Production of Protactinium-229 via Deuteron Irradiation of Thorium-232

A Dissertation Presented for the
Doctor of Philosophy
Degree
The University of Tennessee, Knoxville

Naser Burahmah
December 2021

Copyright © 2021 by Naser Burahmah.
All rights reserved.

DEDICATION

To my father, Tareq, and my mother, Sana this would not have been possible without all the support and love that you provided me since my young age. I dedicate this dissertation to both of you.

ACKNOWLEDGEMENTS

First, I would like to thank the members of my doctoral committee: Dr. Lawrence Heilbronn, Dr. Howard Hall, Dr. Jason Hayward, and Dr. Robert Counce. I am grateful and honored to be one of Dr. Heilbronn's students. He helped me and always welcomed my questions from the first time I met him in my undergraduate courses. Always there to help me whenever I needed help. I could not have reached this level without his constant support and guidance in each step in my academic life. I will always be grateful for all the moments we shared through the years, and I have always had Dr. Heilbronn as a mentor and a father while studying in the states.

Another person whom I need to thank is Dr. Justin Griswold. He was not only my mentor, and he was a friend that guided me in each step for the past three years. From the first day at Oak Ridge National Laboratory, he helped me with many aspects of research and settling in the lab. He was always there to answer my questions and always put a smile and laugh with each story he shared. I would like to thank other members of the Nuclear and Radiochemistry group at ORNL that helped me in the process of this work, including Dr. Roy Copping, Mikayla Molnar, and Dr. Ashleigh Kimberlin.

In addition, I would like to acknowledge our collaborators at Lawrence Berkeley National Laboratory, including Dr. Lee Bernstein, Dr. Andrew Voyles, and Dr. Jonathan Morrell. I am appreciative of their dedication and hard work to the project. They helped with planning and performing the irradiations at LBNL.

I would like to thank my precious friend Dr. Fahad Zaman for being there and helping during the toughest times. Always grateful for the constant support that he provided me.

Finally, I would like to thank the U.S. Department of Energy Isotope Program, managed by the Office of Science for isotope R&D and production, for funding this work through under contract DE-SC0020140. I also thank Kuwait Foundation for the Advancement of Sciences (KFAS) for supporting me in my first year in my Ph.D.

ABSTRACT

^{225}Ac [Actinium-225] is a promising radionuclide for targeted alpha therapy of cancer. ^{229}Pa can lead to the production of ^{229}Th [Thorium-229] and ^{225}Ac [Actinium-225]. Deuteron bombardment on natural thorium targets has been investigated to measure cross sections of protactinium isotopes. In this work, ^{229}Pa [Protactinium-229] excitation function was measured via deuteron energies up to 50 MeV [Mega electron volt] of thin thorium foils. The irradiation took place at Lawrence Berkeley National Laboratory's (LBNL) 88-Inch Cyclotron. The target processing and analysis were performed at Oak Ridge National Laboratory (ORNL). The target consisted of 4 thin foils (~17 mg/cm^2 [milligrams per square centimeter]) in a stacked-target configuration, and were irradiated with 1 μA [microampere] for approximately 11 continuous hours. Column chromatography techniques had been implemented to observe ^{229}Pa due to its weak γ-rays [gamma-rays]. The primary motivation of this work is to quantify the production routes of ^{229}Th. ^{232}Th(d,5n)^{229}Pa reaction cross sections are reported for the first time. The peak of the excitation function of ^{232}Th(d,5n)^{229}Pa at 121.9 ± 12.7 mb [millibarns] occurs at E_d = 35.2 MeV. The production cross sections of ^{232}Th(d,xn)^{228,230,232,233}Pa reactions, where x = 1,2,4, and 6, are also reported. Other measured cross sections are in excellent agreement with published data in the literature. The experimental cross sections were compared with transport code using Particle and Heavy Ion Transport code System (PHITS) and exhibited good agreement.

TABLE OF CONTENTS

Chapter 1 Introduction 1
Section 1.1 Scope 1
Section 1.2 Targeted Alpha Therapy 2
Section 1.3 Current Production of ^{225}Ac 2
Section 1.4 Nuclear Interaction Discussion 5
Chapter 2 Literature Review 8
Chapter 3 Materials and Methods 13
Section 3.1 Experimental 13
Subsection 3.1.1 Target Fabrication 13
Subsection 3.1.2 Target Irradiation 15
Subsection 3.1.3 Chemical Separation and Analysis at ORNL 20
Subsubsection 3.1.3.1 Anion Exchange Column 20
Subsubsection 3.1.3.2 Radiotracer to Determine the Overall Chemical Yield 25
Subsection 3.1.4 Gamma Ray Spectroscopy and Effective Cross Section Measurements 25
Section 3.2 Computational 31
Subsection 3.2.1 PHITS Monte Carlo Calculation 31
Chapter 4 Results and Discussion 37
Section 4.1 ^{232}Th(d,x)^{233}Pa reactions 40
Section 4.2 ^{232}Th(d,2n)^{232}Pa reactions 42
Section 4.3 ^{232}Th(d,4n)^{230}Pa reactions 45
Section 4.4 ^{232}Th(d,5n)^{229}Pa reactions 48
Section 4.5 ^{232}Th(d,6n)^{228}Pa reactions 50
Section 4.6 Discussion 53
Chapter 5 Conclusion and Future Work 54
List of References 56
Appendices 60
Appendix A: Example of Efficiency Curve 61
Appendix B: Sample of PHITS Input File 63
Appendix C: Table of All PHITS Calculated Cross sections 66

Vita..... 86

LIST OF TABLES

Table 2.1. Protactinium production reaction and their threshold energies. 9

Table 3.1. Irradiation Parameters at LBNL. 16

Table 3.2. PHITS-calculated deuteron energies for the stacked-foil experiment. 19

Table 3.3. Gamma-ray energies and intensities used in chemical yield determination and activity calculation [19-23]. 26

Table 4.1. Effective measured production cross section (in mb) of selected radionuclides with 31-50 MeV deuteron energies. 38

Table 4.2. PHITS simulated cross section (in mb) of selected radionuclides with 31-50 MeV deuteron energies. 38

Table 4.3. Ratio of PHITS simulated cross section to experimentally measured cross section. 39

Table A.1. Constants used in the efficiency. 62

Table C.1. PHITS calculated cross sections (in mb) for all product nuclei of deuteron energies of 50, 40, 35, and 30 MeV. 66

LIST OF FIGURES

Figure 1.1. ^{233}U Decay Chain. Prior to its exclusion due to security concerns, ^{233}U was the primary source for the production of ^{229}Th. 4

Figure 1.2. Schematic of incident projectile attenuation with a target. 7

Figure 2.1. Thorium production pathways and nuclides decay scheme. 9

Figure 2.2. ^{232}Th(d,4n)^{230}Pa as a function of deuteron energy [10, 13]. PHITS model calculations for the production of cross sections are also shown. 10

Figure 2.3. ^{232}Th(p,3n)^{230}Pa as a function of proton energy [1, 14-16]. PHITS model calculations for the production of cross sections are also shown. 12

Figure 3.1. Pictures of Th foil fabrication before irradiation. 14

Figure 3.2. The 88-Inch Cyclotron floor plan at LBNL and the location of experiment (Cave 0). 16

Figure 3.3. Foil mounting frame schematic. 17

Figure 3.4. Photo of an individual foil secured to the aluminum holder. 17

Figure 3.5. Example of the stacked-target experiment. 18

Figure 3.6. Deuteron energy at each foil in the stacked-target experiment. 18

Figure 3.7. DOT type A container. 21

Figure 3.8. Target dissolution. 21

Figure 3.9. Ion-exchange chromatography flowchart. 22

Figure 3.10. The MP1 Cl^- column used in the chemical separation process. 22

Figure 3.11. The detector used for gamma spectroscopy analysis. 26

Figure 3.12. Example of gamma-ray spectra of Foil 4 upon arrival to ORNL. 28

Figure 3.13. Example of the method used to calculate net peak area. ^{229}Pa gamma-ray peak is shown above. 28

Figure 3.14. PHITS physics models and their switching energies [24]. 33

Figure 3.15. The geometry of the target and projectile used in the PHITS calculation. 33

Figure 4.1. Excitation function of ^{232}Th(d,x)^{233}Pa reaction. PHITS model calculation is also shown. PHITS cross sections include the direct and cumulative cross sections. 41

Figure 4.2. Effective cross sections and cumulative cross sections from PHITS for ^{232}Th(d,x)^{233}Pa reaction. Literature cross section from the same reaction are shown [10, 13]. 41

Figure 4.3 Excitation function of ^{232}Th(d,2n)^{232}Pa reaction. PHITS model calculation is also shown. 43

Figure 4.4. Effective cross sections and cumulative cross sections from PHITS for ^{232}Th(d,2n)^{232}Pa reaction. Literature cross section from the same reaction are shown [10, 13]. 43

Figure 4.5. Experimental cross sections and simulated cross section for ^{232}Th(p,n)^{232}Pa (red color) and ^{232}Th(d,2n)^{232}Pa (black color) reactions. Literature cross sections from the same reactions are shown [1, 10, 13-15, 17, 18]. 44

Figure 4.6. Excitation function of ^{232}Th(d,4n)^{230}Pa reaction. PHITS model calculation is also shown. 46

Figure 4.7. Effective cross sections and cumulative cross sections from PHITS for ^{232}Th(d,4n)^{230}Pa reaction. Literature cross section from the same reaction are shown [10, 13]. 46

Figure 4.8. Experimental cross sections and simulated cross section for ^{232}Th(p,3n)^{230}Pa (red color) and ^{232}Th(d,4n)^{230}Pa (black color) reactions. Literature cross sections from the same reactions are shown [1, 10, 13-16]. 47

Figure 4.9. Excitation function of ^{232}Th(d,5n)^{229}Pa reaction. PHITS model calculation is also shown. 49

Figure 4.10. Experimental cross sections and simulated cross section for ^{232}Th(p,4n)^{229}Pa (red color) and ^{232}Th(d,5n)^{229}Pa (black color) reactions. Literature cross sections from the same reactions are shown [10, 13]. 49

Figure 4.11. Excitation function of ^{232}Th(d,6n)^{228}Pa reaction. PHITS model calculation is also shown. 51

Figure 4.12. Effective cross sections and cumulative cross sections from PHITS for ^{232}Th(d,2n)^{232}Pa reaction. Literature cross section from the same reaction are shown [10, 13]. 51

Figure 4.13. Experimental cross sections and simulated cross section for $^{232}Th(p,5n)^{228}Pa$ (red color) and $^{232}Th(d,6n)^{228}Pa$ (black color) reactions. Literature cross sections from the same reactions are shown [1, 13, 14]. 52

Figure A.1 A typical efficiency curve used in this work. 62

Chapter 1 Introduction

Section 1.1 Scope

In this work, the effective cross section for the production of ^{229}Pa through deuteron bombardment of ^{232}Th is reported, as well as the effective cross sections for other radioisotopes, including ^{228}Pa, ^{230}Pa, ^{232}Pa, and ^{233}Pa. The goal is to evaluate the production route of ^{229}Th via deuteron-induced reaction of ^{232}Th with low energy deuterons, $E_d \leq 50$ MeV. From previous work, the decay of ^{229}Pa is the main contributor to the overall ^{229}Th production [1]. The deuteron-induced bombardment will be compared with proton-induced bombardment to evaluate each production route. In addition to the experimental cross sections, the PHITS Monte Carlo code is used to produce the simulated cross sections. It is then compared with the experimental cross sections from this work and previously available data. Note that the ^{232}Th(d,5n)^{229}Pa production cross section is reported herein for the first time.

The effective cross sections produced in this work will be referred to as measured cross sections or experimental cross sections, while the cross sections produced from PHITS will be referred to as the simulated cross sections or direct cross sections, or cumulative cross sections. It is important to note that a simulated cross section is a direct cross section that does not include the contribution of any indirect route A cumulative cross section is the sum of the precursors' simulated cross sections, as described in Subsection 3.2.1.

Section 1.2 Targeted Alpha Therapy

The use of α-emitting radioisotopes to treat cancer and other diseases has been given renewed focus in the medical field. One technique that has been given considerable attention is Targeted Alpha Therapy (TAT), a procedure used for cancer therapy that capitalizes on the short range and high linear energy transfer (LET) of alpha (α) particles emitted from isotopes. With a LET on the order of 100 keV/μm, the emitted α particles can produce a lethal dose directed to a tumor cell in human tissue and successfully destroy it without damaging the healthy cells surrounding the tumor [2]. The isotopes ^{211}As ($t_{1/2}$ = 7.2h), ^{223}Ra ($t_{1/2}$ = 11.43d), ^{226}Th ($t_{1/2}$ = 30.57 m), ^{225}Ac ($t_{1/2}$ = 9.92d), and the decay chain product ^{213}Bi ($t_{1/2}$ = 45.59m) are strong contenders for TAT. It has been found through a series of clinical studies that α-emitting radioisotopes have significant potential to treat leukemia, lymphoma, prostate cancer, and other malignancies [3-5]. New means of producing ^{225}Ac need to be investigated, as it is becoming increasingly widespread in clinical research, resulting in the isotope's limited supply.

Section 1.3 Current Production of ^{225}Ac

Currently, the most common method to supply ^{225}Ac is to extract it from the decay of ^{229}Th ($t_{1/2}$ = 7880 y), which has been separated from a supply of ^{233}U. Figure 1.1 shows the decay chain of ^{233}U. The ^{233}U was produced in the 1960s and 1970s as part of a molten salt breeder reactor program, and it is currently in long-term storage. Because of the safeguard and proliferation associated with ^{233}U, it is no longer available for extraction of ^{229}Th, and another method is needed to produce ^{229}Th. The three main

suppliers of ^{229}Th in the world are the Oak Ridge National Laboratory (ORNL) in the United States, the Institute of Physics and Power Engineering (IPPE) in Russia, and the Institute of Transuranium Elements (ITE) in Germany. Together, they yield a yearly total supply of around 1-2 Ci of ^{225}Ac in global production [6]. The ^{225}Ac produced using this method are considered to be “carrier free” nuclides and sufficiently supply a small number of clinical studies. Carrier free refers to a radionuclide having 100 % isotopic abundance. As clinical studies have increased and so has the potential for widespread use of the isotope, it has become more important to identify additional production channels. Recent research offers an alternate method for producing ^{225}Ac by bombarding ^{232}Th targets with high-energy protons, producing ^{225}Ac through spallation reactions [1, 7-12]. After the irradiation, ^{225}Ac is chemically separated from other nuclei produced in the bombardment, such as radium, thorium, protactinium, and fission products. In the production of ^{225}Ac, the presence of ^{226}Ac ($t_{1/2}$ = 29.37 h) and ^{227}Ac ($t_{1/2}$ = 21.8 y) contaminants poses a challenge for the separation method. Since ^{226}Ac has a short half-life, it has little effect on the use of ^{225}Ac in TAT. The longer lived ^{227}Ac cannot be chemically separated from ^{225}Ac, and the impacts of ^{227}Ac and its daughters should be investigated. Any technique that produces ^{227}Ac along with ^{225}Ac needs to quantify the amount of ^{227}Ac produced to decide the viability of this pathway for production.

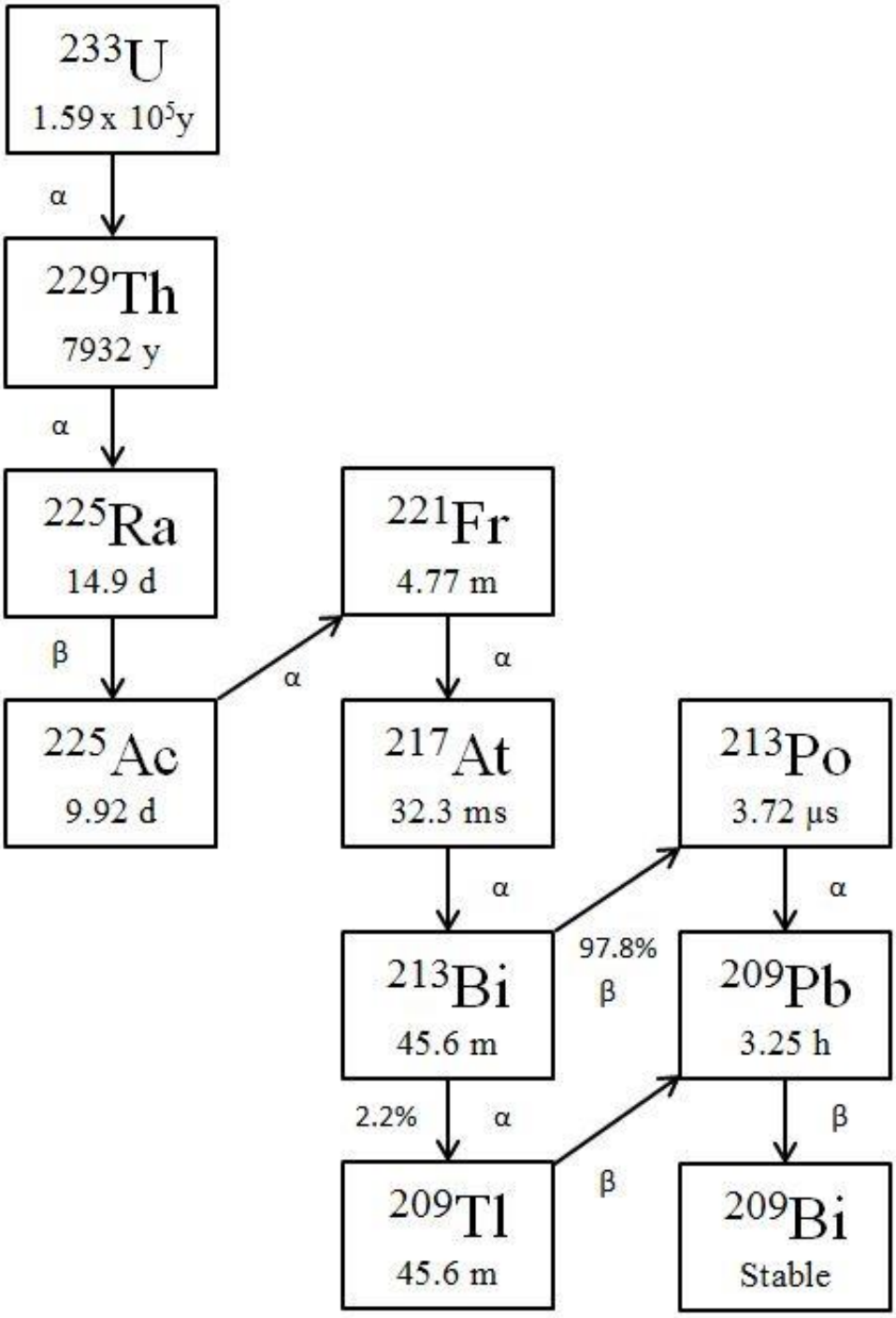


Figure 1.1. ^{233}U Decay Chain. Prior to its exclusion due to security concerns, ^{233}U was the primary source for the production of ^{229}Th.

Section 1.4 Nuclear Interaction Discussion

For nuclear reactions to occur, two options may be considered: exothermic or endothermic reactions. The Q value determines the type of reaction that occurs. The Q value is the difference in mass equivalent energies between the product and reactant species. Using the following example reaction of $A + a \rightarrow B + b$, Equation (1.1 shows Q value calculation for the example reaction, where M_a is the projectile mass energy, M_A is the target mass energy, M_b is the ejected projectile mass energy, and M_B is the ejected target mass energy:

$$Q = (M_A + M_a)c^2 - (M_B + M_b)c^2 \qquad (1.1)$$

If the Q < 0, then the reaction is endothermic, meaning energy is required in order for the reaction to transpire. If Q > 0, then the reaction is exothermic, meaning energy must be released for the reaction to ensue. Note that the exothermic reaction may occur at any energy, while the endothermic reaction requires a threshold energy (E_{th}). Equation 1.2 shows the threshold energy calculation for a two-body interaction:

$$E_{th} = |Q| \cdot \frac{M_A + M_a}{M_A} \qquad 1.2)$$

For the charged particle interaction, the projectile needs to overcome the Coulomb barrier of the projectile-target combination. The Coulomb barrier is the electrostatic

potential energy due to the Coulomb repulsion of the charged particle in the nucleus of the target. The Coulomb barrier is calculated in MKS units using Equation *1.3*, where k is Coulomb's constant (8.9876×10^9 Nm^2C^{-2}) Z_A is the number of protons in the target nucleus, Z_a is the number of protons in the projectile, e is the electric charge ($e = 1.6 \times 10^{-19}\ C$), and R is the radius of the target nucleus (in meters)

$$B = k \frac{Z_A Z_a e^2}{R} \qquad 1.3)$$

The radius of the nucleus can be approximated using Equation (1.4, where A is the atomic mass number and R is in units of meters:

$$R = 1.3 \times 10^{-15} A^{\frac{1}{3}} \qquad (1.4)$$

Nuclear cross section is the mean number of interactions between the projectile and target per unit fluence and has units of cm^2 or barns (b), where 1 b = 10^{-24} cm^2. Referring to Figure 1.2, φ_0 is the incident fluence on the target (attenuated by the target area), and φ is the transmitted fluence. Equation 1.5 displays the cross section σ calculation, where $d\varphi/\varphi$ is the fraction of particles that undergo interactions.

$$\sigma = \frac{d\varphi/\varphi}{n_v\, dx} = \frac{fractional\ change\ in\ transmitted\ flux}{number\ of\ targets\ /\ unit\ area} \qquad 1.5)$$

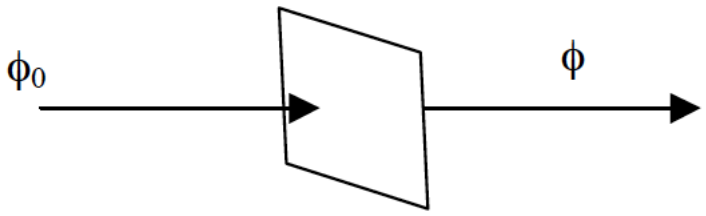


Figure 1.2. Schematic of incident projectile attenuation with a target.

Chapter 2 Literature Review

Figure 2.1 represents the possible production pathways and decay schemes of product nuclides to produce ^{229}Pa, ^{225}Ac, and ^{229}Th. Table 2.1 shows the threshold energies for all possible protactinium isotopes. Note that ^{229}Pa decays via electron capture (EC, 99.5%) to ^{229}Th and via alpha emission (α, 0.5%) to ^{225}Ac. In this study, the production of ^{229}Pa from bombardment of ^{232}Th by deuterons below 50 MeV is the main interest because of its decay channel to ^{229}Th and ^{225}Ac. Noted in the previous work of Griswold et al., ^{229}Pa is the main contributor to ^{229}Th from proton bombardment of ^{232}Th at low energies $E \leq 50$ MeV [1].

Few studies had been conducted that use deuteron projectiles on ^{232}Th targets, with just two relevant measurements [10, 13], both of which measured the ^{228,230,232,233}Pa production cross section. Neither measured the production of ^{225}Ac or ^{229}Pa. Duchemin et al. measured the reaction of ^{232}Th(d,xn)^{230,232,233}Pa, where x = 1, 2, and 4, and Rao et al. measured the reaction of ^{232}Th(d,xn)^{228,230,232,233}Pa. Duchemin et al. used deuteron energies from 16.6 to 33.1 MeV, while Rao et al. used energies from 16 to 80 MeV. Figure 2.2 shows modeled cross sections (modeling discussed later) for the ^{232}Th(d,4n)^{230}Pa reaction together with the experimental data of Duchemin and Rao [10, 13]. The simulated cross sections are in excellent agreement with the experimental data. No experimental data were found in the literature for the ^{232}Th(d,5n)^{229}Pa reaction.

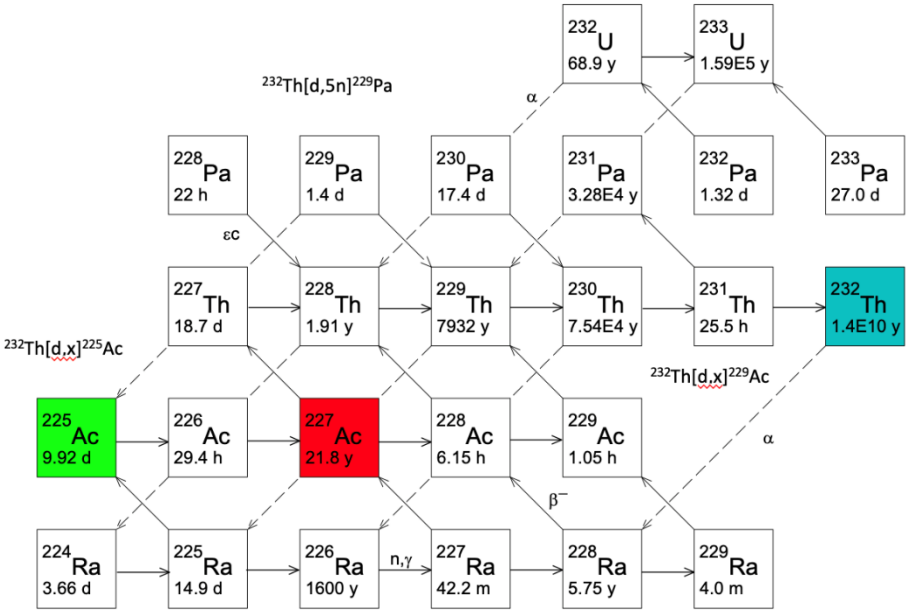


Figure 2.1. Thorium production pathways and nuclides decay scheme.

Table 2.1. Protactinium production reaction and their threshold energies.

Reaction	**Threshold (MeV)**
^{232}Th(d,n)^{233}Pa	0
^{232}Th(d,2n)^{232}Pa	3.54
^{232}Th(d,4n)^{230}Pa	16.01
^{232}Th(d,5n)^{229}Pa	21.86
^{232}Th(d,6n)^{228}Pa	29.02

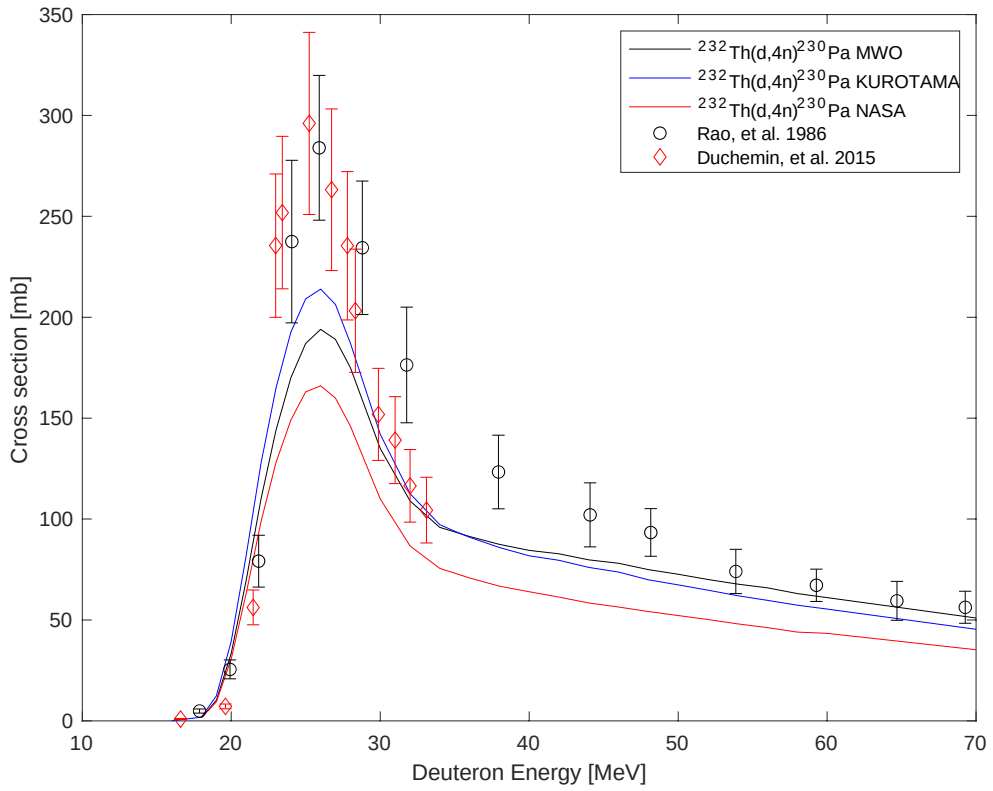


Figure 2.2. ^{232}Th(d,4n)^{230}Pa as a function of deuteron energy [10, 13]. PHITS model calculations for the production of cross sections are also shown.

On the other hand, several more measurements using proton projectile had been conducted [1, 14-18]. Those measurements are compared to the deuteron data results in chapter 4. Griswold et al. measured the reaction of ^{232}Th(p,xn)^{228,229,230,232}Pa, where x = 1, 3, 4, and 5, at proton energies ranges of 12 to 40 MeV [1]. Kudo et al. measured the excitation function for ^{232}Th(p,xn) ^{230,232}Pa, where x = 1 and 3, in the proton energy range of 8 to 22 MeV [15]. Radchenko et al. evaluated the cross sections of ^{232}Th(p,xn) ^{228,230,232}Pa, where x = 1, 3, and 5, in the energy ranges of 44 to 195 MeV [14]. Morgenstern et al. measured the excitation function for ^{232}Th(p,3n) ^{230}Pa reaction up to 34 MeV proton energy [16]. For the ^{232}Th(p,n) ^{232}Pa reaction, both Tewes and Celler et al. measured the cross section up to energies of 32 MeV [17, 18]. Note that all the previous studies measured the cross sections using the stacked-target technique, where a single, high-energy beam strikes a target composed of several foils sandwiched between energy degraders. Figure 2.3 shows the excitation function for the ^{232}Th(p,3n) ^{230}Pa reaction from the literature with the simulated cross sections from PHITS (modeling discussed in section 3.2).

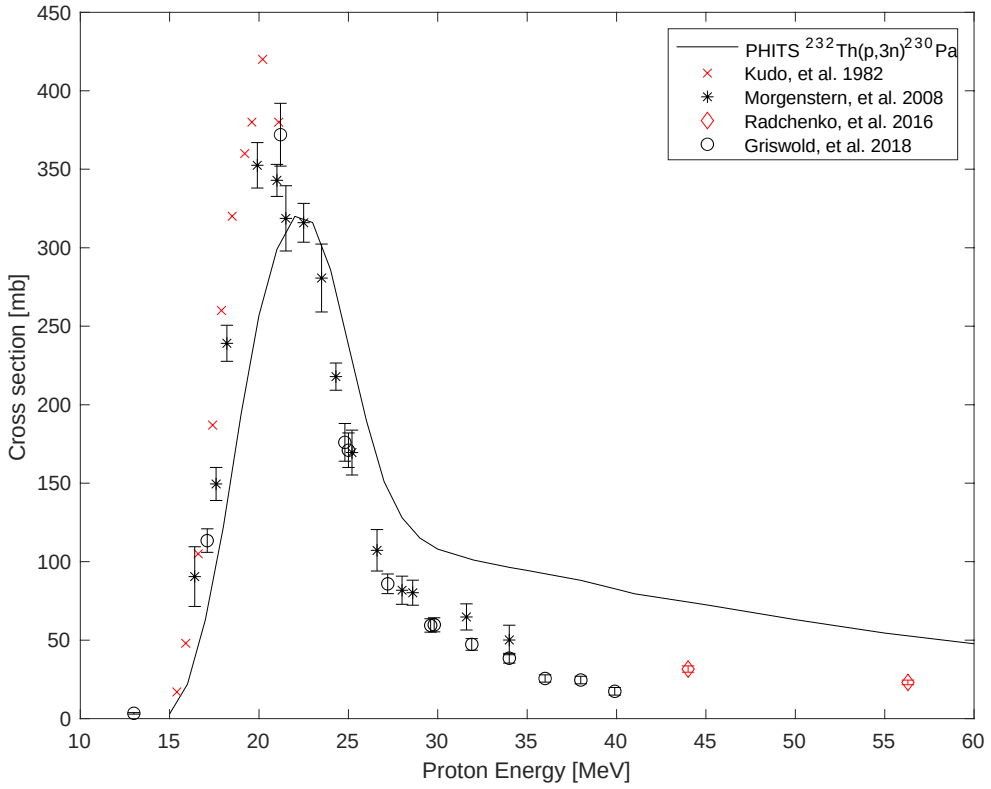


Figure 2.3. ^{232}Th(p,3n)^{230}Pa as a function of proton energy [1, 14-16]. PHITS model calculations for the production of cross sections are also shown.

Chapter 3 Materials and Methods

Section 3.1 Experimental

The experiment was conducted at the 88-Inch Cyclotron located at Lawrence Berkeley National Laboratory (LBNL). The irradiation consisted of deuteron bombardment up to 50 MeV on natural thorium foils using a stacked-target technique. The foils were then sent back to ORNL for chemical separation and gamma spectroscopy analysis. Following separation, the end of bombardment activities were determined by using a well calibrated high-purity germanium (HPGe) detector. The effective cross sections were then calculated from the end of bombardment activities.

Subsection 3.1.1 Target Fabrication

A natural thorium foil (0.0125 mm, 99.5% purity) was purchased from Goodfellow Corporation (Coraopolis, PA 15108, USA) and was sent to ORNL for preparation. The original foil was 50x50 mm with a thickness of 0.0125mm. The foil was then cut into nine 16x16mm foils, providing enough foils to perform a stacked-target experiment. The foils were measured and weighed before sending them to LBNL for irradiation. Figure 3.1 shows the foils after cutting and wrapped in Al foils to prevent contamination. The foils were designated with numbers on the accompanying Al foils and sent to LBNL for Irradiation.

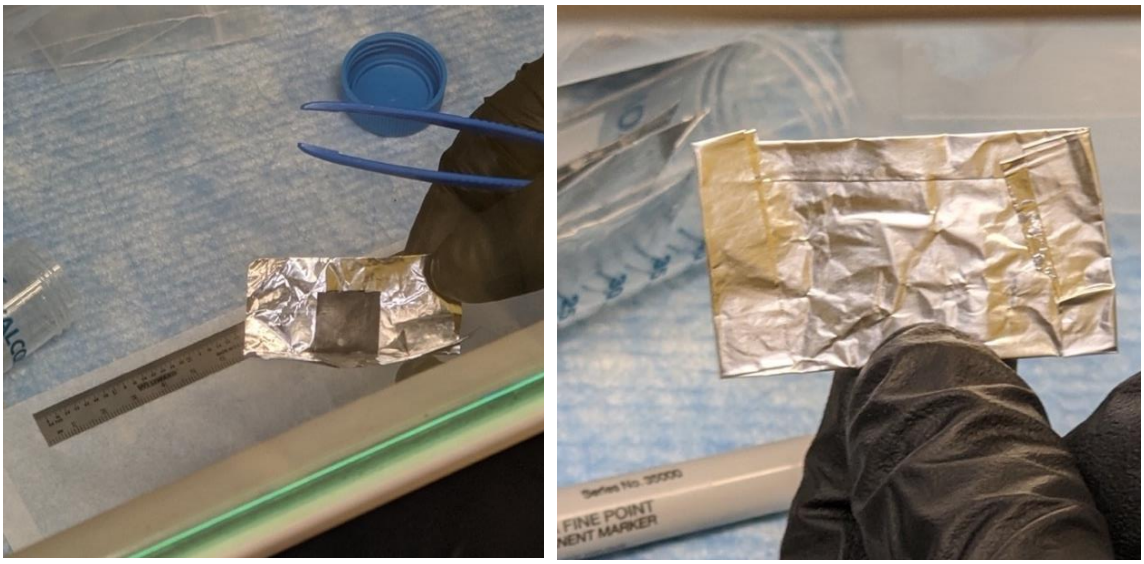


Figure 3.1. Pictures of Th foil fabrication before irradiation.

Subsection 3.1.2 Target Irradiation

The experiment was performed in the 88-inch cyclotron in LBNL. The 88-inch cyclotron can provide light ion beams with intensities of up to 1-2 μA and energies of up to 65 MeV for deuterons. The experiment took a place in Cave 0, a location typically used for experiments that potentially create high levels of target activation. Figure 3.2 graphically represents of the 88-Inch Cyclotron floor plan. The preliminary PHITS calculations indicated cross sections ranging from millibarn to hundreds of millibarn for Pa, Ac, Th, and light fission products. Based on the cross section calculation, eight hours of deuteron beamtime at those intensities was calculated to provide sufficient activity from the product nuclei to calculate their production cross section. The irradiation parameters used in the experiment are shown in Table 3.1. The foils were irradiated on the 18^{th} of May 2021 with ~1 μA of deuteron beam current and lasted for 10.9 hours.

Figure 3.3 shows the target holder at LBNL where the foil was placed in the center of the frame. An example of foil placement to the aluminum holder where it was sealed in Kapton film tape is shown in Figure 3.4 The irradiation setup was to irradiate four foils at once using the stacked-target technique, as shown in Figure 3.5. Utilizing a stacked-foil configuration, each foil was irradiated at different deuteron energy; as the beam travels through the Th foils, monitor foils, and aluminum degraders, the energy was degraded to reach the proposed energies at each foil. Figure 3.6 displays the PHITS calculated deuteron energy distribution before reaching each foil. From the simulation, the aluminum degrader thicknesses were estimated to acquire the proposed energies shown in Table 3.2.

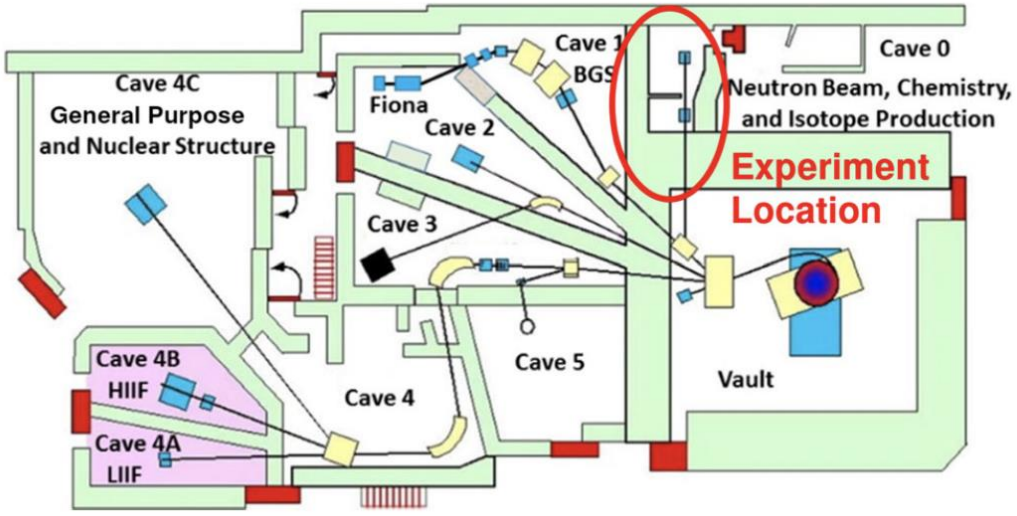


Figure 3.2. The 88-Inch Cyclotron floor plan at LBNL and the location of experiment (Cave 0).

Table 3.1. Irradiation Parameters at LBNL.

Foil (#)	Target Thickness (mg cm^{-2})	Energy (MeV)	Uncertainty (MeV)	Average Current (μA)	Uncertainty in Current (%)
1	17.15	49.61	0.54	1.08	4.09
2	17.17	41.34	0.62	1.07	4.00
3	17.37	35.01	0.71	1.10	3.96
4	17.51	30.76	0.77	1.10	3.88

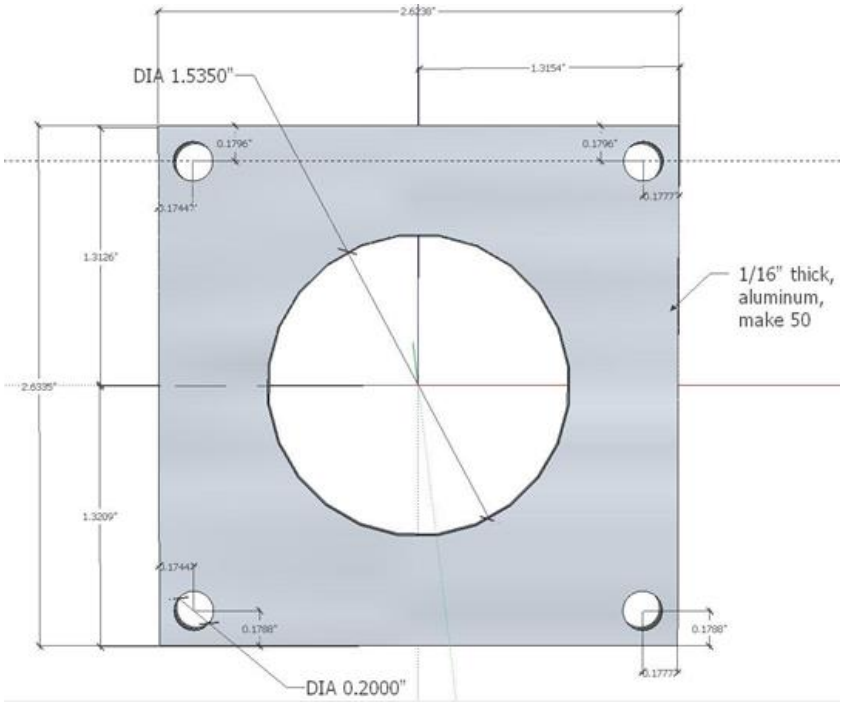
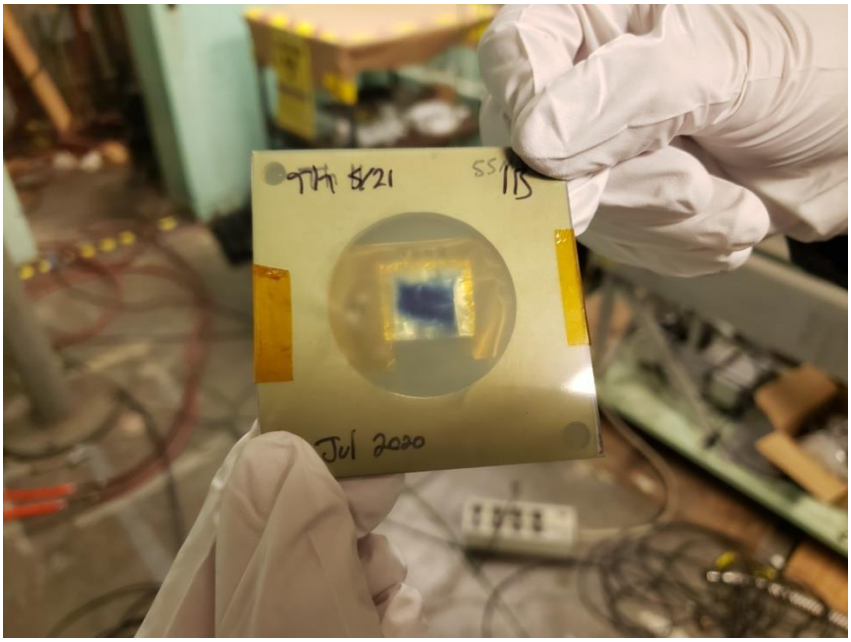


Figure 3.3. Foil mounting frame schematic.


Figure 3.4. Photo of an individual foil secured to the aluminum holder.

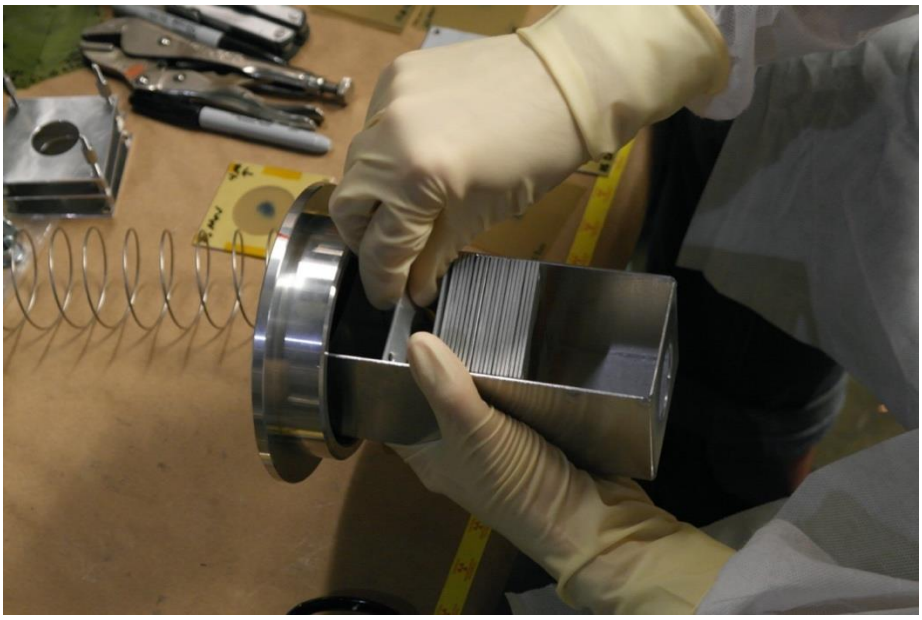


Figure 3.5. Example of the stacked-target experiment.

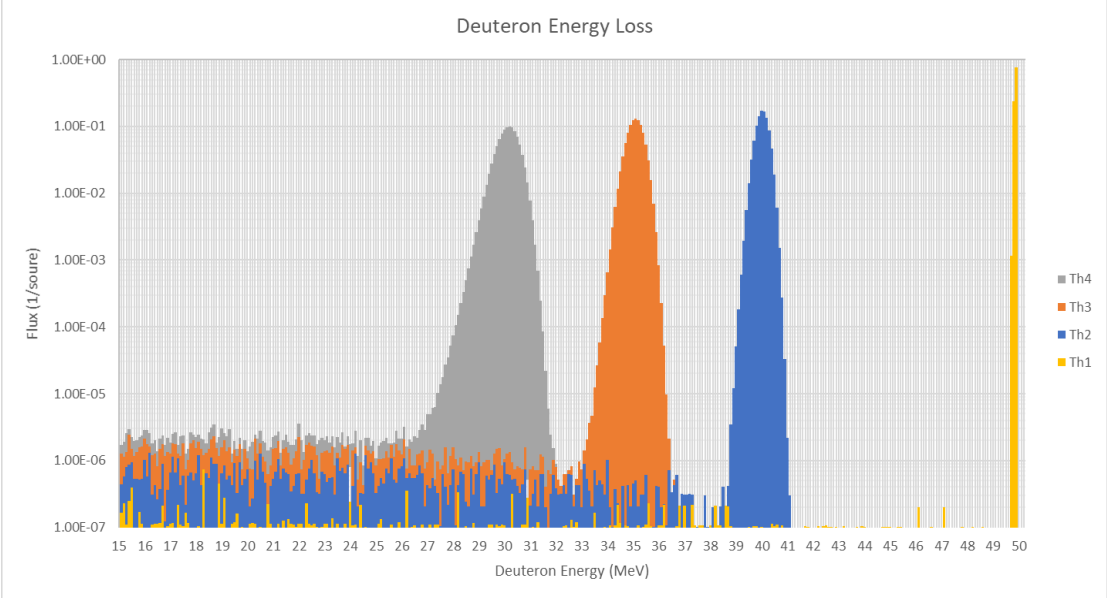


Figure 3.6. Deuteron energy at each foil in the stacked-target experiment.

Table 3.2. PHITS-calculated deuteron energies for the stacked-foil experiment.

Foil (#)	Al Thickness (mm)	Average Energy (MeV)	Uncertainty (%)	FWHM (MeV)
1	0	49.646	0.001	0.122
2	1.55	41.346	0.002	0.509
3	0.97	35.012	0.003	0.732
4	0.51	30.695	0.003	0.931

Subsection 3.1.3 Chemical Separation and Analysis at ORNL

The foils were sent to ORNL post-irradiation for chemical separation in building 4501. The reagent and ion exchange columns were prepared before the foils arrived, and the chemical separation was completed in a fume hood. The targets were shipped to ORNL in a DOT Type A container, as displayed in Figure 3.7. To prevent any contamination, the foils were transferred into the fume hood for processing. Then, each foil was removed from the aluminum foil and placed into 20 mL glass scintillation vials, as exhibited in Figure 3.8. The highest dose measured on contact with the foils was 1.5 mSv/hr (150 mrem/hr). The foils were assayed via γ-ray spectroscopy for 10 minutes. Then, each foil was dissolved in 10 mL of 10 M optima-grade HCl and a few drops of 2M HF, as seen in Figure 3.8. Heating through hot plate and heat lamp were used to aid the dissolution. Figure 3.9 presents a flowchart of the process of ion-exchange chromatography. After the chemical separation process, fractions coming from the columns were assayed using gamma spectroscopy.

Subsubsection 3.1.3.1 Anion Exchange Column

In this work, anion exchange chromatography was used to separate actinium, thorium, and other actinides and fission products. The column was a BioRad disposable polypropylene (PP) with 2 mL bed volume (BV) and 0.8 cm diameter. For the separation, 0.5 and 1 mL of MP1 Cl^- anion exchange resin was used with resin size of 100-200 mesh, as shown in Figure 3.10.



Figure 3.7. DOT type A container.



Figure 3.8. Target dissolution.

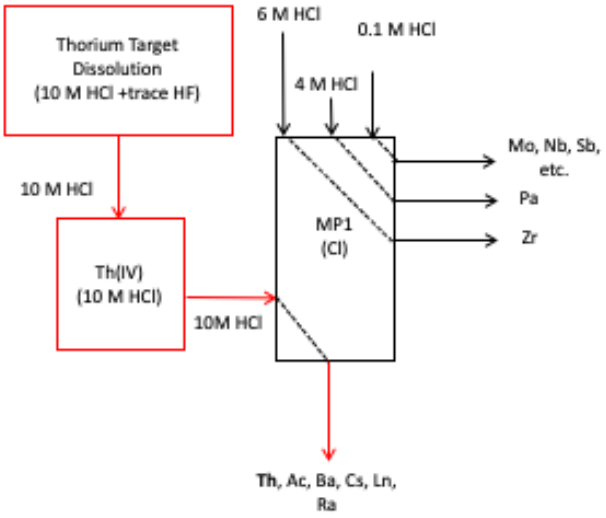


Figure 3.9. Ion-exchange chromatography flowchart.

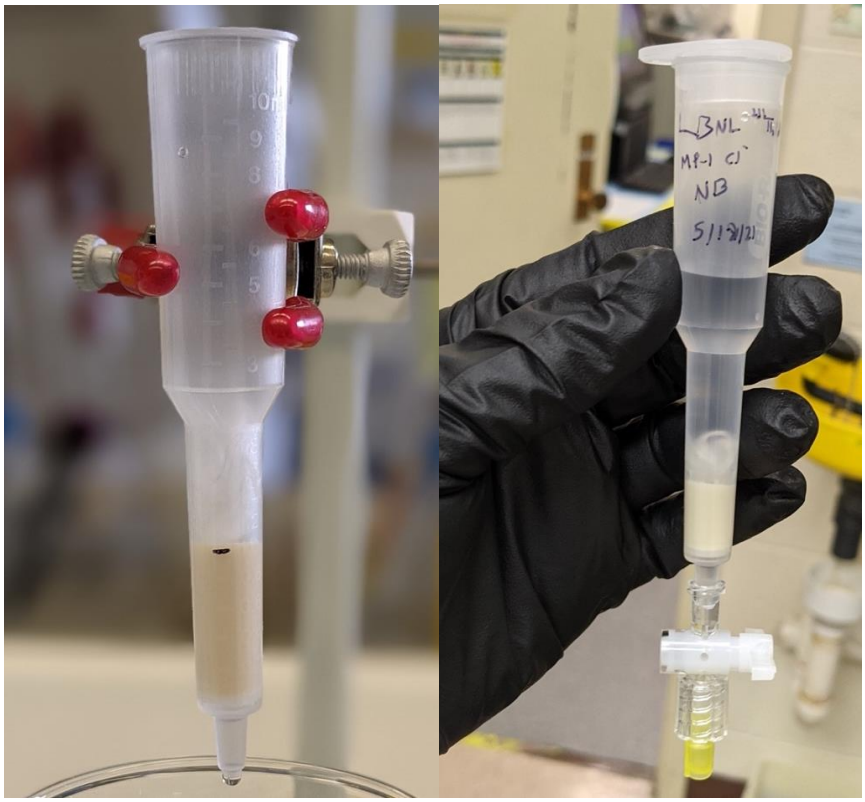


Figure 3.10. The MP1 Cl^- column used in the chemical separation process.

In this MP1 Cl^- column, fission products such as molybdenum, niobium, zirconium, and iron were attached to the resin in addition to uranium and protactinium, while other elements such as thorium, actinium, radium, barium, cesium, and lanthanum went through the resin.

The procedure of loading the target was very similar for each foil. The steps are as follows:

1. The column was conditioned with 4 BV of 10 M HCl.
2. The target solution was added to the column using a glass pipette, and the fraction coming out was loaded into a clean glass scintillation vial labeled "Load Wash" with the foil number. In this fraction, the thorium, actinium, radium, and other actinides were collected. Note: All fractions coming from the column were assayed for 5 minutes with a HPGe detector.
3. 1 BV of 10 M HCl was added to the empty target vial to rinse, ensuring that all of the target went into the column. The fraction was collected in a clean scintillation vial labeled "W1" with the foil number.
4. Step 3 repeated twice. The fractions were collected in the same vial used in step 3.
5. 10 BV of 6 M HCl were added to the column. In this fraction, zirconium and niobium was stripped out of the column. The fraction was collected in a clean vial and labeled "W2" with the foil number.

6. 1 BV of 6 M HCl was added to the column, and the same collection process was repeated in step 5. The collected fraction was assayed in the HPGe detector to certify that protactinium was still attached to the column.
7. Step 6 was repeated 4-5 times. The fractions were assayed, and it was verified that protactinium did not leak from the column.
8. 1 BV of 4 M HCl was added to the column. In this fraction, protactinium was stripped out of the column. The fraction was then collected in a clean vial and labeled “W3” with the foil number.
9. 2 BV of 4 M HCl was added to the column. The same collection process was repeated in step 8.
10. Step 9 repeated twice. What could have been considered a main impurity, molybdenum, did not leak into the fraction.
11. The column was washed with 5 BV of 0.1 M HCl to strip it of molybdenum and other fission products. The fraction was collected in a clean vial and labeled “E1” with the foil number.
12. Next, the column was cleaned with 5 BV of 8 M HNO_3 to strip it of other fission products. The fraction was collected in a clean vial and labeled “E2” with the foil number.
13. Lastly, 5 BV of distilled H2O was added to the column to strip off what was left on the column. The fraction was collected in a clean vial and labeled “WW” with the foil number.

Subsubsection 3.1.3.2 Radiotracer to Determine the Overall Chemical Yield

Column chromatography techniques were implemented to isolate Pa. This is required in order to observe the low intensity γ-rays emitted by ^{229}Pa. Table 3.3 shows the γ-ray emissions used in this work to assess protactinium isotopes, and those data were taken from the Nuclear Data Sheets [19-23]. In addition to the low γ-rays intensity, having a half-life of 1.5 days raised another complication to the chemistry separation since the transit time from LBNL to ORNL took a day and another day for target preparation. $^{228\&230}$Pa may be quantified directly from the thorium foil but their γ-rays were interfered with other fission products. Strong γ-rays with fairly good intensity and no interfering γ-rays from other isotopes were the reasons for choosing ^{232}Pa as an internal tracer. Protactinium-232 activity before and after chemistry separation process was used to determine the overall chemical efficiency of each fraction.

Subsection 3.1.4 Gamma Ray Spectroscopy and Effective Cross Section Measurements

The gamma ray spectroscopy measurements were conducted using a well shielded HPGe detector with relative efficiency of 20% as shown in Figure 3.11. The detector was coupled with multichannel analyzer using Canberra Genie 2000 software. According to the manufacturer, the detector resolution is 0.74 keV at 122 keV and 2.0 keV at 1332 keV The detector efficiency and energy calibration were performed using well known sources to the National Institute of Standards and Technology (NIST). An example of the efficiency curve used in this work presented in Appendix A.

Table 3.3. Gamma-ray energies and intensities used in chemical yield determination and activity calculation [19-23].

Radionuclide	**Half-life**	**E_γ (keV)**	**I_γ (%)**
^{228}Pa	22 h	911.2	23.0
^{229}Pa	1.5 d	119.0	0.13
^{230}Pa	17.4 d	951.9	29.6
^{232}Pa	1.32 d	894.4	19.6
^{233}Pa	26.98 d	311.9	38.5



Figure 3.11. The detector used for gamma spectroscopy analysis.

The targets were assayed for the cross section calculation. The targets were assayed to determine the number of counts in each isotope's relevant gamma-ray peak, and the production cross sections for each isotope could then be determined using the efficiency-corrected gamma-ray counts along with the relevant spectroscopic information on half-life and gamma-ray intensities.

Counting times varied from five minutes to 36-hour counts depending on the sample collected. An example of γ-ray spectrum of the foil is presented in Figure 3.12. Genie reported the value of counts per second (CPS) with the uncertainty in percentage. In some cases, the 119-keV peak of ^{229}Pa was too small for the MCA to recognize it; in this case, the peak was calculated using an end-point averaging method. First, the gross counts of each channel under the peak were determined. The background counts under the peak were calculated by locating areas to the left and right of the peak that appear to be just background, and then taking the average number of counts per channel in that background region, when possible. The net peak area calculation is shown in Equation (3.1 where P is the total counts under the photopeak, n is number of channels under the photopeak, B_1 average background counts over n_1 channels before the photopeak, and B_2 average background counts over n_2 channels after the photopeak. Figure 3.13 demonstrates the methodology used to calculate the net peak area.

$$C = P - n\left(\frac{\left({}^{B_1}/_{n_1}\right) + \left({}^{B_2}/_{n_2}\right)}{2}\right) \qquad (3.1)$$

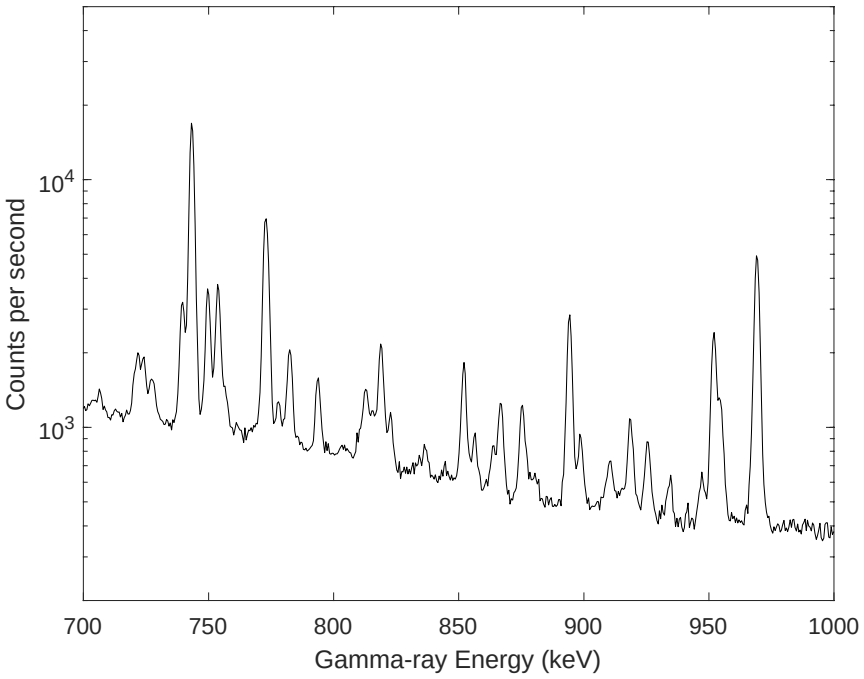


Figure 3.12. Example of gamma-ray spectra of Foil 4 upon arrival to ORNL.

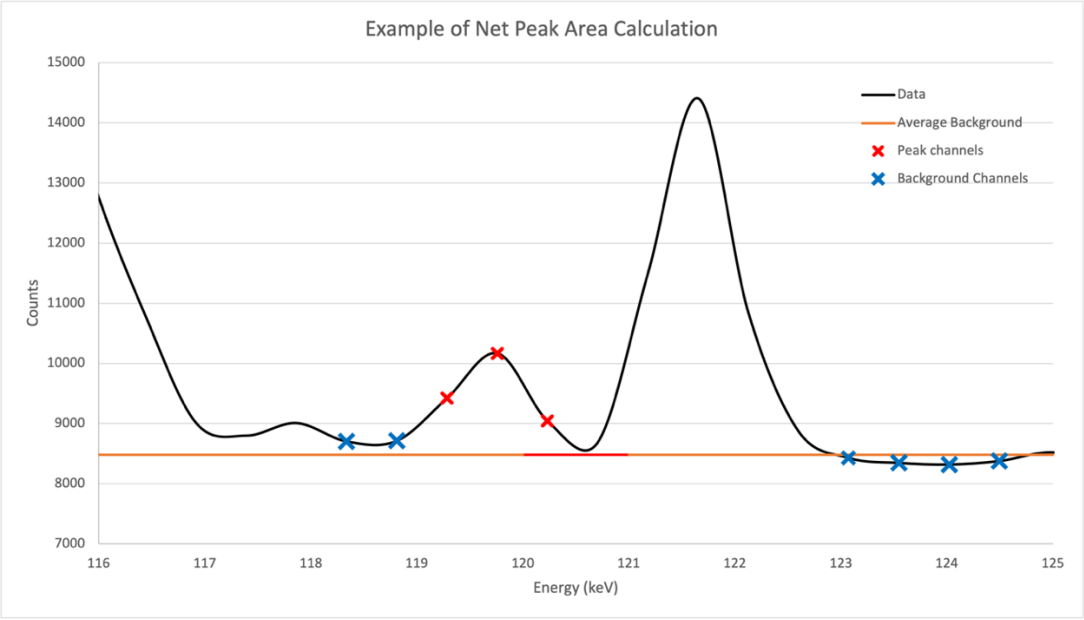


Figure 3.13. Example of the method used to calculate net peak area. ^{229}Pa gamma-ray peak is shown above.

For the uncertainty of net peak area calculation is shown in Equation (3.2.

$$\sigma_C = \sqrt{P + \left(\frac{n}{2}\right)^2 \left(\frac{B_1}{{n_1}^2} + \frac{B_2}{{n_2}^2}\right)} \tag{3.2}$$

For short-lived isotopes and long count times, a correction for the activity must considered, as shown in Equation (3.3, where CPS_u is the uncorrected count rate from Genie, λ is the decay constant (s^{-1}) for the radionuclide, and t is the time of acquisition (s).

$$CPS_c = \frac{CPS_u \times t \times \lambda}{1 - e^{-\lambda t}} \tag{3.3}$$

The activity in becquerels (Bq) of each radionuclide based on the number of background corrected counts under each γ-ray energy (E) peak will be calculated using Equation (3.4, where ε_E is the fractional absolute efficiency of the detector for a gamma-ray with energy E, and I_γ is the fractional intensity of the γ-ray.

$$A_{E,TOC} = \frac{CPS_c}{\varepsilon_E \times I_\gamma} \tag{3.4}$$

Equation (3.5 was used to correct the activity at the time of the count to the end of the bombardment (EOB) where t is the time from EOB to the time of acquisition.

$$A_{i,EOB} = \frac{A_{E,i,TOC}}{e^{-\lambda t}} \tag{3.5}$$

Fractional uncertainty for the activity of each γ-ray is given in Equation (3.6, where σ_g is the fractional uncertainty of the net peak provided by Genie, and σ_{I_γ} is the uncertainty of the intensity of each γ-ray reported in the Nuclear Data Sheets [19-23]. The half-lives are assumed to have a negligible uncertainty.

$$\sigma_{A,EOB} = \sqrt{{\sigma_g}^2 + {\sigma_{I_\gamma}}^2} \tag{3.6}$$

The cross section was calculated using Equation (3.7 below, where $A_{i,EOB}$ is the activity at the end of the bombardment, N is the areal density of the target (atoms · cm^{-2}), *SF* is the saturation factor for the radionuclide during irradiation, φ is the deuteron beam's current (deuteron · s^{-1}), and ε_{chem} is the overall chemical efficiency.

$$\sigma = \frac{A_{i,EOB}}{N \times \varphi \times SF \times \varepsilon_{chem}} \tag{3.7}$$

The saturation factor is the maximum value for the activity where the rate of production is affected by the radioactive decay of the same radionuclide. It plays an

important role in short lived isotopes and explains the reason of requiring long time irradiations to produce long lived radionuclides. Equation 3.8 has been used to calculate the saturation factor where λ is the decay constant of the radionuclide and t is the irradiation time.

$$SF = 1 - e^{-\lambda t} \qquad (3.8)$$

For cross section uncertainty, which governs an error propagation of the activity calculated in Equation (3.6, the fractional uncertainties for beam intensity (~5%), detector efficiencies (~5%), overall chemical efficiency (~4%), and target mass (~5%) are calculated using Equation (3.9.

$$uncertainty\ in\ \sigma = \sqrt{\left(\frac{\sigma_{A,EOB}}{A_{i,EOB}}\right)^2 + \left(\frac{\sigma_{\varphi}}{\varphi}\right)^2 + \left(\frac{\sigma_{\varepsilon_{chem}}}{\varepsilon_{chem}}\right)^2 + \left(\frac{\sigma_{\varepsilon_E}}{\varepsilon_E}\right)^2 + \left(\frac{\sigma_m}{m}\right)^2} \qquad (3.9)$$

Section 3.2 Computational

Subsection 3.2.1 PHITS Monte Carlo Calculation

PHITS (Particle and Heavy Ion Transport code System) [24] was used for the theoretical calculations of the isotope production cross sections. PHITS is a general-purpose Monte Carlo particle transport simulation code developed through collaboration between Japan Atomic Energy Agency (JAEA), Research Organization for Information

Science and Technology (RIST), High Energy Accelerator Research Organization (KEK), and several other institutes. It can deal with the transport of all particles across a wide range of energies using several nuclear reaction models and nuclear data libraries. PHITS version 3.2 was employed with a combination of the intra-nuclear cascade (INCL 4.6) and evaporation (GEM) models to determine the deuteron reaction cross sections of irradiations occurring in the 5-75 MeV/n incident projectile energy range [25]. The continuous slowing down approximation was applied to charged particle transport using the ATIMA computer code [26].

Starting with version 3.00, the KUROTAMA model [27, 28] became the default model for nucleus-nucleus reaction cross sections instead of the NASA model [29-31]. A total reaction cross section for deuteron-induced reactions, the MWO formula, was implemented in the simulation [32]. To determine any perceptible variances within production cross sections due to choice of physics models, all of these three models were utilized. I am the first author of a journal article published in *Applied Radiation and Isotope* that discusses the differences between the models and production cross sections [33]. Figure 3.14 shows the physics models used in the PHITS as a function of particle type and energy. Figure 3.15 illustrates the simple geometry used in the PHITS calculations—a rectangular solid representing a ^{232}Th foil target with a thickness of 0.0125 mm.

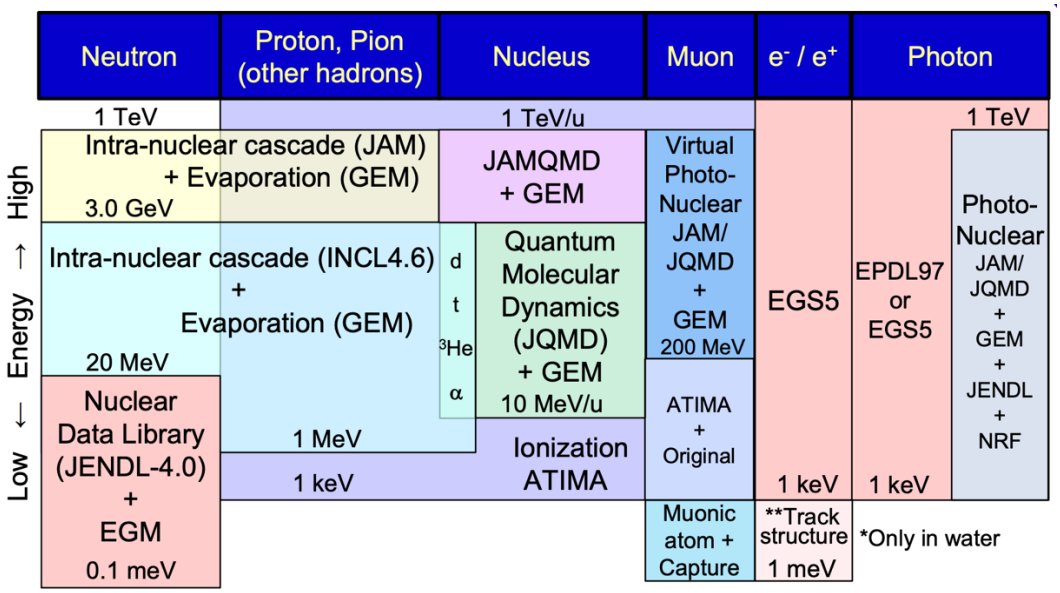


Figure 3.14. PHITS physics models and their switching energies [24].

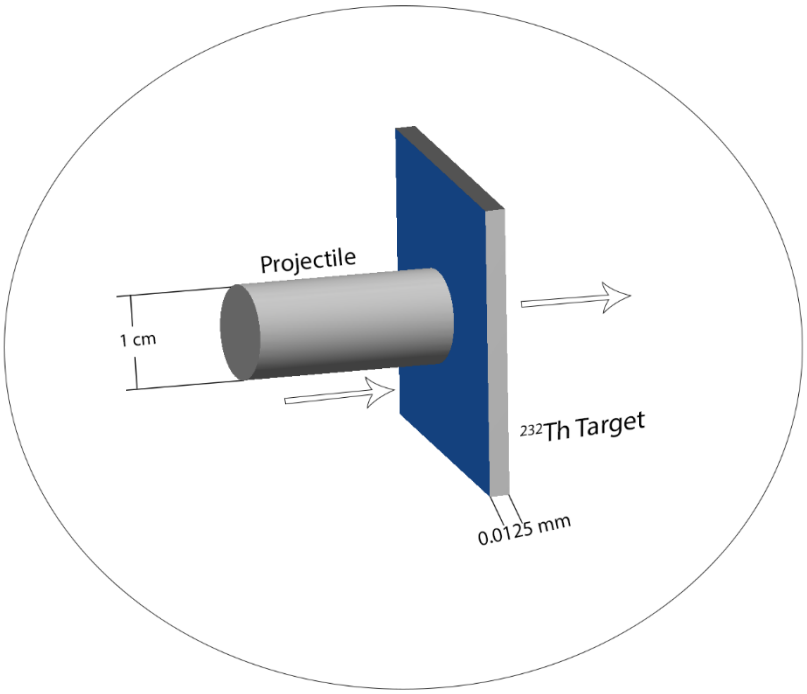


Figure 3.15. The geometry of the target and projectile used in the PHITS calculation.

The PHITS *T-Yield* tally was used to track the production of nuclides through deuteron beam interactions with the target. *T-Yield* can tally nuclei and particles produced by nuclear interaction, and fission. PHITS was used to determine the thickness of the degraders for the experiment and the incident deuteron energy at each thorium foil. PHITS *T-Cross* tally was used to determine the flux of deuterons after interactions with the target, as seen in Figure 3.6.

The calculation in this study used a series of simulations at different energies to create an excitation function for the target nuclei production of all isotopes produced. This was used to help determine the energy necessary for the actual experiment as well as determine the predicted cross sections. In summary, 43 simulations were performed by varying the incident energy from 5 to 75 MeV/n, and the same number of simulations were used for the three models mentioned before. A total of 129 simulations were performed to get the simulated cross section in this work.

To eliminate any human errors associated with processing a large data set, a Microsoft Macro code was developed to analyze the output files and calculate the cross sections. The code loops over files in a folder, taking all output files from each simulation, placing each simulation run into a new sheet, and arranging each by isotope. Then, the cross section for each isotope was calculated using Equation (3.10.

It is important to note that the PHITS-calculated cross sections are time independent and do not include contributions from the decay of any precursors, nor do they include the decay of the product nuclei itself.

In this work, some of the simulated cross section was called the cumulative cross section. Since the measured cross sections in this work are considered the effective cross sections, some of the measured cross section cannot be compared to the direct cross section; hence, the cumulative cross section or the precursors should be added to have a practical comparison (as shown later in Figure 4.1). The cumulative cross section was calculated by summing the isotopes or isobars fed or decayed to the produced radionuclide. An example of such calculation is displayed in section 4.1.

Once the number of targeted product nuclei was tallied from the simulation, the simulated cross section was calculated using Equation (3.10 .

$$\sigma = \frac{-ln\left(1 - \frac{\phi_{int}}{\phi_o}\right)}{nx} \qquad (3.10)$$

Equation (3.10 was derived from Equation (3.11, where σ is the simulated cross section for the interaction with a specific target, ϕ_{int} is the number of product nuclei, ϕ_o is the number of projectile particles incident on the target, *n* is the number of target nuclei per cm^3, and *x* is the thickness of the target in cm.

$$\phi_{int} = \phi_o(1 - e^{-n\sigma x}) \qquad (3.11)$$

The fractional uncertainty of the PHITS cross section calculation was calculated using Equation (3.12, where N is the total number of product nuclei generated in each simulation.

$$\sigma_f = \frac{\sqrt{N}}{N} \qquad (3.12)$$

Chapter 4 Results and Discussion

Measured and simulated cross sections in this work are presented in Table 4.1-Table 4.3 and illustrated in Figure 4.1-Figure 4.13. As mentioned previously, the measured cross sections were compared with PHITS simulated cross sections. The results of all radionuclides produced in PHITS are presented in Appendix C. Effective cross sections for ^{232}Th(d,xn)^{228,229,230,232,233}Pa reactions at 31, 35.2, 41.4, and 49.6 MeV are presented in Table 4.1. Table 4.2 shows the PHITS simulated cross sections using the default model (KUROTAMA) at the same energies conducted in the experiment. The ratios between the simulated cross sections and experimentally measured cross sections are given in Table 4.3. The excitation functions for each radionuclide are indicated with reported cross sections in the literature if available [1, 10, 13-18]. The measured cross sections from deuteron bombardment were compared to cross sections produced using proton bombardment on thorium targets.

PHITS simulated cross sections were produced using three different models for the deuteron simulated cross sections, as mentioned in Section Subsection 3.2.1. For the proton simulated cross sections, only the default model (KUROTAMA) was implemented. The reason for using only the default model for the simulated proton cross sections was discussed in [33]; there were no noticeable differences in the cross sections between the two models. The PHITS simulated cross sections were the direct cross sections, which do not include any precursors or decay of the radionuclide itself. In some cases, the cumulative cross section was used to have a valid comparison with the effective cross section.

Table 4.1. Effective measured production cross section (in mb) of selected radionuclides with 31-50 MeV deuteron energies.

Radionuclide	**Half-life**	**31 MeV**	**35.2 MeV**	**41.4 MeV**	**49.6 MeV**
^{228}Pa	22 h	0	2.3 ± 0.2	34.9 ± 3.4	31.6 ± 3.5
^{229}Pa	1.55 d	89.3 ± 9.6	121.9 ± 12.7	43.7 ± 5.0	38.2 ± 5.1
^{230}Pa	17.4 d	161.4 ± 16.8	71.9 ± 7.6	58.0 ± 6.1	47.3 ± 5.4
^{232}Pa	1.32 d	40.6 ± 3.3	31.3 ± 2.6	21.9 ± 1.8	20.4 ± 1.7
^{233}Pa	26.98 d	75.0 ± 6.4	56.1 ± 8.4	33.1 ± 2.9	30.5 ± 3.0

Table 4.2. PHITS simulated cross section (in mb) of selected radionuclides with 31-50 MeV deuteron energies.

Radionuclide	**Half-life**	**31 MeV**	**35.2 MeV**	**41.4 MeV**	**49.6 MeV**
^{228}Pa	22 h	0	2.3 ± 0.05	23.2 ± 0.02	16.0 ± 0.02
^{229}Pa	1.55 d	68.4 ± 0.01	86.9 ± 0.01	51.8 ± 0.01	38.1 ± 0.01
^{230}Pa	17.4 d	127.6 ± 0.01	93.9 ± 0.01	80.4 ± 0.01	68.1 ± 0.01
^{232}Pa	1.32 d	117.8 ± 0.01	101.9 ± 0.01	83.8 ± 0.01	65.7 ± 0.01
^{233}Pa*	26.98 d	105.2 ± 0.02	92.5 ± 0.02	77.8 ± 0.03	62.6 ± 0.03

*Presented as cumulative cross sections includes the contribution of ^{232}Th(d,p)^{233}Th. Look in text for explanation.

Table 4.3. Ratio of PHITS simulated cross section to experimentally measured cross section.

Radionuclide	Half-life	31 MeV	35.2 MeV	41.4 MeV	49.6 MeV
^{228}Pa	22 h	0.00	1.00	0.66	0.51
^{229}Pa	1.55 d	0.77	0.71	1.19	1.00
^{230}Pa	17.4 d	0.79	1.31	1.39	1.44
^{232}Pa	1.32 d	2.90	3.26	3.83	3.22
^{233}Pa	26.98 d	1.40	1.65	2.35	2.05

Section 4.1 ^{232}Th(d,x)^{233}Pa reactions

The measured cross sections for ^{233}Pa are presented in Figure 4.1 and Figure 4.2. As mentioned earlier, the PHITS simulated cross sections were direct and do not include any contribution from the precursors. In Figure 4.1 the cross sections were cumulative and included the contribution of ^{232}Th(d,p)^{233}Th. ^{233}Th ($t_{1/2}$ = 21.83 m) decays via beta emission (β^-, 100%) to ^{233}Pa. Since the target arrived a day after irradiation, it is a safe assumption that ^{233}Th decayed into ^{233}Pa. As seen in Figure 4.1, direct simulated cross sections were also included to show the importance of having the cumulative cross sections for comparison purposes. The peak of the excitation function of ^{232}Th(d,x)^{233}Pa is 75.0 ± 6.4 mb, and it occurs at E_d = 31 MeV. The simulated cross sections were in good agreement with the measured cross section at 31 MeV. While above 31 MeV, the measurements were agreed by a factor of 1-2 between all three models of PHITS.

Figure 4.2 displays the effective cross sections compared with cross sections from the literature from the same reaction [10, 13]. The measurements agree with the data reported from Duchemin et al. [10] and Rao et al. [13]. It is important to note Rao et al. conducted the experiment in 1986 and used different γ-rays intensity values than reported in National Nuclear Data Center [34]. Also, the target thicknesses used in Rao et al. [13] were 10-100 mg/cm^2, this might explain the discripinses in the cross sections.

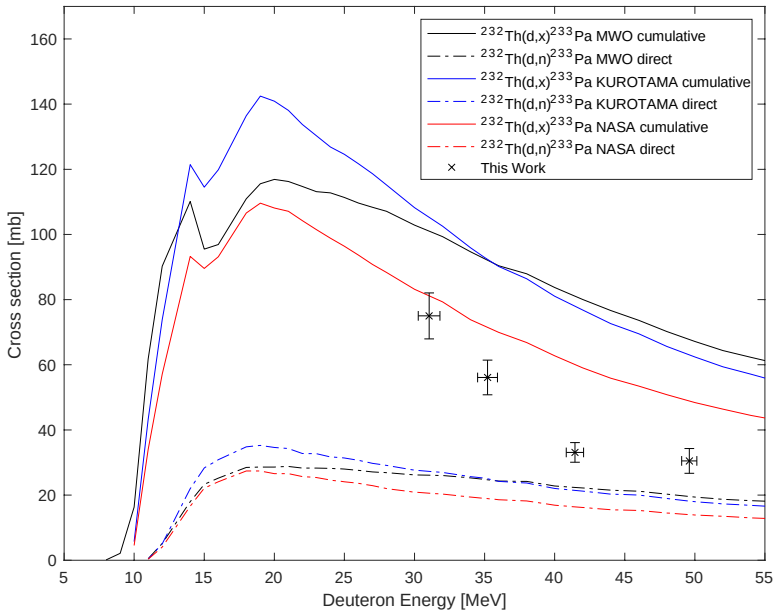


Figure 4.1. Excitation function of ^{232}Th(d,x)^{233}Pa reaction. PHITS model calculation is also shown. PHITS cross sections include the direct and cumulative cross sections.

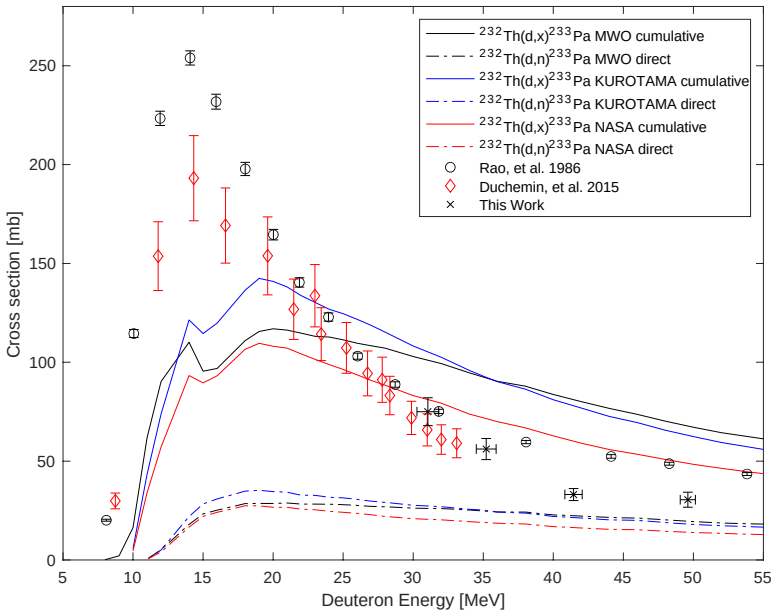


Figure 4.2. Effective cross sections and cumulative cross sections from PHITS for ^{232}Th(d,x)^{233}Pa reaction. Literature cross section from the same reaction are shown [10, 13].

Section 4.2 ^{232}Th(d,2n)^{232}Pa reactions

Effective measured and simulated cross sections for Th(d,2n)^{232}Pa reaction are shown in Figure 4.3 - Figure 4.5. ^{232}Pa ($t_{1/2}$ = 1.32 d) decays via beta emission (β^-, 100%) to ^{232}Th. As noted previously, ^{232}Pa was used as an internal tracer for the chemical separation. Figure 4.3 demonstrates the experimentally measured cross section compared with the simulated cross sections. The peak of the excitation function of ^{232}Th(d,2n)^{232}Pa is 40.6 ± 3.3 mb, and it occurs at E_d = 31 MeV. The data were within a factor of 2 to PHITS NASA model and a factor of 3 for both KUROTAMA and MWO models.

Figure 4.4 illustrates the experimental cross section compared with reported cross sections from the literature [10, 13]. Cross sections from this work agree with reported data from Duchemin et al. [10] and Rao et al. [13]. Above 15 MeV deuetron energies, measured cross sections reported were differ than PHITS simulated cross section by a factor of 2-4.

Figure 4.5 displays the cross sections using proton and deuteron projectiles of ^{232}Th target compared with data values from the literature [1, 10, 13-15, 17, 18]. As stated before, only the default model was implemented for the proton induced reaction. The general trends seen in the deuteron-induced experimental cross sections indicate larger cross sections than the proton-induced experimental cross sections. In the energy range of 10 – 15 MeV/n, the deuteron effective cross sections were larger by a factor 12 when compared to proton cross sections.

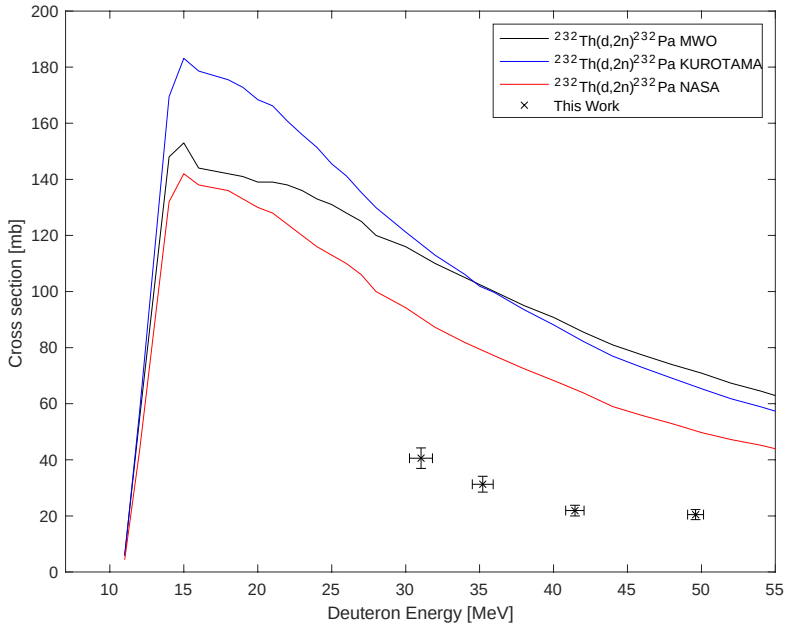


Figure 4.3 Excitation function of ^{232}Th(d,2n)^{232}Pa reaction. PHITS model calculation is also shown.

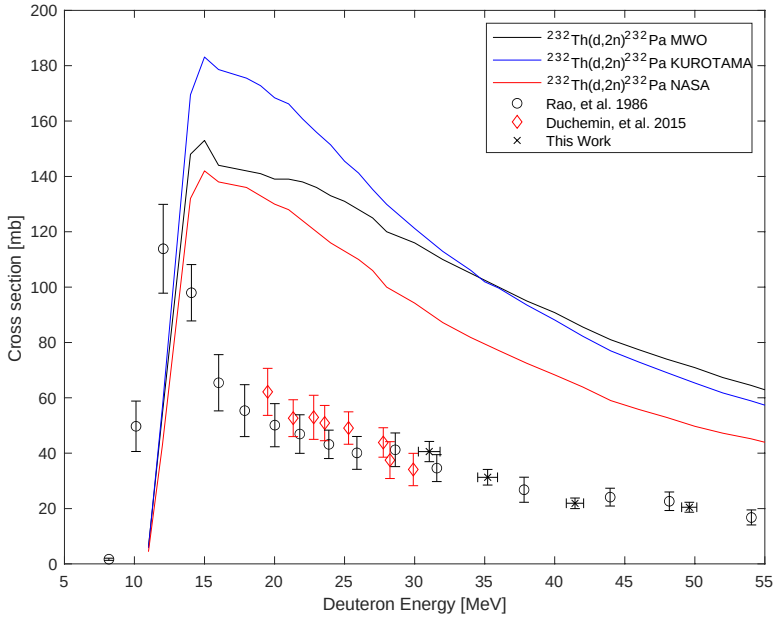


Figure 4.4. Effective cross sections and cumulative cross sections from PHITS for ^{232}Th(d,2n)^{232}Pa reaction. Literature cross section from the same reaction are shown [10, 13].

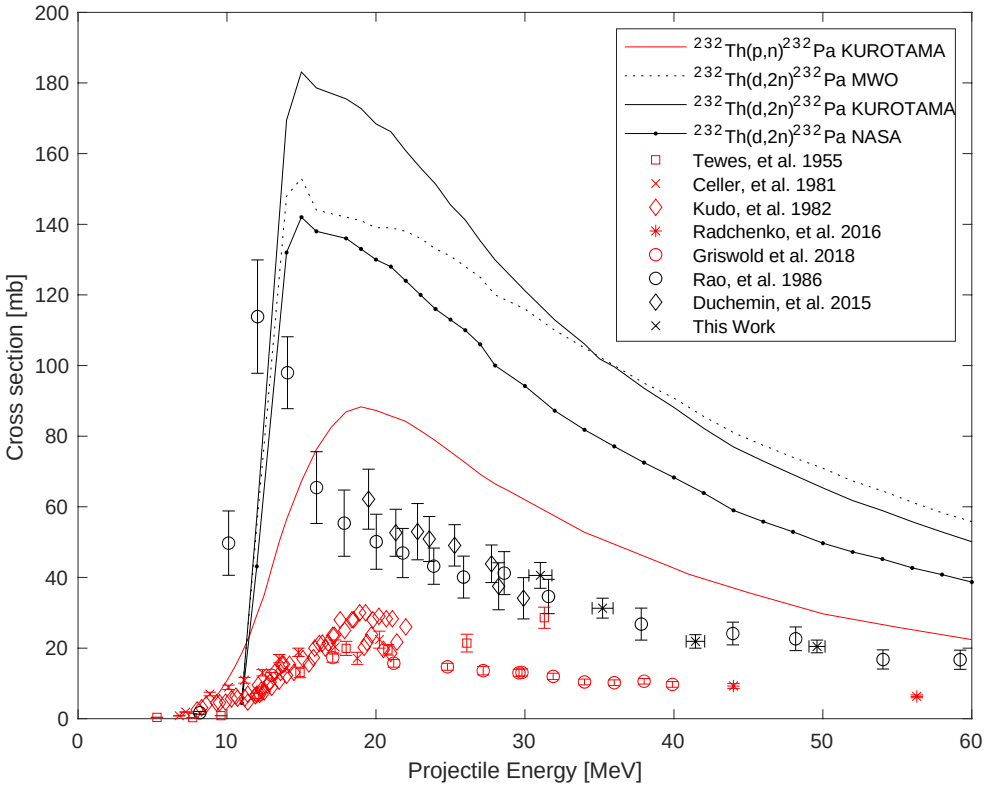


Figure 4.5. Experimental cross sections and simulated cross section for ^{232}Th(p,n)^{232}Pa (red color) and ^{232}Th(d,2n)^{232}Pa (black color) reactions. Literature cross sections from the same reactions are shown [1, 10, 13-15, 17, 18].

Section 4.3 ^{232}Th(d,4n)^{230}Pa reactions

Figure 4.6 - Figure 4.8 demonstrate the experimental and simulated cross sections for ^{230}Pa production. ^{230}Pa ($t_{1/2}$ = 17.4 d) decays via electron capture (EC, 92.2%) to ^{230}Th and via beta emission (β^-, 7.8%) to ^{230}U ($t_{1/2}$ = 20.8 d). ^{230}U is another candidate for targeted alpha therapy for cancer. The excitation function of ^{232}Th(d,4n)^{230}Pa reaction is shown in Figure 4.6. As presented, the peak of ^{230}Pa at 161.4 ± 16.8 occurs at E_d = 31 MeV. ^{230}Pa has been evaluated by direct gamma ray spectroscopy and ion exchange chromatography. As seen in Figure 4.6, the measured cross sections using the direct assessment were higher than the chemically separated cross section. Interference by γ-rays of other fission products was the reason for the increase in the activity and cross section. This demonstrates the importance of the chemical separation techniques to quantify and calculate the cross section. The data point at 31 MeV is within 75% of both KUROTAMA and MWO models and by a factor of 1 of NASA model.

Figure 4.7 shows the experimental and simulated cross sections for the ^{232}Th(d,4n)^{230}Pa reaction compared with literature values [10, 13]. The cross sections measured from this work are in excellent agree with reported values in the literature. This also illustrates the importance of utilizing the chemical separation in this work.

The effective cross section from both ^{232}Th(p,3n)^{230}Pa and ^{232}Th(d,4n)^{230}Pa reactions compared with reported cross sections in the literature are shown in Figure 4.8 [1, 10, 13-16]. The measured cross sections by deuteron and proton induced reactions are fairly similar at most of the energies. The peak cross section for the proton projectile is larger than the deuteron projectile.

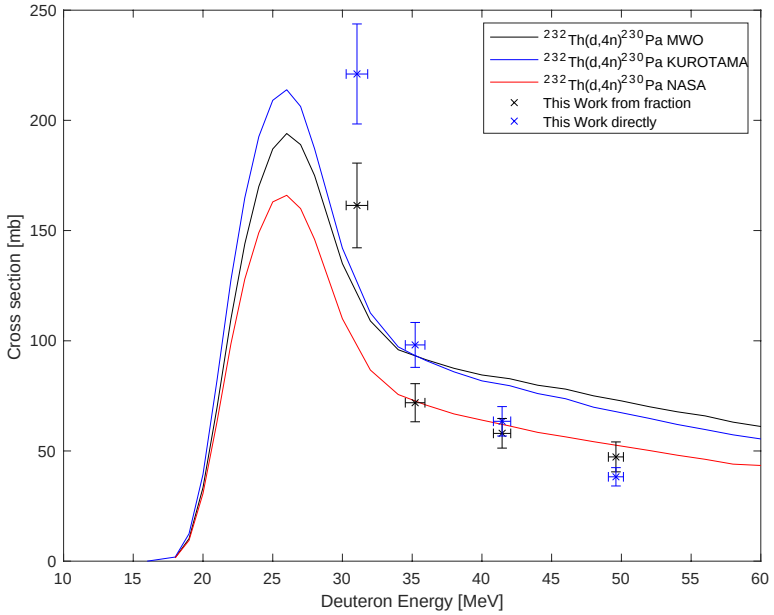


Figure 4.6. Excitation function of ^{232}Th(d,4n)^{230}Pa reaction. PHITS model calculation is also shown.

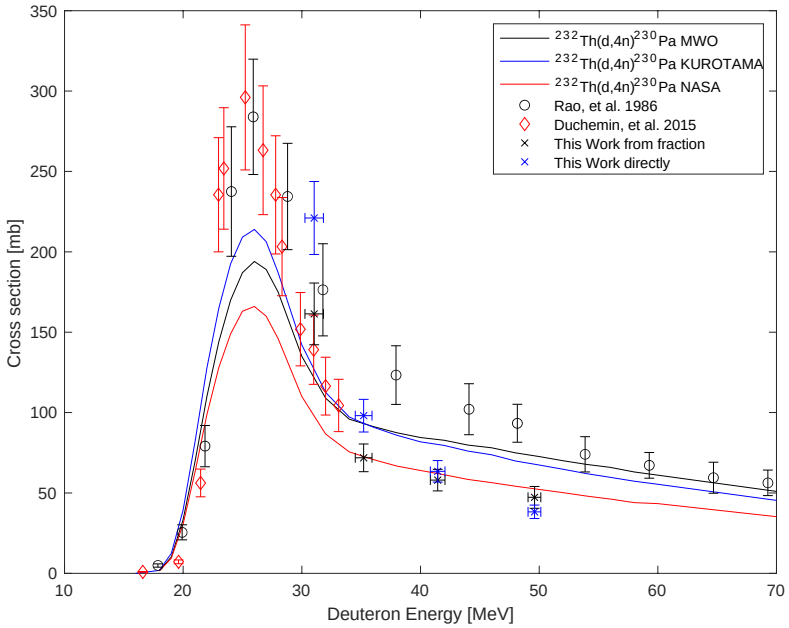


Figure 4.7. Effective cross sections and cumulative cross sections from PHITS for ^{232}Th(d,4n)^{230}Pa reaction. Literature cross section from the same reaction are shown [10, 13].

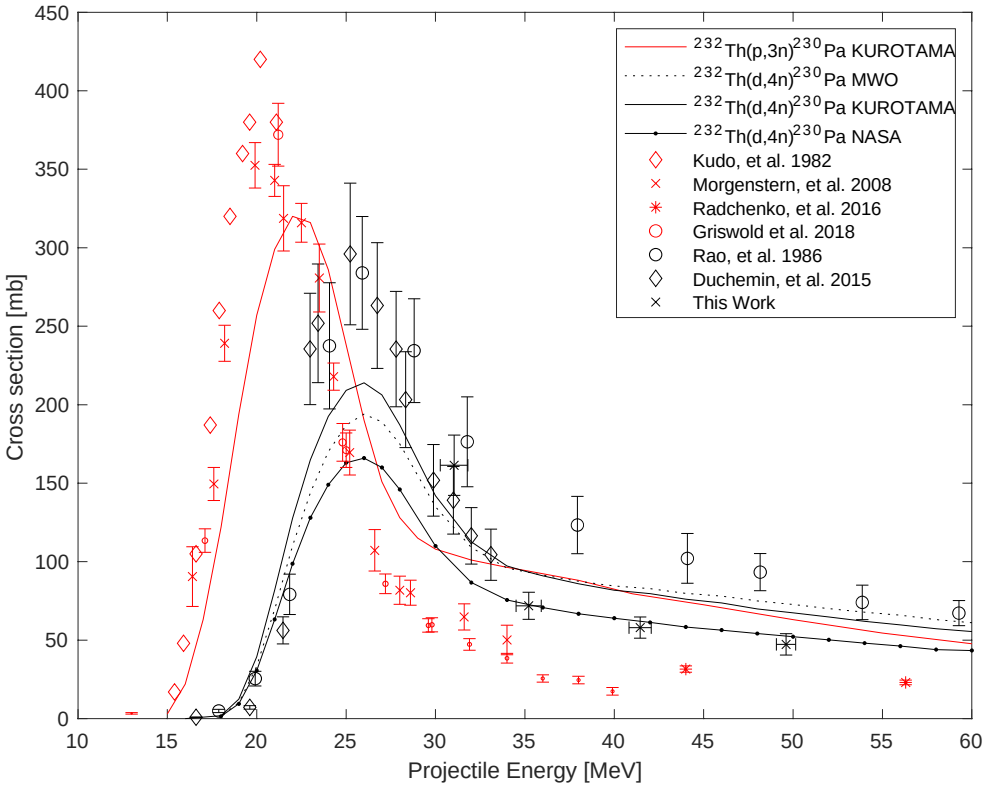


Figure 4.8. Experimental cross sections and simulated cross section for ^{232}Th(p,3n)^{230}Pa (red color) and ^{232}Th(d,4n)^{230}Pa (black color) reactions. Literature cross sections from the same reactions are shown [1, 10, 13-16].

Section 4.4 ^{232}Th(d,5n)^{229}Pa reactions

The excitation functions for ^{232}Th(p,4n)^{229}Pa and ^{232}Th(d,5n)^{229}Pa are graphically illustrated in Figure 4.9 and Figure 4.10. ^{229}Pa ($t_{1/2}$ = 1.55 d) decays via electron capture (EC, 99.5%) to ^{229}Th ($t_{1/2}$ = 7932 y) and via alpha emission (α, 0.5%) to ^{225}Ac ($t_{1/2}$ = 9.92 d). In this work, the production of ^{229}Pa from bombardment of ^{232}Th by deuterons below 50 MeV is the main interest because of its decay channels. Since the ^{233}U is not a viable resource for ^{229}Th and there is increased demand for ^{225}Ac in various clinical trials, looking for another possible pathway to produce ^{229}Th is the main aim of this work. The measured cross sections for ^{232}Th(d,5n)^{229}Pa reaction are reported for the first time.

Figure 4.9 shows the experimental and simulated cross sections for deuteron induced reactions. The peak of the excitation function at 121.9 ± 12.7 mb occurs at E_d = 35.2 MeV. Above 40 MeV, the data are slightly higher than the NASA model and agree with both KUROTAMA and MWO models. Below 40 MeV, the measured cross sections differ than all other models by a factor of 1-2.

Figure 4.10 demonstrates the effective measured cross sections for both ^{232}Th(p,4n)^{229}Pa and ^{232}Th(d,5n)^{229}Pa reactions and compares them with reported cross sections in the literature [1]. Griswold et al. was the only available measurement for ^{229}Pa [1]. As displayed, the cross sections are generally within the same magnitude for both projectiles.

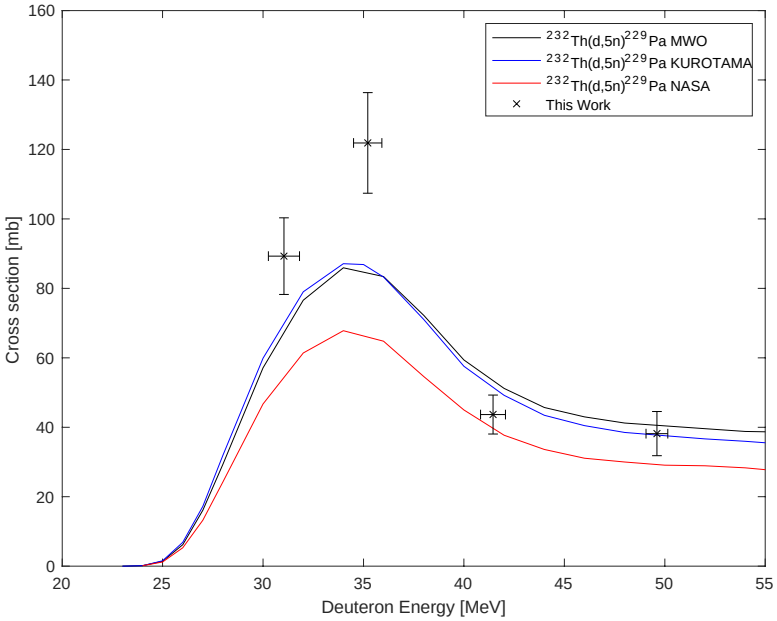


Figure 4.9. Excitation function of ^{232}Th(d,5n)^{229}Pa reaction. PHITS model calculation is also shown.

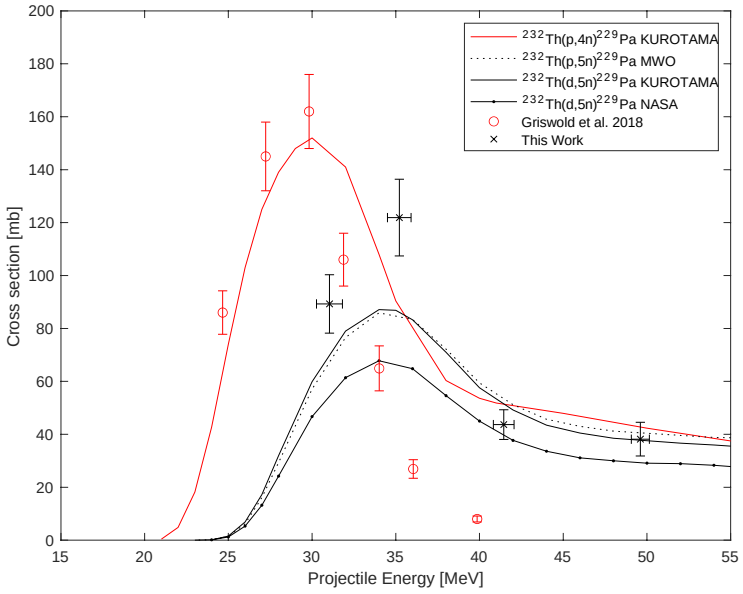


Figure 4.10. Experimental cross sections and simulated cross section for ^{232}Th(p,4n)^{229}Pa (red color) and ^{232}Th(d,5n)^{229}Pa (black color) reactions. Literature cross sections from the same reactions are shown [10, 13].

Section 4.5 ^{232}Th(d,6n)^{228}Pa reactions

The measured and simulated cross sections for ^{232}Th(d,6n)^{228}Pa and ^{232}Th(p,5n)^{228}Pa reactions are presented in Figure 4.11 – Figure 4.13. ^{228}Pa ($t_{1/2}$ = 22 h) decays via electron capture (EC, 98.15%) to ^{228}Th ($t_{1/2}$ = 1.91 y) and alpha emission (α, 1.85%) to ^{224}Ac ($t_{1/2}$ = 2.78 h). Figure 4.11 illustrates excitation function for ^{232}Th(d,6n)^{228}Pa reaction compared with PHITS simulated cross sections. Since the last foil in this work was near threshold for ^{232}Th(d,6n)^{228}Pa reaction, only three data values have been detected. As shown, the cross sections show a maximum of 34.9 ± 3.4 mb at 41.4 MeV. Above 35 MeV, the measured cross sections are within a factor of 2-3 to all predictions from PHITS.

Data from the same reaction were compared to the experimental values from this work is shown in Figure 4.12. The data from Rao et al. [13] reported a slightly higher cross section values than experimental cross sections. As mentioned before, Rao et al. [13] have been using different γ-rays intensity than are available nowadays and target thicknesses of 10-100 mg/cm^2.

Both proton and deuteron-induced reactions cross sections were compared with reported data as presented in Figure 4.13 [1, 13, 14]. For ^{232}Th(p,5n)^{228}Pa reaction, only two measurements were conducted by Griswold et al. [1] and Radchenko et al. [14]. Cross sections from both projectiles exhibit the same peak magnitude of cross sections.

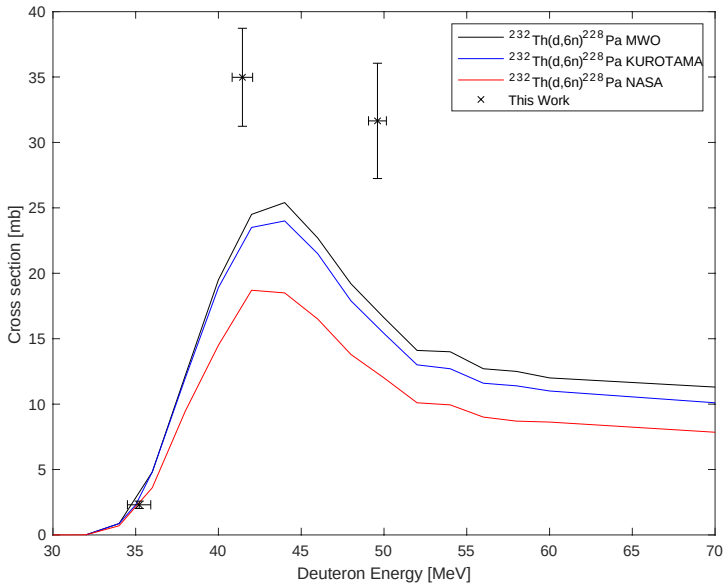


Figure 4.11. Excitation function of ^{232}Th(d,6n)^{228}Pa reaction. PHITS model calculation is also shown.

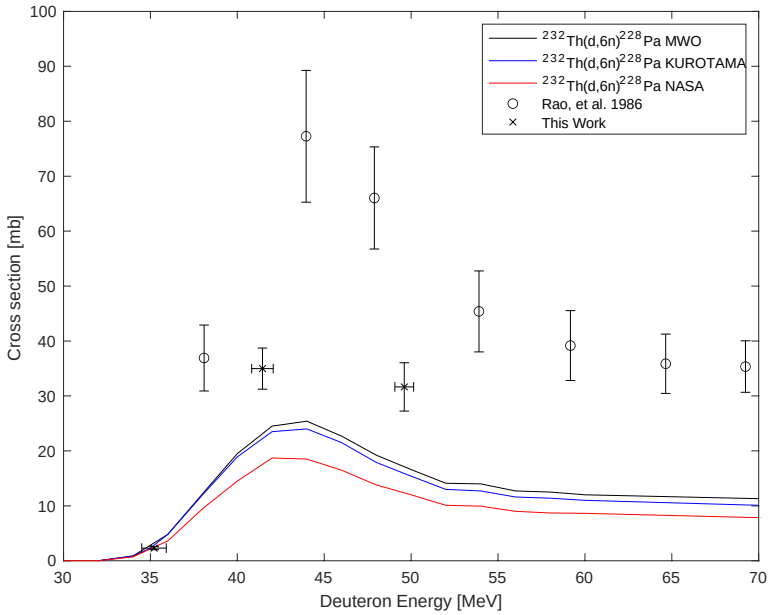


Figure 4.12. Effective cross sections and cumulative cross sections from PHITS for ^{232}Th(d,2n)^{232}Pa reaction. Literature cross section from the same reaction are shown [10, 13].

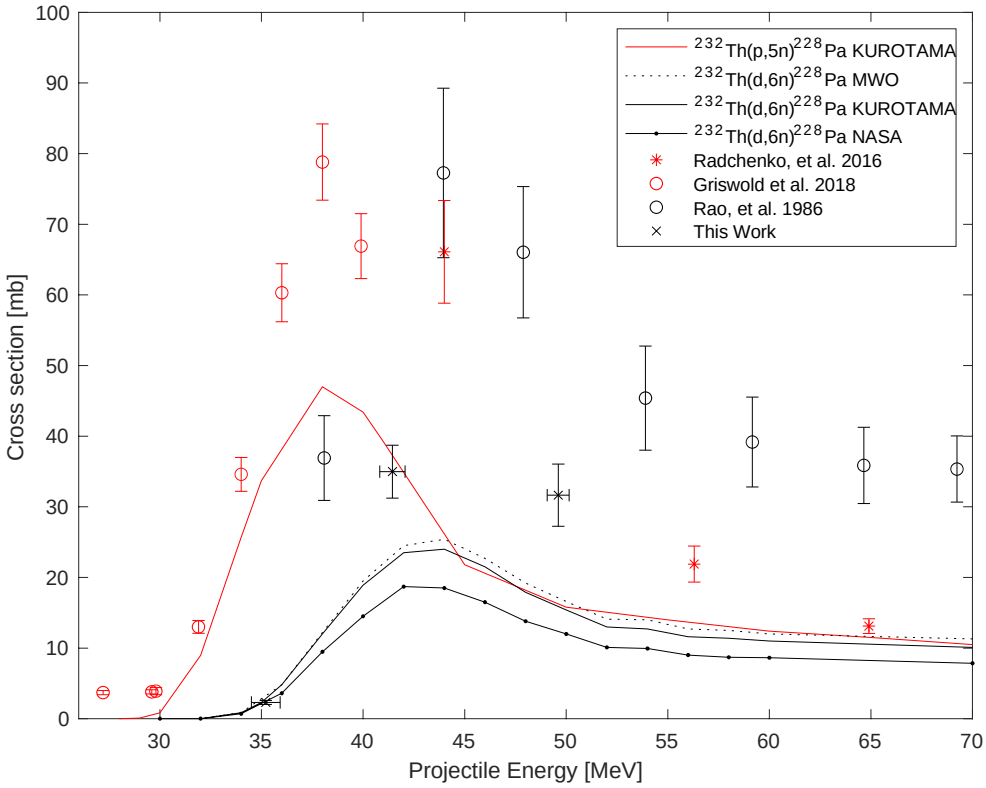


Figure 4.13. Experimental cross sections and simulated cross section for ^{232}Th(p,5n)^{228}Pa (red color) and ^{232}Th(d,6n)^{228}Pa (black color) reactions. Literature cross sections from the same reactions are shown [1, 13, 14].

Section 4.6 Discussion

Measurements from this work agree with reported cross sections in the literature except for ^{232}Th(d,6n)^{228}Pa reaction. Cross sections from ^{232}Th(d,6n)^{228}Pa reaction were lower than published values by Rao et al. [13], as shown in Figure 4.12. Target thicknesses and different γ-rays intensity could explain the discrepancies between the cross sections. In general, proton and deuteron-induced reactions exhibit the same order of magnitude for the experimentally measured cross sections. In ^{229}Pa production pathways, proton beam showed slightly higher cross sections than deuteron beam but using a thick target (usually in production), deuteron beam may result in higher integral cross sections over broad energies as presented in Figure 4.10. PHITS simulated cross section showed good agreement with the trend of the measured cross sections. Across the data spectrum, there was no systematic underprediction or overprediction for the simulated cross sections, and the comparison depends on the isotope of interest. However, a trend was found, with removing more neutrons (d,xn); the simulated cross sections were generally underestimated.

Chapter 5 Conclusion and Future Work

Experimentally measured cross sections are reported for all protactinium isotopes produced from deuteron-induced reactions on thorium targets. The ^{232}Th(d,5n)^{229}Pa reaction cross sections are reported for the first time. The data from this work on other Pa isotopes agree with published results from previous measurements. The measured cross sections from proton and deuteron projectiles were compared for all protoactinium isotopes when available—there are no significant discrepancies in magnitude between projectiles' excitation functions. Cross sections for ^{232}Th(d,5n)^{229}Pa reaction are generally within the same magnitude as ^{232}Th(p,4n)^{229}Pa cross sections. Due to the long half-life of ^{229}Th, long irradiation is needed to achieve a sufficient quantity of ^{229}Th (mCi levels). PHITS simulated cross section had been evaluated with the effective cross sections. The KUROTAMA model showed slightly larger cross sections than the MWO model. The NASA model demonstrated lower cross sections than both KUROTAMA and MWO models. Generally, the results exhibited good agreement with all models, especially the default model (KUROTAMA).

Future work includes an investigation of the effects of the secondary particles from the stacked-foil configuration by performing another irradiation for the same system but using the lowest energy used in this work; the results should then be compared. In addition, measurements should be made at more energies to fill the gap between the data points in this work in order to have a complete excitation function for all reactions.

The results from PHITS should also be compared to different transport codes like MCNP or TALYS. This will help to validate the physics models implemented in those

codes. Finally, a code should be developed that helps implement the decay of isotopes and precursors in order to calculate the cumulative cross section calculations for future PHITS simulations. It will help to acquire an accurate comparison between experimental effective cross sections and simulated cross sections, as shown in this work.

List of References

1. Griswold, J.R., et al., *Production of Th229 for medical applications: Excitation functions of low-energy protons on Th232 targets.* Physical Review C, 2018. **98**(4).
2. Kennel, S., et al., *Radiotoxicity of Bismuth-213 Bound to Membranes of Monolayer and Spheroid Cultures of Tumor Cells.* Radiation research, 1999. **151**: p. 244-56.
3. McDevitt, M., et al., *Tumor therapy with targeted atomic nanogenerators.* Science, 2001. **294**(5546): p. 1537-40.
4. Ballangrud, A.M., et al., *Alpha-particle emitting atomic generator (Actinium-225)-labeled trastuzumab (herceptin) targeting of breast cancer spheroids: efficacy versus HER2/neu expression.* Clin Cancer Res, 2004. **10**(13): p. 4489-97.
5. Morgenstern, A., et al., *An Overview of Targeted Alpha Therapy with (225)Actinium and (213)Bismuth.* Curr Radiopharm, 2018. **11**(3): p. 200-208.
6. IAEA, *Alpha Emitting Radionuclides and Radiopharmaceuticals for Therapy,*, in *Technical Meeting Report*. 2013: Vienna, Austria.
7. Weidner, J.W., et al., *225Ac and 223Ra production via 800MeV proton irradiation of natural thorium targets.* Applied Radiation and Isotopes, 2012. **70**(11): p. 2590-2595.
8. Weidner, J.W., et al., *Proton-induced cross sections relevant to production of 225Ac and 223Ra in natural thorium targets below 200MeV.* Applied Radiation and Isotopes, 2012. **70**(11): p. 2602-2607.
9. Ermolaev, S.V., et al., *Production of actinium, thorium and radium isotopes from natural thorium irradiated with protons up to 141 MeV,* in *Radiochimica Acta International journal for chemical aspects of nuclear science and technology*. 2012. p. 223.
10. Duchemin, C., et al., *Production of medical isotopes from a thorium target irradiated by light charged particles up to 70 MeV.* Phys Med Biol, 2015. **60**(3): p. 931-46.
11. Griswold, J.R., et al., *Large scale accelerator production of (225)Ac: Effective cross sections for 78-192MeV protons incident on (232)Th targets.* Appl Radiat Isot, 2016. **118**: p. 366-374.
12. Robertson, A.K.H., et al., *Design of a Thorium Metal Target for 225Ac Production at TRIUMF.* Instruments, 2019. **3**(1): p. 18.
13. Rao, J.R., J. Ernst, and H. Machner, *Comparative study of d- and 6Li-induced reactions on 232Th in terms of breakup and preequilibrium processes.* Nuclear Physics, Section A, 1986. **448**(2): p. 365-380.
14. Radchenko, V., et al., *Formation cross-sections and chromatographic separation of protactinium isotopes formed in proton-irradiated thorium metal.* Radiochimica Acta, 2016. **104**(5): p. 291-304.
15. Kudo, H., et al., *Fission fragment yields in the fission of Th 232 by protons of energies 8 to 22 MeV.* Physical Review C, 1982. **25**(6): p. 3011-3023.
16. Morgenstern, A., et al., *Cross-sections of the reaction 232Th(p,3n) 230Pa for production of 230U for targeted alpha therapy.* Applied Radiation and Isotopes, 2008. **66**(10): p. 1275-1280.

17. Tewes, H.A., *Excitation Functions for Some Proton-Induced Reactions of Thorium.* Physical Review, 1955. **98**(1): p. 25-27.
18. Celler, A., et al., *Cross Sections of232Th (p,xn+yp) Reactions at Ep= 6.8 to 20.2 MeV.* Physica Scripta, 1981. **24**(6): p. 930-934.
19. Abusaleem, K., *Nuclear Data Sheets for A=228.* Nuclear Data Sheets, 2014. **116**: p. 163-262.
20. Browne, E., *Nuclear Data Sheets for A = 232.* Nuclear Data Sheets, 2006. **107**(10): p. 2579-2648.
21. Browne, E. and J.K. Tuli, *Nuclear Data Sheets for A = 230.* Nuclear Data Sheets, 2012. **113**(8): p. 2113-2185.
22. Browne, E. and J.K. Tuli, *Nuclear Data Sheets for A = 229.* Nuclear Data Sheets, 2008. **109**(11): p. 2657-2724.
23. Singh, B., J.K. Tuli, and E. Browne, *Nuclear Data Sheets for A=233.* Nuclear Data Sheets, 2020. **170**: p. 499-705.
24. Sato, T., et al., *Features of Particle and Heavy Ion Transport code System (PHITS) version 3.02.* Journal of Nuclear Science and Technology, 2018. **55**(6): p. 684-690.
25. Boudard, A., et al., *New potentialities of the Li\`ege intranuclear cascade model for reactions induced by nucleons and light charged particles.* Physical Review C, 2013. **87**(1): p. 014606.
26. Scheidenberger, C. and H. Geissel, *Penetration of relativistic heavy ions through matter.* Nuclear Instruments and Methods in Physics Research Section B: Beam Interactions with Materials and Atoms, 1998. **135**(1): p. 25-34.
27. Iida, K., A. Kohama, and K. Oyamatsu, *Formula for Proton–Nucleus Reaction Cross Section at Intermediate Energies and Its Application.* Journal of the Physical Society of Japan, 2007. **76**(4): p. 044201.
28. Sihver, L., et al., *Current status of the "Hybrid Kurotama model" for total reaction cross sections.* Nuclear Instruments and Methods in Physics Research Section B: Beam Interactions with Materials and Atoms, 2014. **334**: p. 34-39.
29. Tripathi, R.K., F.A. Cucinotta, and J.W. Wilson, *Accurate universal parameterization of absorption cross sections.* Nuclear Instruments and Methods in Physics Research Section B: Beam Interactions with Materials and Atoms, 1996. **117**(4): p. 347-349.
30. Tripathi, R.K., J.W. Wilson, and F.A. Cucinotta, *Accurate universal parameterization of absorption cross sections II — neutron absorption cross sections.* Nuclear Instruments and Methods in Physics Research Section B: Beam Interactions with Materials and Atoms, 1997. **129**(1): p. 11-15.
31. Tripathi, R.K., F.A. Cucinotta, and J.W. Wilson, *Accurate universal parameterization of absorption cross sections III – light systems.* Nuclear Instruments and Methods in Physics Research Section B: Beam Interactions with Materials and Atoms, 1999. **155**(4): p. 349-356.
32. Minomo, K., K. Washiyama, and K. Ogata, *Deuteron–nucleus total reaction cross sections up to 1 GeV.* Journal of Nuclear Science and Technology, 2017. **54**(1): p. 127-130.

33. Burahmah, N., et al., *Transport model predictions of 225Ac production cross sections via energetic p, d and α irradiation of 232Th targets.* Applied Radiation and Isotopes, 2021. **172**: p. 109676.
34. Firestone, R.B., et al., *The 8th edition of the Table of Isotopes*. 1997, Hungary: Springer.

Appendices

Appendix A: Example of Efficiency Curve

An example of the calibration curve used in this work is shown in Figure 5.1. The calibration was calculated by measuring a well-known source and the calibration curve was generated using dual efficiency function via a 4^{th} order polynomial function. It is important to note that the calibration is total efficiency which includes the geometric and intrinsic efficiency. Efficiency was calculated using Equation A.1, where E is the incident photon energy in keV, and constants are shown in Table 5.1.

$$efficiency = exp\left[a + b \times ln(E) + c \times ln(E)^2 + d \times ln(E)^3 \right] \qquad (5.1)$$

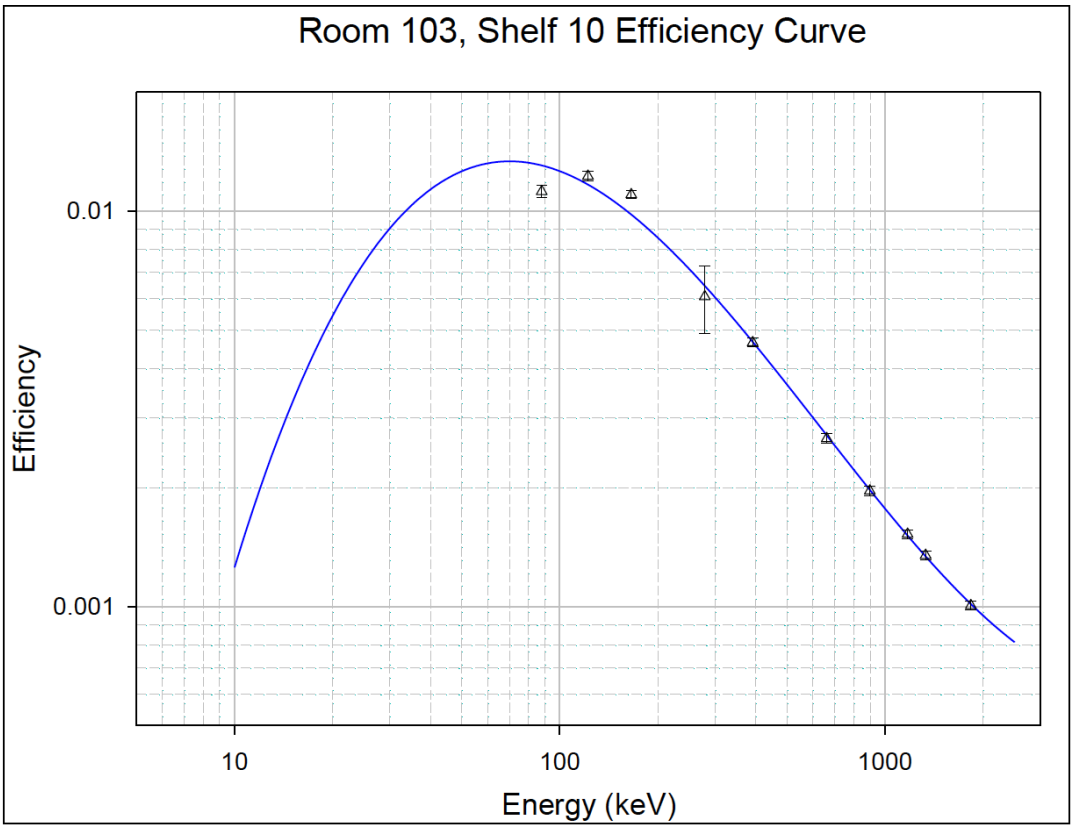


Figure 5.1 A typical efficiency curve used in this work.

Table 5.1. Constants used in the efficiency.

a	b	c	d
-18.63	8.059	-1.415	0.073

Appendix B: Sample of PHITS Input File

```
[ T i t l e ]
Deteron Beam on a 232Th target

[ P a r a m e t e r s ]

 icntl    =          0       # (D=0) 3:ECH 5:NOR 6:SRC 7,8:GSH 11:DSH 12:DUMP
 maxcas   =    10000000     # (D=10) number of particles per one batch
 maxbch   =         50     # (D=10) number of batches
 emin(1)  = 1.000000000E-01 # (D=1.0) cut-off energy of proton (MeV)
 emin(2)  = 1.000000000E-02 # (D=1.0) cut-off energy of neutron (MeV)
 dmax(2)  =  10.0000000     # (D=emin(2)) data max. energy of neutron (MeV)
 emin(12) = 1.000000000     # (D=1.d9) cut-off energy of electron (MeV)
 emin(13) = 1.000000000     # (D=1.d9) cut-off energy of positron (MeV)
 emin(14) = 1.000000000     # (D=1.d9) cut-off energy of photon (MeV)
 dmax(12) =  1000.00000     # (D=emin(12)) data max. energy of electron (MeV)
 dmax(13) =  1000.00000     # (D=emin(13)) data max. energy of positron (MeV)
 dmax(14) =  1000.00000     # (D=emin(14)) data max. energy of photon (MeV)
 emin(15) = 1.000000000     # (D=1.0) cut-off energy of deuteron (MeV/u)
 emin(16) = 1.000000000     # (D=1.0) cut-off energy of triton (MeV/u)
 emin(17) = 1.000000000     # (D=1.0) cut-off energy of 3He (MeV/u)
 emin(18) = 1.000000000     # (D=1.0) cut-off energy of Alpha (MeV/u)
 emin(19) = 1.000000000     # (D=1.0) cut-off energy of Nucleus (MeV/u)
 igamma   =          3     # (D=0) 0:No, 1:Old, 2:EBITEM, 3:EBITEM+Isomer
 ipnint   =          1     # (D=0) 0: no, 1: consider photo-nuclear reaction
 negs     =         -1     # (D=0) =1 EGS photon and electron
 e-mode   =          2     # (D=0) 0: Normal, 1: Event generator mode
 inmed    =          2   #  (Cugnon new is 2)
 icrhi    =          2  # Kurotama cross section model
 icrdm    =          0    # the MWO formula
 nspred   =          2
 ndedx    =          3  # ATIMA
 nedisp   =          1
 itall    =         1
 Infout   =     8


 file(6)  = phits232Th.out       # (D=phits.out) general output file name

 maxbnk = 100000

[ S o u r c e ]
  s-type =   1           # mono-energetic axial source
```

```
    proj = deuteron       # He4
      e0 =   25        # energy of beam [MeV/n]
      r0 =  0.500         # radius [cm]
      x0 =   0.0000        # (D=0.0) center position of x-axis [cm]
      y0 =   0.0000        # (D=0.0) center position of y-axis [cm]
      z0 =  -0.1000        # minimum position of z-axis [cm]
      z1 =  -0.1000        # maximum position of z-axis [cm]
     dir =   1.0000        # z-direction of beam [cosine]

[ M a t e r i a l ]
 $ Thorium density =  11.724g/cm3
 MAT[1] 232Th   1.0

set: c91[11.724]  $ density of target [g/cm3]
set: c92[232] $ molecular weight [g/mol]
set: c20[10.0]    $ radius
set: c30[0.0125]   $ depth of sample
set: c50[c91/c92*6.02e23*c30] $ target density particles/cm^2



[ M a t N a m e C o l o r]
  mat    name      color
  1      Thorium   red


[ S u r f a c e ]

$  1       cz      c40
  1    RPP     -1 1 -1 1 0 c30 $ target
$  2       pz     0.0
$  3       pz      c30
  99      so     c20

[ C e l l ]
    1     1 -c91               -1 $ 2 -3  Target
    2     0                     -99 #1
   10    -1               99


[ T - Y i e l d ]
    title = Production yield of isotopes in region mesh
     mesh =  reg           # mesh type is region-wise
      reg = 1
```

```
  special =  0           # (D=0) number of repeated nuclear reactions
 material =  1
1
   mother =  all          # (D=all) number of specific mother
  nucleus =  all          # (D=all) number of detected nucleus
     unit =    1          # unit is [1/source]
     axis = dchain         # axis of output
     file = yield_reg.out   # file name of output for the above axis
     info =    0          # 0-> no, 1-> write magic number and stable nuclei
     part =  all
   output = product        # (D=product) normal yeild
      factor = 1/c50*1.0E27
   epsout =    1          # (D=0) generate eps file by ANGEL


[END]
```

Appendix C: Table of All PHITS Calculated Cross sections

The simulated cross sections in Table 5.2 were produced using PHITS 3.2 and the KUROTAMA model for nucleus-nucleus reaction cross sections since it is the default model. The input file from Appendix B was used to get the simulated cross section in Table 5.2.

Table 5.2. PHITS calculated cross sections (in mb) for all product nuclei of deuteron energies of 50, 40, 35, and 30 MeV.

Isotope	50 MeV	40 MeV	35 MeV	30 MeV
H-2	41.38 ± 0.01	24.8 ± 0.01	16.18 ± 0.02	9.4 ± 0.02
H-3	18.38 ± 0.02	9.19 ± 0.02	5.5 ± 0.03	3 ± 0.04
He-3	0.55 ± 0.1	0.09 ± 0.24	0.1 ± 0.23	1.37 ± 0.06
He-4	14.71 ± 0.02	5.82 ± 0.03	3.07 ± 0.04	-
He-5	-	-	-	-
He-6	0.03 ± 0.53	-	-	-
V-65	0.01 ± 1	-	-	-
Mn-64	0.01 ± 1	-	-	-
Fe-62	0.01 ± 1	-	-	-
Fe-63	-	-	-	-
Fe-64	0.01 ± 0.71	-	-	-
Fe-65	0.01 ± 1	-	-	-
Fe-66	0.02 ± 0.5	0.01 ± 1	0.01 ± 1	0.01 ± 1
Fe-67	0.01 ± 1	0.01 ± 1	-	-
Fe-68	0.01 ± 1	0.01 ± 1	0.01 ± 1	0.01 ± 1
Fe-69	0.01 ± 1	-	0.01 ± 1	0.01 ± 1
Fe-70	-	-	-	-
Fe-71	-	-	-	-
Fe-72	-	-	-	-
Fe-73	0.01 ± 1	-	-	-
Co-65	0.01 ± 0.5	0.01 ± 0.71	0.01 ± 1	0.01 ± 1
Co-66	0.01 ± 0.71	0.01 ± 1	0.01 ± 1	0.01 ± 0.71
Co-67	0.01 ± 0.71	0.03 ± 0.41	0.02 ± 0.58	0.01 ± 0.71
Co-68	0.02 ± 0.5	0.01 ± 0.71	0.02 ± 0.58	0.02 ± 0.58
Co-69	0.01 ± 1	0.02 ± 0.5	0.02 ± 0.5	0.01 ± 0.71
Co-70	0.03 ± 0.45	0.02 ± 0.58	0.02 ± 0.58	0.01 ± 0.71
Co-71	0.02 ± 0.5	0.03 ± 0.45	0.02 ± 0.5	0.01 ± 0.71
Co-72	0.01 ± 1	-	-	-
Co-73	0.01 ± 1	-	-	-

Table C.1 Continued.

Isotope	50 MeV	40 MeV	35 MeV	30 MeV
Ni-66	0.02 ± 0.58	0.01 ± 0.71	-	-
Ni-67	0.02 ± 0.58	0.01 ± 1	0.01 ± 1	0.01 ± 1
Ni-68	0.05 ± 0.33	0.02 ± 0.5	0.02 ± 0.5	0.03 ± 0.45
Ni-69	0.06 ± 0.29	0.02 ± 0.5	0.05 ± 0.33	0.01 ± 1
Ni-70	0.04 ± 0.35	0.07 ± 0.27	0.06 ± 0.3	0.06 ± 0.29
Ni-71	0.07 ± 0.26	0.04 ± 0.35	0.03 ± 0.41	0.04 ± 0.35
Ni-72	0.07 ± 0.28	0.04 ± 0.38	0.06 ± 0.29	0.03 ± 0.41
Ni-73	0.04 ± 0.38	0.03 ± 0.45	0.04 ± 0.35	0.04 ± 0.35
Ni-74	0.03 ± 0.44	0.04 ± 0.38	0.01 ± 0.71	0.03 ± 0.45
Ni-75	0.01 ± 0.71	0.01 ± 1	0.02 ± 0.58	0.01 ± 0.71
Ni-76	0.01 ± 1	0.01 ± 1	-	-
Ni-77	0.01 ± 1	-	-	-
Cu-67	0.01 ± 1	-	-	-
Cu-68	0.02 ± 0.5	-	-	-
Cu-69	0.05 ± 0.33	0.03 ± 0.45	0.05 ± 0.33	0.03 ± 0.41
Cu-70	0.06 ± 0.29	0.03 ± 0.41	0.06 ± 0.29	0.04 ± 0.35
Cu-71	0.18 ± 0.18	0.13 ± 0.2	0.17 ± 0.18	0.13 ± 0.2
Cu-72	0.21 ± 0.16	0.17 ± 0.18	0.11 ± 0.22	0.08 ± 0.26
Cu-73	0.29 ± 0.14	0.32 ± 0.13	0.24 ± 0.15	0.21 ± 0.16
Cu-74	0.14 ± 0.2	0.13 ± 0.2	0.19 ± 0.17	0.1 ± 0.23
Cu-75	0.18 ± 0.16	0.15 ± 0.19	0.15 ± 0.19	0.15 ± 0.19
Cu-76	0.08 ± 0.26	0.07 ± 0.28	0.09 ± 0.24	0.04 ± 0.35
Cu-77	0.05 ± 0.32	0.04 ± 0.35	0.09 ± 0.24	0.05 ± 0.33
Cu-78	0.02 ± 0.58	-	0.01 ± 0.71	0.02 ± 0.58
Cu-79	0.01 ± 1	0.01 ± 1	-	0.01 ± 0.71
Cu-80	0.01 ± 1	0.01 ± 1	-	-
Zn-69	0.01 ± 0.71	-	-	-
Zn-70	0.03 ± 0.53	0.03 ± 0.45	0.02 ± 0.5	0.03 ± 0.45
Zn-71	0.03 ± 0.41	0.04 ± 0.38	0.04 ± 0.35	0.02 ± 0.5
Zn-72	0.28 ± 0.13	0.14 ± 0.2	0.22 ± 0.16	0.23 ± 0.15
Zn-73	0.32 ± 0.13	0.26 ± 0.14	0.26 ± 0.14	0.2 ± 0.16
Zn-74	0.74 ± 0.08	0.6 ± 0.09	0.52 ± 0.1	0.56 ± 0.1
Zn-75	0.54 ± 0.1	0.54 ± 0.1	0.47 ± 0.11	0.44 ± 0.11
Zn-76	0.74 ± 0.08	0.69 ± 0.09	0.62 ± 0.09	0.64 ± 0.09
Zn-77	0.34 ± 0.13	0.41 ± 0.11	0.35 ± 0.12	0.32 ± 0.13
Zn-78	0.43 ± 0.11	0.29 ± 0.14	0.27 ± 0.14	0.33 ± 0.13
Zn-79	0.13 ± 0.21	0.18 ± 0.17	0.16 ± 0.18	0.18 ± 0.17
Zn-80	0.09 ± 0.24	0.08 ± 0.25	0.11 ± 0.22	0.09 ± 0.24
Zn-81	0.03 ± 0.45	-	-	-
Zn-82	0.01 ± 0.71	-	-	-

Table C.1 Continued.

Isotope	50 MeV	40 MeV	35 MeV	30 MeV
Ga-71	0.04 ± 0.35	0.01 ± 1	0.02 ± 0.5	0.01 ± 1
Ga-72	0.05 ± 0.33	0.03 ± 0.45	0.02 ± 0.58	0.02 ± 0.5
Ga-73	0.2 ± 0.17	0.13 ± 0.2	0.15 ± 0.19	0.11 ± 0.22
Ga-74	0.39 ± 0.11	0.26 ± 0.14	0.28 ± 0.14	0.24 ± 0.15
Ga-75	1.02 ± 0.07	0.84 ± 0.08	0.93 ± 0.08	0.66 ± 0.09
Ga-76	0.91 ± 0.08	0.98 ± 0.07	0.89 ± 0.08	0.91 ± 0.08
Ga-77	1.72 ± 0.06	1.67 ± 0.06	1.57 ± 0.06	1.64 ± 0.06
Ga-78	1.51 ± 0.06	1.28 ± 0.06	1.38 ± 0.06	1.43 ± 0.06
Ga-79	1.56 ± 0.06	1.27 ± 0.06	1.46 ± 0.06	1.4 ± 0.06
Ga-80	0.63 ± 0.09	0.75 ± 0.08	0.67 ± 0.09	0.64 ± 0.09
Ga-81	0.74 ± 0.08	0.52 ± 0.1	0.56 ± 0.1	0.56 ± 0.1
Ga-82	0.11 ± 0.21	0.12 ± 0.21	0.15 ± 0.19	0.12 ± 0.21
Ga-83	0.08 ± 0.27	0.07 ± 0.28	0.09 ± 0.24	0.06 ± 0.29
Ga-84	0.03 ± 0.45	0.02 ± 0.58	0.01 ± 1	0.01 ± 0.71
Ga-85	0.01 ± 1	0.01 ± 1	0.01 ± 1	0.01 ± 1
Ga-86	0.01 ± 1	-	-	-
Ge-72	0.01 ± 1	0.01 ± 1	-	-
Ge-73	0.01 ± 1	-	0.01 ± 1	0.01 ± 1
Ge-74	0.08 ± 0.27	0.08 ± 0.25	0.04 ± 0.35	0.03 ± 0.45
Ge-75	0.08 ± 0.25	0.09 ± 0.24	0.07 ± 0.28	0.06 ± 0.3
Ge-76	0.8 ± 0.08	0.79 ± 0.08	0.76 ± 0.08	0.69 ± 0.09
Ge-77	0.91 ± 0.08	0.93 ± 0.08	0.71 ± 0.09	0.8 ± 0.08
Ge-78	2.98 ± 0.04	2.7 ± 0.04	2.85 ± 0.04	2.74 ± 0.04
Ge-79	2.72 ± 0.04	2.43 ± 0.05	2.47 ± 0.05	2.66 ± 0.04
Ge-80	4.24 ± 0.04	4.06 ± 0.04	4.02 ± 0.04	3.9 ± 0.04
Ge-81	2.33 ± 0.05	2.25 ± 0.05	2.18 ± 0.05	2.28 ± 0.05
Ge-82	2.57 ± 0.05	2.43 ± 0.05	2.6 ± 0.04	2.67 ± 0.04
Ge-83	0.83 ± 0.08	0.68 ± 0.09	0.67 ± 0.09	0.78 ± 0.08
Ge-84	0.6 ± 0.09	0.49 ± 0.1	0.49 ± 0.1	0.54 ± 0.1
Ge-85	0.09 ± 0.22	0.15 ± 0.19	0.12 ± 0.21	0.07 ± 0.27
Ge-86	0.08 ± 0.25	0.05 ± 0.33	0.07 ± 0.28	0.07 ± 0.28
Ge-87	0.01 ± 0	0.01 ± 0.71	0.01 ± 0.71	0.01 ± 1
Ge-88	0.02 ± 0.5	0.01 ± 0.71	0.01 ± 1	-
Ge-90	0.01 ± 1	-	-	-
As-75	0.02 ± 0.5	0.03 ± 0.45	0.01 ± 1	0.02 ± 0.58
As-76	0.06 ± 0.29	0.04 ± 0.38	0.04 ± 0.38	0.04 ± 0.38
As-77	0.4 ± 0.11	0.37 ± 0.12	0.3 ± 0.13	0.26 ± 0.14
As-78	0.92 ± 0.08	0.71 ± 0.09	0.62 ± 0.09	0.69 ± 0.09
As-79	2.61 ± 0.04	2.49 ± 0.05	2.31 ± 0.05	2.17 ± 0.05
As-80	3.75 ± 0.04	3.38 ± 0.04	3.49 ± 0.04	3.56 ± 0.04

Table C.1 Continued.

Isotope	50 MeV	40 MeV	35 MeV	30 MeV
As-81	6.78 ± 0.03	6.68 ± 0.03	6.83 ± 0.03	6.64 ± 0.03
As-82	5.71 ± 0.03	5.51 ± 0.03	5.6 ± 0.03	5.99 ± 0.03
As-83	6.91 ± 0.03	6.94 ± 0.03	6.85 ± 0.03	7.67 ± 0.03
As-84	3.26 ± 0.04	2.94 ± 0.04	3.06 ± 0.04	3.4 ± 0.04
As-85	2.47 ± 0.05	2.21 ± 0.05	2.35 ± 0.05	2.31 ± 0.05
As-86	0.87 ± 0.08	0.94 ± 0.07	0.7 ± 0.09	0.84 ± 0.08
As-87	0.48 ± 0.11	0.43 ± 0.11	0.48 ± 0.1	0.42 ± 0.11
As-88	0.13 ± 0.2	0.12 ± 0.21	0.17 ± 0.18	0.18 ± 0.17
As-89	0.07 ± 0.28	0.03 ± 0.45	0.04 ± 0.38	0.03 ± 0.45
As-90	-	0.03 ± 0.45	0.02 ± 0.58	0.01 ± 1
As-91	0.01 ± 1	0.01 ± 0.71	0.01 ± 1	0.01 ± 1
Se-77	0.01 ± 1	-	-	-
Se-78	0.1 ± 0.24	0.07 ± 0.27	0.06 ± 0.29	0.05 ± 0.33
Se-79	0.27 ± 0.15	0.17 ± 0.17	0.12 ± 0.21	0.1 ± 0.23
Se-80	1.67 ± 0.06	1.36 ± 0.06	1.22 ± 0.07	1.26 ± 0.06
Se-81	1.46 ± 0.06	1.4 ± 0.06	1.24 ± 0.07	1.23 ± 0.07
Se-82	7.4 ± 0.03	7.2 ± 0.03	7.35 ± 0.03	7.08 ± 0.03
Se-83	4.62 ± 0.03	4.97 ± 0.03	4.69 ± 0.03	5.25 ± 0.03
Se-84	13.91 ± 0.02	13.3 ± 0.02	14.23 ± 0.02	15.5 ± 0.02
Se-85	7.82 ± 0.03	7.78 ± 0.03	8.01 ± 0.03	8.24 ± 0.03
Se-86	7.16 ± 0.03	7.34 ± 0.03	7.25 ± 0.03	7.79 ± 0.03
Se-87	3.07 ± 0.04	3.06 ± 0.04	3.35 ± 0.04	3.32 ± 0.04
Se-88	2.07 ± 0.05	2.08 ± 0.05	2.1 ± 0.05	2.04 ± 0.05
Se-89	0.73 ± 0.09	0.62 ± 0.09	0.76 ± 0.08	0.79 ± 0.08
Se-90	0.44 ± 0.11	0.41 ± 0.11	0.3 ± 0.13	0.3 ± 0.13
Se-91	0.04 ± 0.35	0.1 ± 0.23	0.06 ± 0.3	0.06 ± 0.29
Se-92	0.02 ± 0.58	0.05 ± 0.33	0.05 ± 0.33	0.05 ± 0.33
Se-93	0.01 ± 1	0.01 ± 1	0.01 ± 0.71	0.02 ± 0.58
Se-94	0.01 ± 1	0.01 ± 0.71	0.01 ± 1	-
Br-79	0.02 ± 0.58	-	-	-
Br-80	0.04 ± 0.38	0.03 ± 0.45	0.02 ± 0.5	0.01 ± 0.71
Br-81	0.35 ± 0.12	0.33 ± 0.13	0.28 ± 0.14	0.26 ± 0.14
Br-82	1.25 ± 0.06	0.98 ± 0.07	0.94 ± 0.07	0.73 ± 0.08
Br-83	4.43 ± 0.03	4.19 ± 0.04	4.1 ± 0.04	3.68 ± 0.04
Br-84	4.92 ± 0.03	5.1 ± 0.03	4.68 ± 0.03	4.82 ± 0.03
Br-85	15.66 ± 0.02	16 ± 0.02	16 ± 0.02	17 ± 0.02
Br-86	12.41 ± 0.02	12.6 ± 0.02	13.1 ± 0.02	14.1 ± 0.02
Br-87	14.07 ± 0.02	14.6 ± 0.02	15.01 ± 0.02	16.3 ± 0.02
Br-88	9.6 ± 0.02	9.23 ± 0.02	9.59 ± 0.02	10.7 ± 0.02
Br-89	6.79 ± 0.03	7.2 ± 0.03	7.18 ± 0.03	7.83 ± 0.03

Table C.1 Continued.

Isotope	50 MeV	40 MeV	35 MeV	30 MeV
Br-90	2.7 ± 0.04	2.58 ± 0.05	2.85 ± 0.04	3.01 ± 0.04
Br-91	1.48 ± 0.06	1.74 ± 0.06	1.58 ± 0.06	1.62 ± 0.06
Br-92	0.45 ± 0.11	0.51 ± 0.1	0.53 ± 0.1	0.48 ± 0.1
Br-93	0.21 ± 0.15	0.25 ± 0.15	0.3 ± 0.13	0.22 ± 0.15
Br-94	0.04 ± 0.4	0.04 ± 0.35	0.06 ± 0.3	0.06 ± 0.3
Br-95	0.04 ± 0.38	0.03 ± 0.41	0.05 ± 0.33	0.03 ± 0.45
Br-96	0.01 ± 1	0.02 ± 0.5	0.01 ± 0.71	0.01 ± 1
Br-97	0.01 ± 1	-	-	-
Kr-82	0.06 ± 0.27	0.05 ± 0.32	0.03 ± 0.45	0.03 ± 0.45
Kr-83	0.17 ± 0.17	0.14 ± 0.2	0.06 ± 0.29	0.09 ± 0.24
Kr-84	1.25 ± 0.06	1.17 ± 0.07	1.01 ± 0.07	1.07 ± 0.07
Kr-85	2.41 ± 0.05	2.17 ± 0.05	2.03 ± 0.05	2.11 ± 0.05
Kr-86	11.57 ± 0.02	11.4 ± 0.02	11.59 ± 0.02	11.1 ± 0.02
Kr-87	12.86 ± 0.02	12.5 ± 0.02	13.73 ± 0.02	13.3 ± 0.02
Kr-88	19.8 ± 0.02	20.3 ± 0.02	21.06 ± 0.02	22.3 ± 0.02
Kr-89	15.6 ± 0.02	16.7 ± 0.02	16.48 ± 0.02	17.6 ± 0.02
Kr-90	14.86 ± 0.02	15.2 ± 0.02	15.77 ± 0.02	16.9 ± 0.02
Kr-91	7.86 ± 0.03	7.59 ± 0.03	8.44 ± 0.02	8.43 ± 0.03
Kr-92	5.04 ± 0.03	5.2 ± 0.03	5.65 ± 0.03	5.64 ± 0.03
Kr-93	1.54 ± 0.06	1.7 ± 0.06	1.73 ± 0.06	1.75 ± 0.05
Kr-94	0.99 ± 0.07	1.02 ± 0.07	1.08 ± 0.07	1.19 ± 0.07
Kr-95	0.31 ± 0.13	0.32 ± 0.13	0.26 ± 0.14	0.26 ± 0.14
Kr-96	0.21 ± 0.16	0.19 ± 0.17	0.22 ± 0.15	0.25 ± 0.15
Kr-97	0.05 ± 0.32	0.07 ± 0.28	0.03 ± 0.41	0.01 ± 0.71
Kr-98	0.03 ± 0.44	0.05 ± 0.33	0.03 ± 0.41	0.03 ± 0.41
Kr-99	0.01 ± 1	0.01 ± 1	-	-
Rb-83	0.01 ± 1	-	-	-
Rb-84	0.01 ± 0.71	0.02 ± 0.58	-	-
Rb-85	0.19 ± 0.17	0.14 ± 0.2	0.1 ± 0.23	0.14 ± 0.19
Rb-86	0.6 ± 0.09	0.55 ± 0.1	0.46 ± 0.11	0.48 ± 0.1
Rb-87	4.47 ± 0.03	4.25 ± 0.04	3.95 ± 0.04	3.69 ± 0.04
Rb-88	7.8 ± 0.03	8.12 ± 0.03	7.82 ± 0.03	7.34 ± 0.03
Rb-89	15.38 ± 0.02	14.9 ± 0.02	16.54 ± 0.02	16.6 ± 0.02
Rb-90	18.13 ± 0.02	18.4 ± 0.02	18.77 ± 0.02	20.2 ± 0.02
Rb-91	20.61 ± 0.02	22.1 ± 0.02	23.01 ± 0.02	24.2 ± 0.01
Rb-92	14.78 ± 0.02	15.6 ± 0.02	16.92 ± 0.02	18.2 ± 0.02
Rb-93	11.7 ± 0.02	11.9 ± 0.02	12.74 ± 0.02	13.4 ± 0.02
Rb-94	5.05 ± 0.03	5.26 ± 0.03	5.14 ± 0.03	5.62 ± 0.03
Rb-95	3.22 ± 0.04	3.69 ± 0.04	3.81 ± 0.04	3.59 ± 0.04
Rb-96	1.3 ± 0.06	1.28 ± 0.06	1.25 ± 0.06	1.26 ± 0.06

Table C.1 Continued.

Isotope	50 MeV	40 MeV	35 MeV	30 MeV
Rb-97	0.9 ± 0.08	0.91 ± 0.08	0.86 ± 0.08	0.87 ± 0.08
Rb-98	0.35 ± 0.12	0.38 ± 0.12	0.32 ± 0.13	0.34 ± 0.12
Rb-99	0.12 ± 0.21	0.18 ± 0.17	0.15 ± 0.19	0.21 ± 0.16
Rb-100	0.08 ± 0.26	0.08 ± 0.26	0.05 ± 0.32	0.02 ± 0.5
Rb-101	0.02 ± 0.58	0.03 ± 0.41	0.04 ± 0.38	0.04 ± 0.38
Sr-85	0.01 ± 1	-	-	-
Sr-86	0.01 ± 0.71	0.02 ± 0.58	0.01 ± 1	-
Sr-87	0.06 ± 0.29	0.05 ± 0.32	0.07 ± 0.28	0.04 ± 0.35
Sr-88	1.07 ± 0.07	0.78 ± 0.08	0.84 ± 0.08	0.68 ± 0.09
Sr-89	2.71 ± 0.04	2.46 ± 0.05	2.18 ± 0.05	2.14 ± 0.05
Sr-90	7.74 ± 0.03	7.44 ± 0.03	7.91 ± 0.03	7.26 ± 0.03
Sr-91	11.68 ± 0.02	12 ± 0.02	12.29 ± 0.02	11.8 ± 0.02
Sr-92	20.44 ± 0.02	20.1 ± 0.02	21.84 ± 0.02	22.6 ± 0.02
Sr-93	17.84 ± 0.02	19.1 ± 0.02	19.68 ± 0.02	20.5 ± 0.02
Sr-94	19.09 ± 0.02	20.5 ± 0.02	21.17 ± 0.02	22.5 ± 0.02
Sr-95	10.06 ± 0.02	10.6 ± 0.02	10.57 ± 0.02	10.8 ± 0.02
Sr-96	8.39 ± 0.02	8.98 ± 0.02	8.5 ± 0.02	8.73 ± 0.02
Sr-97	3.44 ± 0.04	3.72 ± 0.04	3.66 ± 0.04	3.76 ± 0.04
Sr-98	2.82 ± 0.04	3.04 ± 0.04	2.8 ± 0.04	2.78 ± 0.04
Sr-99	1.02 ± 0.07	1.01 ± 0.07	1.02 ± 0.07	0.99 ± 0.07
Sr-100	0.8 ± 0.08	0.95 ± 0.07	0.75 ± 0.08	0.74 ± 0.08
Sr-101	0.19 ± 0.17	0.23 ± 0.15	0.22 ± 0.16	0.25 ± 0.15
Sr-102	0.12 ± 0.21	0.13 ± 0.2	0.15 ± 0.19	0.15 ± 0.19
Sr-103	0.04 ± 0.38	0.04 ± 0.38	0.03 ± 0.45	0.03 ± 0.41
Sr-104	0.01 ± 0.71	0.02 ± 0.58	0.02 ± 0.58	0.02 ± 0.5
Sr-105	0.01 ± 1	0.01 ± 1	-	-
Y-88	0.01 ± 0.71	-	-	-
Y-89	0.08 ± 0.26	0.05 ± 0.32	0.04 ± 0.35	0.03 ± 0.41
Y-90	0.32 ± 0.13	0.26 ± 0.14	0.2 ± 0.16	0.27 ± 0.14
Y-91	1.05 ± 0.07	1.06 ± 0.07	0.96 ± 0.07	0.77 ± 0.08
Y-92	4.76 ± 0.03	4.27 ± 0.04	4.28 ± 0.04	4.31 ± 0.03
Y-93	6.9 ± 0.03	6.89 ± 0.03	7.23 ± 0.03	7.08 ± 0.03
Y-94	15.08 ± 0.02	15 ± 0.02	15.31 ± 0.02	16 ± 0.02
Y-95	19.88 ± 0.02	2-.02	20.99 ± 0.02	22.1 ± 0.02
Y-96	14.54 ± 0.02	15.6 ± 0.02	15.72 ± 0.02	16.2 ± 0.02
Y-97	13.49 ± 0.02	13.6 ± 0.02	13.78 ± 0.02	14.1 ± 0.02
Y-98	7.81 ± 0.03	7.84 ± 0.03	7.71 ± 0.03	7.69 ± 0.03
Y-99	7.2 ± 0.03	7.24 ± 0.03	6.94 ± 0.03	6.77 ± 0.03
Y-100	4.16 ± 0.04	4.16 ± 0.04	4.15 ± 0.04	4.15 ± 0.04
Y-101	2.37 ± 0.05	2.59 ± 0.05	2.8 ± 0.04	2.53 ± 0.05

Table C.1 Continued.

Isotope	50 MeV	40 MeV	35 MeV	30 MeV
Y-102	1.19 ± 0.07	1.15 ± 0.07	1.24 ± 0.07	1.33 ± 0.06
Y-103	0.52 ± 0.1	0.5 ± 0.1	0.53 ± 0.1	0.57 ± 0.1
Y-104	0.18 ± 0.16	0.23 ± 0.15	0.26 ± 0.14	0.18 ± 0.17
Y-105	0.09 ± 0.24	0.09 ± 0.24	0.11 ± 0.22	0.07 ± 0.28
Y-106	0.03 ± 0.41	0.03 ± 0.45	0.02 ± 0.58	0.03 ± 0.41
Y-107	0.01 ± 1	0.01 ± 1	0.01 ± 0.71	0.03 ± 0.41
Y-108	-	-	-	-
Y-109	0.01 ± 1	-	-	-
Zr-91	0.04 ± 0.38	0.02 ± 0.5	0.01 ± 0.71	0.01 ± 1
Zr-92	0.28 ± 0.14	0.17 ± 0.17	0.18 ± 0.17	0.11 ± 0.22
Zr-93	0.99 ± 0.07	0.83 ± 0.08	0.73 ± 0.08	0.55 ± 0.1
Zr-94	3.49 ± 0.04	3.24 ± 0.04	3 ± 0.04	2.68 ± 0.04
Zr-95	7.06 ± 0.03	6.95 ± 0.03	6.7 ± 0.03	6.09 ± 0.03
Zr-96	14.3 ± 0.02	13.6 ± 0.02	13.84 ± 0.02	14.4 ± 0.02
Zr-97	13 ± 0.02	13 ± 0.02	12.55 ± 0.02	13.6 ± 0.02
Zr-98	15.36 ± 0.02	14.9 ± 0.02	14.87 ± 0.02	14.6 ± 0.02
Zr-99	10.89 ± 0.02	10.7 ± 0.02	10.65 ± 0.02	10.7 ± 0.02
Zr-100	12.87 ± 0.02	12.7 ± 0.02	12.56 ± 0.02	12.5 ± 0.02
Zr-101	7.23 ± 0.03	7.68 ± 0.03	7.4 ± 0.03	6.85 ± 0.03
Zr-102	6.03 ± 0.03	6.57 ± 0.03	6.29 ± 0.03	6.02 ± 0.03
Zr-103	2.89 ± 0.04	2.84 ± 0.04	3.15 ± 0.04	2.98 ± 0.04
Zr-104	2.15 ± 0.05	2.14 ± 0.05	2.07 ± 0.05	1.94 ± 0.05
Zr-105	0.7 ± 0.09	0.78 ± 0.08	0.75 ± 0.08	0.69 ± 0.09
Zr-106	0.41 ± 0.11	0.44 ± 0.11	0.41 ± 0.11	0.47 ± 0.11
Zr-107	0.12 ± 0.23	0.13 ± 0.2	0.19 ± 0.16	0.14 ± 0.2
Zr-108	0.08 ± 0.25	0.07 ± 0.27	0.09 ± 0.24	0.11 ± 0.22
Zr-109	0.04 ± 0.35	0.01 ± 1	0.02 ± 0.58	0.01 ± 0.71
Zr-110	0.01 ± 1	-	-	-
Nb-92	0.01 ± 1	-	-	-
Nb-93	0.02 ± 0.58	-	-	-
Nb-94	0.05 ± 0.33	0.02 ± 0.58	0.03 ± 0.41	0.01 ± 0.71
Nb-95	0.54 ± 0.1	0.36 ± 0.12	0.34 ± 0.12	0.27 ± 0.14
Nb-96	1.9 ± 0.05	1.55 ± 0.06	1.35 ± 0.06	1.17 ± 0.07
Nb-97	4 ± 0.04	3.75 ± 0.04	3.37 ± 0.04	3.04 ± 0.04
Nb-98	2.98 ± 0.04	2.93 ± 0.04	2.81 ± 0.04	2.85 ± 0.04
Nb-99	11.53 ± 0.02	10.2 ± 0.02	10.28 ± 0.02	9.92 ± 0.02
Nb-100	11.82 ± 0.02	11.1 ± 0.02	11.02 ± 0.02	10.2 ± 0.02
Nb-101	14.97 ± 0.02	15 ± 0.02	13.3 ± 0.02	13.4 ± 0.02
Nb-102	12.09 ± 0.02	11.4 ± 0.02	10.83 ± 0.02	10.3 ± 0.02
Nb-103	11.95 ± 0.02	12 ± 0.02	11.68 ± 0.02	11.1 ± 0.02

Table C.1 Continued.

Isotope	50 MeV	40 MeV	35 MeV	30 MeV
Nb-104	7.05 ± 0.03	7.18 ± 0.03	6.47 ± 0.03	6.21 ± 0.03
Nb-105	5.59 ± 0.03	6.11 ± 0.03	6.01 ± 0.03	5.57 ± 0.03
Nb-106	2.43 ± 0.05	2.5 ± 0.05	2.36 ± 0.05	2.21 ± 0.05
Nb-107	1.54 ± 0.06	1.92 ± 0.05	1.84 ± 0.05	1.83 ± 0.05
Nb-108	0.53 ± 0.1	0.56 ± 0.1	0.64 ± 0.09	0.59 ± 0.09
Nb-109	0.38 ± 0.12	0.42 ± 0.11	0.38 ± 0.12	0.42 ± 0.11
Nb-110	0.09 ± 0.24	0.11 ± 0.22	0.05 ± 0.32	0.14 ± 0.19
Nb-111	0.08 ± 0.24	0.07 ± 0.28	0.05 ± 0.33	0.06 ± 0.29
Nb-112	0.01 ± 0.71	-	0.01 ± 0.71	-
Nb-113	0.01 ± 0.71	0.01 ± 1	0.03 ± 0.45	-
Mo-96	0.03 ± 0.45	0.02 ± 0.58	0.03 ± 0.45	0.01 ± 0.71
Mo-97	0.16 ± 0.18	0.11 ± 0.22	0.08 ± 0.26	0.08 ± 0.25
Mo-98	0.85 ± 0.08	0.72 ± 0.09	0.62 ± 0.09	0.39 ± 0.12
Mo-99	1.99 ± 0.05	1.63 ± 0.06	1.52 ± 0.06	1.14 ± 0.07
Mo-100	5.88 ± 0.03	4.67 ± 0.03	4.2 ± 0.04	3.95 ± 0.04
Mo-101	6.42 ± 0.03	5.98 ± 0.03	5.12 ± 0.03	4.99 ± 0.03
Mo-102	13.53 ± 0.02	11.5 ± 0.02	11.29 ± 0.02	9.92 ± 0.02
Mo-103	12.1 ± 0.02	10.6 ± 0.02	9.7 ± 0.02	8.93 ± 0.02
Mo-104	16.59 ± 0.02	15.8 ± 0.02	14.82 ± 0.02	13.3 ± 0.02
Mo-105	11.24 ± 0.02	10.8 ± 0.02	9.99 ± 0.02	8.9 ± 0.02
Mo-106	11.94 ± 0.02	12.4 ± 0.02	11.2 ± 0.02	10.4 ± 0.02
Mo-107	5.79 ± 0.03	6.04 ± 0.03	5.83 ± 0.03	5.88 ± 0.03
Mo-108	4.84 ± 0.03	5.18 ± 0.03	4.95 ± 0.03	4.78 ± 0.03
Mo-109	2.06 ± 0.05	2.12 ± 0.05	2.08 ± 0.05	2.03 ± 0.05
Mo-110	1.25 ± 0.06	1.67 ± 0.06	1.56 ± 0.06	1.47 ± 0.06
Mo-111	0.41 ± 0.11	0.37 ± 0.12	0.5 ± 0.1	0.42 ± 0.11
Mo-112	0.23 ± 0.16	0.31 ± 0.13	0.25 ± 0.14	0.3 ± 0.13
Mo-113	0.08 ± 0.23	0.07 ± 0.28	0.08 ± 0.26	0.04 ± 0.38
Mo-114	0.05 ± 0.32	0.03 ± 0.45	0.03 ± 0.41	0.04 ± 0.38
Mo-115	0.01 ± 1	0.01 ± 1	0.01 ± 0.71	0.01 ± 0.71
Mo-116	0.01 ± 0.5	-	0.01 ± 1	-
Tc-98	0.01 ± 1	-	-	-
Tc-99	0.06 ± 0.3	0.03 ± 0.45	0.01 ± 1	0.01 ± 0.71
Tc-100	0.26 ± 0.15	0.15 ± 0.19	0.22 ± 0.15	0.11 ± 0.22
Tc-101	1.19 ± 0.07	0.79 ± 0.08	0.68 ± 0.09	0.51 ± 0.1
Tc-102	2.41 ± 0.05	1.82 ± 0.05	1.36 ± 0.06	1.13 ± 0.07
Tc-103	6.33 ± 0.03	5.22 ± 0.03	4.17 ± 0.04	3.38 ± 0.04
Tc-104	8.18 ± 0.03	6.94 ± 0.03	5.91 ± 0.03	4.63 ± 0.03
Tc-105	14.28 ± 0.02	12.5 ± 0.02	10.74 ± 0.02	9.92 ± 0.02
Tc-106	13.04 ± 0.02	11.8 ± 0.02	10.51 ± 0.02	9.18 ± 0.02

Table C.1 Continued.

Isotope	50 MeV	40 MeV	35 MeV	30 MeV
Tc-107	17.06 ± 0.02	16.1 ± 0.02	14.79 ± 0.02	13 ± 0.02
Tc-108	10.43 ± 0.02	10.8 ± 0.02	10.18 ± 0.02	9 ± 0.02
Tc-109	11.18 ± 0.02	10.9 ± 0.02	11.22 ± 0.02	10.4 ± 0.02
Tc-110	5.37 ± 0.03	5.6 ± 0.03	5.55 ± 0.03	5.39 ± 0.03
Tc-111	4.4 ± 0.03	4.81 ± 0.03	4.83 ± 0.03	4.52 ± 0.03
Tc-112	1.79 ± 0.05	1.93 ± 0.05	1.9 ± 0.05	1.81 ± 0.05
Tc-113	1.22 ± 0.06	1.41 ± 0.06	1.45 ± 0.06	1.48 ± 0.06
Tc-114	0.24 ± 0.15	0.3 ± 0.13	0.37 ± 0.12	0.43 ± 0.11
Tc-115	0.23 ± 0.15	0.24 ± 0.15	0.21 ± 0.16	0.2 ± 0.16
Tc-116	0.05 ± 0.37	0.06 ± 0.3	0.04 ± 0.38	0.05 ± 0.32
Tc-117	0.03 ± 0.41	0.02 ± 0.5	0.04 ± 0.35	0.03 ± 0.41
Tc-118	0.01 ± 0	0.01 ± 1	-	-
Ru-101	0.02 ± 0.58	0.01 ± 0.71	0.01 ± 1	-
Ru-102	0.11 ± 0.23	0.07 ± 0.27	0.09 ± 0.24	0.05 ± 0.33
Ru-103	0.36 ± 0.12	0.21 ± 0.16	0.09 ± 0.24	0.17 ± 0.18
Ru-104	2.01 ± 0.05	1.24 ± 0.07	0.86 ± 0.08	0.65 ± 0.09
Ru-105	3.39 ± 0.04	2.34 ± 0.05	1.89 ± 0.05	1.38 ± 0.06
Ru-106	8.97 ± 0.02	6.8 ± 0.03	5.78 ± 0.03	4.5 ± 0.03
Ru-107	10.31 ± 0.02	8.33 ± 0.03	6.71 ± 0.03	5.72 ± 0.03
Ru-108	17.75 ± 0.02	15 ± 0.02	13.51 ± 0.02	10.9 ± 0.02
Ru-109	13.67 ± 0.02	12.3 ± 0.02	11.13 ± 0.02	9.63 ± 0.02
Ru-110	17.7 ± 0.02	16.5 ± 0.02	15.76 ± 0.02	13.2 ± 0.02
Ru-111	9.34 ± 0.02	9.65 ± 0.02	9.37 ± 0.02	8.36 ± 0.03
Ru-112	10.2 ± 0.02	10.2 ± 0.02	9.42 ± 0.02	9.35 ± 0.02
Ru-113	3.92 ± 0.04	4.83 ± 0.03	4.58 ± 0.03	4.12 ± 0.04
Ru-114	3.38 ± 0.04	3.99 ± 0.04	3.82 ± 0.04	3.88 ± 0.04
Ru-115	1.13 ± 0.07	1.21 ± 0.07	1.33 ± 0.06	1.27 ± 0.06
Ru-116	0.78 ± 0.08	1.03 ± 0.07	1.05 ± 0.07	0.89 ± 0.08
Ru-117	0.25 ± 0.15	0.25 ± 0.14	0.27 ± 0.14	0.29 ± 0.14
Ru-118	0.11 ± 0.22	0.11 ± 0.22	0.09 ± 0.24	0.15 ± 0.19
Ru-119	0.02 ± 0.5	0.03 ± 0.41	0.02 ± 0.5	0.03 ± 0.45
Ru-120	0.02 ± 0.58	0.01 ± 0.71	0.02 ± 0.58	0.01 ± 1
Rh-103	0.01 ± 1	-	-	-
Rh-104	0.02 ± 0.58	0.02 ± 0.5	-	-
Rh-105	0.2 ± 0.16	0.06 ± 0.29	0.06 ± 0.29	0.04 ± 0.35
Rh-106	0.21 ± 0.16	0.09 ± 0.24	0.08 ± 0.26	0.06 ± 0.29
Rh-107	2.76 ± 0.04	1.78 ± 0.05	1.35 ± 0.06	0.86 ± 0.08
Rh-108	4.63 ± 0.03	3.57 ± 0.04	2.7 ± 0.04	1.91 ± 0.05
Rh-109	11.37 ± 0.02	8.52 ± 0.02	6.87 ± 0.03	5.68 ± 0.03
Rh-110	12.41 ± 0.02	10.6 ± 0.02	8.99 ± 0.02	6.9 ± 0.03

Table C.1 Continued.

Isotope	50 MeV	40 MeV	35 MeV	30 MeV
Rh-111	17.83 ± 0.02	15.8 ± 0.02	14.1 ± 0.02	11.3 ± 0.02
Rh-112	13.49 ± 0.02	12.8 ± 0.02	11.75 ± 0.02	10.3 ± 0.02
Rh-113	16.35 ± 0.02	15.4 ± 0.02	14.79 ± 0.02	12.9 ± 0.02
Rh-114	9.05 ± 0.02	9.14 ± 0.02	9 ± 0.02	8.31 ± 0.03
Rh-115	8.44 ± 0.03	8.69 ± 0.03	8.7 ± 0.03	8.35 ± 0.03
Rh-116	3.61 ± 0.04	3.92 ± 0.04	3.69 ± 0.04	3.81 ± 0.04
Rh-117	2.54 ± 0.05	2.94 ± 0.04	2.97 ± 0.04	3.07 ± 0.04
Rh-118	0.92 ± 0.08	0.98 ± 0.07	1.03 ± 0.07	1.04 ± 0.07
Rh-119	0.56 ± 0.1	0.76 ± 0.08	0.65 ± 0.09	0.62 ± 0.09
Rh-120	0.17 ± 0.18	0.18 ± 0.17	0.22 ± 0.16	0.14 ± 0.19
Rh-121	0.1 ± 0.24	0.05 ± 0.32	0.06 ± 0.29	0.05 ± 0.32
Rh-122	0.02 ± 0.58	0.03 ± 0.41	0.01 ± 1	0.02 ± 0.5
Pd-106	0.02 ± 0.58	-	-	-
Pd-107	0.08 ± 0.26	-	-	-
Pd-108	0.52 ± 0.1	0.28 ± 0.14	0.11 ± 0.22	0.11 ± 0.22
Pd-109	0.8 ± 0.08	0.46 ± 0.11	0.37 ± 0.12	0.24 ± 0.15
Pd-110	4.48 ± 0.03	3.06 ± 0.04	2.12 ± 0.05	1.66 ± 0.06
Pd-111	4.63 ± 0.03	3.34 ± 0.04	2.66 ± 0.04	2.1 ± 0.05
Pd-112	13.96 ± 0.02	11.3 ± 0.02	9.5 ± 0.02	7.06 ± 0.03
Pd-113	12.32 ± 0.02	11 ± 0.02	9.67 ± 0.02	7.87 ± 0.03
Pd-114	19.59 ± 0.02	17.5 ± 0.02	16.09 ± 0.02	13.6 ± 0.02
Pd-115	12.09 ± 0.02	11.9 ± 0.02	11.11 ± 0.02	9.67 ± 0.02
Pd-116	14.95 ± 0.02	14.8 ± 0.02	14.36 ± 0.02	13.2 ± 0.02
Pd-117	6.6 ± 0.03	7.58 ± 0.03	7.48 ± 0.03	6.56 ± 0.03
Pd-118	6.75 ± 0.03	6.91 ± 0.03	6.84 ± 0.03	6.43 ± 0.03
Pd-119	2.57 ± 0.05	2.92 ± 0.04	3.06 ± 0.04	3.05 ± 0.04
Pd-120	1.86 ± 0.05	1.96 ± 0.05	2.1 ± 0.05	2.08 ± 0.05
Pd-121	0.53 ± 0.1	0.6 ± 0.09	0.57 ± 0.1	0.61 ± 0.09
Pd-122	0.4 ± 0.12	0.41 ± 0.11	0.39 ± 0.12	0.35 ± 0.12
Pd-123	0.09 ± 0.26	0.05 ± 0.32	0.07 ± 0.28	0.08 ± 0.25
Pd-124	0.05 ± 0.33	0.06 ± 0.3	0.04 ± 0.35	0.07 ± 0.28
Pd-125	0.01 ± 0.71	0.01 ± 1	0.01 ± 0.71	0.02 ± 0.58
Pd-126	0.01 ± 1	0.01 ± 1	0.01 ± 1	0.01 ± 1
Ag-109	0.01 ± 1	-	-	-
Ag-110	0.09 ± 0.24	0.06 ± 0.3	0.04 ± 0.35	0.01 ± 1
Ag-111	0.32 ± 0.13	0.24 ± 0.15	0.15 ± 0.19	0.07 ± 0.27
Ag-112	1.89 ± 0.05	1.13 ± 0.07	0.9 ± 0.08	0.61 ± 0.09
Ag-113	1.93 ± 0.05	1.53 ± 0.06	1.12 ± 0.07	0.89 ± 0.08
Ag-114	3.14 ± 0.04	2.72 ± 0.04	1.98 ± 0.05	1.78 ± 0.05
Ag-115	2.85 ± 0.04	2.69 ± 0.04	2.31 ± 0.05	1.68 ± 0.06

Table C.1 Continued.

Isotope	50 MeV	40 MeV	35 MeV	30 MeV
Ag-116	13.66 ± 0.02	12 ± 0.02	10.22 ± 0.02	8.85 ± 0.02
Ag-117	18.27 ± 0.02	17.1 ± 0.02	15.81 ± 0.02	13 ± 0.02
Ag-118	12.19 ± 0.02	11.9 ± 0.02	11.5 ± 0.02	9.69 ± 0.02
Ag-119	11.92 ± 0.02	11.9 ± 0.02	11.57 ± 0.02	10.8 ± 0.02
Ag-120	6.37 ± 0.03	6.9 ± 0.03	6.81 ± 0.03	6.49 ± 0.03
Ag-121	4.89 ± 0.03	5.29 ± 0.03	5.6 ± 0.03	5.52 ± 0.03
Ag-122	2.07 ± 0.05	2.1 ± 0.05	2.2 ± 0.05	2.35 ± 0.05
Ag-123	1.2 ± 0.07	1.52 ± 0.06	1.6 ± 0.06	1.66 ± 0.06
Ag-124	0.47 ± 0.11	0.61 ± 0.09	0.52 ± 0.1	0.46 ± 0.11
Ag-125	0.26 ± 0.14	0.3 ± 0.13	0.24 ± 0.15	0.28 ± 0.14
Ag-126	0.07 ± 0.27	0.07 ± 0.27	0.12 ± 0.21	0.1 ± 0.23
Ag-127	0.04 ± 0.35	0.03 ± 0.45	0.02 ± 0.5	0.03 ± 0.41
Ag-128	0.01 ± 0.71	0.02 ± 0.58	0.01 ± 1	0.01 ± 1
Cd-110	0.01 ± 0	-	-	-
Cd-111	-	0.01 ± 1	0.01 ± 1	-
Cd-112	0.09 ± 0.24	0.02 ± 0.58	0.02 ± 0.5	0.02 ± 0.5
Cd-113	0.17 ± 0.17	0.09 ± 0.24	0.05 ± 0.33	0.03 ± 0.41
Cd-114	1.42 ± 0.06	0.73 ± 0.09	0.52 ± 0.1	0.35 ± 0.12
Cd-115	1.74 ± 0.06	1.22 ± 0.07	0.92 ± 0.08	0.72 ± 0.09
Cd-116	8.28 ± 0.03	5.69 ± 0.03	4.53 ± 0.03	3.26 ± 0.04
Cd-117	4.72 ± 0.03	4.09 ± 0.04	3.34 ± 0.04	2.52 ± 0.05
Cd-118	16.25 ± 0.02	13.7 ± 0.02	12.14 ± 0.02	10.1 ± 0.02
Cd-119	11.57 ± 0.02	11 ± 0.02	10.05 ± 0.02	8.63 ± 0.02
Cd-120	16.6 ± 0.02	16.1 ± 0.02	15.2 ± 0.02	13.9 ± 0.02
Cd-121	9.66 ± 0.02	1-.02	9.26 ± 0.02	8.6 ± 0.02
Cd-122	10.07 ± 0.02	10.7 ± 0.02	10.39 ± 0.02	10.1 ± 0.02
Cd-123	4.69 ± 0.03	5.03 ± 0.03	4.9 ± 0.03	4.92 ± 0.03
Cd-124	4.28 ± 0.03	4.88 ± 0.03	4.88 ± 0.03	4.82 ± 0.03
Cd-125	1.53 ± 0.06	1.76 ± 0.05	1.98 ± 0.05	1.84 ± 0.05
Cd-126	1.19 ± 0.07	1.27 ± 0.06	1.14 ± 0.07	1.22 ± 0.07
Cd-127	0.38 ± 0.12	0.31 ± 0.13	0.37 ± 0.12	0.39 ± 0.12
Cd-128	0.22 ± 0.15	0.2 ± 0.16	0.21 ± 0.16	0.21 ± 0.16
Cd-129	0.05 ± 0.33	0.04 ± 0.35	0.03 ± 0.41	0.04 ± 0.38
Cd-130	0.02 ± 0.58	0.01 ± 0.71	0.01 ± 0.71	0.01 ± 1
In-114	0.01 ± 1	-	-	-
In-115	0.09 ± 0.23	0.04 ± 0.35	0.03 ± 0.45	0.01 ± 0.71
In-116	0.14 ± 0.19	0.13 ± 0.2	0.06 ± 0.29	0.08 ± 0.25
In-117	1.43 ± 0.06	0.79 ± 0.08	0.55 ± 0.1	0.34 ± 0.12
In-118	1.59 ± 0.06	0.93 ± 0.08	0.85 ± 0.08	0.62 ± 0.09
In-119	6.64 ± 0.03	4.95 ± 0.03	3.69 ± 0.04	2.82 ± 0.04

Table C.1 Continued.

Isotope	50 MeV	40 MeV	35 MeV	30 MeV
In-120	9.56 ± 0.02	7.97 ± 0.03	6.3 ± 0.03	5.21 ± 0.03
In-121	15.06 ± 0.02	13.8 ± 0.02	12.09 ± 0.02	1-.02
In-122	11.98 ± 0.02	11 ± 0.02	10.1 ± 0.02	9.16 ± 0.02
In-123	14.12 ± 0.02	14.7 ± 0.02	13.89 ± 0.02	13.3 ± 0.02
In-124	8.86 ± 0.02	9.31 ± 0.02	9.29 ± 0.02	8.73 ± 0.02
In-125	8.84 ± 0.02	9.9 ± 0.02	10.31 ± 0.02	10.2 ± 0.02
In-126	4.7 ± 0.03	4.95 ± 0.03	5.45 ± 0.03	5.58 ± 0.03
In-127	3.85 ± 0.04	4.41 ± 0.03	4.28 ± 0.04	4.63 ± 0.03
In-128	1.59 ± 0.06	1.77 ± 0.05	2 ± 0.05	2.09 ± 0.05
In-129	1 ± 0.07	0.96 ± 0.07	1.01 ± 0.07	1.06 ± 0.07
In-130	0.39 ± 0.12	0.4 ± 0.12	0.35 ± 0.12	0.4 ± 0.12
In-131	0.13 ± 0.2	0.13 ± 0.2	0.16 ± 0.18	0.1 ± 0.23
In-132	0.02 ± 0.5	0.01 ± 1	0.01 ± 1	0.02 ± 0.5
In-133	0.01 ± 1	-	0.01 ± 0.71	0.01 ± 0.71
Sn-116	0.01 ± 0	-	-	-
Sn-117	0.01 ± 0.71	0.02 ± 0.58	0.01 ± 0.71	0.01 ± 0.71
Sn-118	0.23 ± 0.15	0.11 ± 0.22	0.08 ± 0.25	0.04 ± 0.38
Sn-119	0.47 ± 0.11	0.23 ± 0.15	0.14 ± 0.19	0.12 ± 0.21
Sn-120	2.85 ± 0.04	1.97 ± 0.05	1.32 ± 0.06	0.84 ± 0.08
Sn-121	2.84 ± 0.04	1.86 ± 0.05	1.44 ± 0.06	0.95 ± 0.07
Sn-122	9.16 ± 0.02	7.68 ± 0.03	6.56 ± 0.03	5.05 ± 0.03
Sn-123	5.04 ± 0.03	4.23 ± 0.04	3.61 ± 0.04	3.12 ± 0.04
Sn-124	15 ± 0.02	13.7 ± 0.02	12.43 ± 0.02	11 ± 0.02
Sn-125	6.42 ± 0.03	6.27 ± 0.03	5.91 ± 0.03	5.33 ± 0.03
Sn-126	13.63 ± 0.02	14.6 ± 0.02	14.08 ± 0.02	14 ± 0.02
Sn-127	5.75 ± 0.03	5.9 ± 0.03	6.14 ± 0.03	6.13 ± 0.03
Sn-128	8.14 ± 0.03	8.85 ± 0.02	9.73 ± 0.02	10.5 ± 0.02
Sn-129	4.93 ± 0.03	4.98 ± 0.03	5.28 ± 0.03	6.04 ± 0.03
Sn-130	3.95 ± 0.04	4.39 ± 0.03	4.27 ± 0.04	4.79 ± 0.03
Sn-131	1.31 ± 0.06	1.57 ± 0.06	1.53 ± 0.06	1.73 ± 0.06
Sn-132	0.74 ± 0.09	0.74 ± 0.08	0.86 ± 0.08	0.82 ± 0.08
Sn-133	0.08 ± 0.25	0.1 ± 0.23	0.08 ± 0.25	0.09 ± 0.24
Sn-134	0.05 ± 0.33	0.06 ± 0.3	0.05 ± 0.33	0.05 ± 0.32
Sn-135	0.02 ± 0.58	0.01 ± 1	0.01 ± 0.71	0.01 ± 1
Sn-136	0.02 ± 0.58	-	-	-
Sb-119	0.02 ± 0.5	0.01 ± 1	0.01 ± 1	-
Sb-120	-	-	-	-
Sb-121	0.31 ± 0.13	0.21 ± 0.16	0.11 ± 0.22	0.06 ± 0.3
Sb-122	0.89 ± 0.08	0.47 ± 0.11	0.37 ± 0.12	0.22 ± 0.15
Sb-123	3.42 ± 0.04	1.86 ± 0.05	1.57 ± 0.06	1.04 ± 0.07

Table C.1 Continued.

Isotope	50 MeV	40 MeV	35 MeV	30 MeV
Sb-124	3.32 ± 0.04	2.61 ± 0.04	2.06 ± 0.05	1.57 ± 0.06
Sb-125	9.53 ± 0.02	8.11 ± 0.03	7.05 ± 0.03	5.33 ± 0.03
Sb-126	2.86 ± 0.04	2.29 ± 0.05	1.9 ± 0.05	1.42 ± 0.06
Sb-127	14.1 ± 0.02	14 ± 0.02	13.33 ± 0.02	12.3 ± 0.02
Sb-128	2.95 ± 0.04	2.62 ± 0.04	2.26 ± 0.05	1.98 ± 0.05
Sb-129	13.44 ± 0.02	14.8 ± 0.02	15.04 ± 0.02	15.7 ± 0.02
Sb-130	6.08 ± 0.03	5.96 ± 0.03	6.42 ± 0.03	6.95 ± 0.03
Sb-131	10.7 ± 0.02	11.5 ± 0.02	12.12 ± 0.02	13.4 ± 0.02
Sb-132	5.53 ± 0.03	5.7 ± 0.03	6.25 ± 0.03	6.94 ± 0.03
Sb-133	3.51 ± 0.04	3.25 ± 0.04	3.49 ± 0.04	3.78 ± 0.04
Sb-134	0.68 ± 0.09	0.71 ± 0.09	0.69 ± 0.09	0.72 ± 0.09
Sb-135	0.42 ± 0.11	0.39 ± 0.12	0.3 ± 0.13	0.35 ± 0.12
Sb-136	0.1 ± 0.23	0.16 ± 0.18	0.12 ± 0.21	0.13 ± 0.2
Sb-137	0.04 ± 0.35	0.08 ± 0.25	0.04 ± 0.38	0.07 ± 0.28
Sb-138	0.02 ± 0.58	0.02 ± 0.58	0.03 ± 0.45	0.02 ± 0.58
Te-121	0.01 ± 1	-	-	-
Te-122	0.02 ± 0.58	0.01 ± 1	0.01 ± 1	0.01 ± 1
Te-123	0.05 ± 0.33	0.03 ± 0.41	0.02 ± 0.5	-
Te-124	0.66 ± 0.09	0.27 ± 0.14	0.19 ± 0.17	0.13 ± 0.2
Te-125	0.73 ± 0.09	0.47 ± 0.11	0.35 ± 0.12	0.17 ± 0.17
Te-126	3.63 ± 0.04	2.81 ± 0.04	2.03 ± 0.05	1.38 ± 0.06
Te-127	2.53 ± 0.05	1.92 ± 0.05	1.77 ± 0.05	1.19 ± 0.07
Te-128	9.9 ± 0.02	8.3 ± 0.03	7.27 ± 0.03	6.3 ± 0.03
Te-129	6.57 ± 0.03	6.42 ± 0.03	6.19 ± 0.03	5.8 ± 0.03
Te-130	16.3 ± 0.02	16.5 ± 0.02	15.82 ± 0.02	15.5 ± 0.02
Te-131	9.37 ± 0.02	9.93 ± 0.02	10.97 ± 0.02	10.7 ± 0.02
Te-132	18.96 ± 0.02	20.3 ± 0.02	22.13 ± 0.02	22.6 ± 0.02
Te-133	7.18 ± 0.03	8.04 ± 0.03	8.45 ± 0.02	1-.02
Te-134	9.9 ± 0.02	10.4 ± 0.02	10.88 ± 0.02	12.3 ± 0.02
Te-135	2.77 ± 0.04	2.93 ± 0.04	3.18 ± 0.04	3.29 ± 0.04
Te-136	2.04 ± 0.05	2.04 ± 0.05	2.23 ± 0.05	2.51 ± 0.05
Te-137	0.74 ± 0.09	0.69 ± 0.09	0.76 ± 0.08	0.86 ± 0.08
Te-138	0.46 ± 0.11	0.33 ± 0.13	0.37 ± 0.12	0.5 ± 0.1
Te-139	0.12 ± 0.24	0.12 ± 0.21	0.09 ± 0.24	0.08 ± 0.25
Te-140	0.03 ± 0.47	0.07 ± 0.28	0.05 ± 0.33	0.06 ± 0.3
I-124	0.01 ± 1	-	-	-
I-125	0.04 ± 0.35	-	0.01 ± 1	0.01 ± 1
I-126	0.15 ± 0.19	0.04 ± 0.38	0.03 ± 0.41	0.02 ± 0.58
I-127	0.72 ± 0.09	0.31 ± 0.13	0.24 ± 0.15	0.15 ± 0.19
I-128	1.42 ± 0.06	0.91 ± 0.08	0.59 ± 0.09	0.41 ± 0.11

Table C.1 Continued.

Isotope	50 MeV	40 MeV	35 MeV	30 MeV
I-129	3.77 ± 0.04	2.82 ± 0.04	1.96 ± 0.05	1.5 ± 0.06
I-130	3.23 ± 0.04	2.64 ± 0.04	1.83 ± 0.05	1.68 ± 0.06
I-131	10.27 ± 0.02	10.1 ± 0.02	8.46 ± 0.02	7.22 ± 0.03
I-132	8.64 ± 0.02	9.31 ± 0.02	9.48 ± 0.02	9.47 ± 0.02
I-133	17.56 ± 0.02	19.3 ± 0.02	20.56 ± 0.02	20.6 ± 0.02
I-134	12.56 ± 0.02	14.5 ± 0.02	15.74 ± 0.02	17.5 ± 0.02
I-135	19.15 ± 0.02	21 ± 0.02	23.19 ± 0.02	24.6 ± 0.01
I-136	7.78 ± 0.03	8.17 ± 0.03	8.64 ± 0.02	9.48 ± 0.02
I-137	6.53 ± 0.03	6.52 ± 0.03	7.59 ± 0.03	7.94 ± 0.03
I-138	3.15 ± 0.04	3.07 ± 0.04	3.01 ± 0.04	3.55 ± 0.04
I-139	1.87 ± 0.05	1.82 ± 0.05	1.9 ± 0.05	2.16 ± 0.05
I-140	0.65 ± 0.09	0.64 ± 0.09	0.78 ± 0.08	0.84 ± 0.08
I-141	0.47 ± 0.1	0.38 ± 0.12	0.41 ± 0.11	0.35 ± 0.12
I-142	0.1 ± 0.23	0.06 ± 0.3	0.1 ± 0.23	0.09 ± 0.24
I-143	0.04 ± 0.38	0.05 ± 0.33	0.02 ± 0.5	0.02 ± 0.5
Xe-128	0.04 ± 0.38	0.01 ± 0.71	-	-
Xe-129	0.13 ± 0.2	0.04 ± 0.35	0.02 ± 0.58	0.01 ± 0.71
Xe-130	0.7 ± 0.09	0.48 ± 0.1	0.25 ± 0.15	0.14 ± 0.19
Xe-131	0.82 ± 0.08	0.54 ± 0.1	0.38 ± 0.12	0.26 ± 0.14
Xe-132	3.66 ± 0.04	2.99 ± 0.04	2.46 ± 0.05	1.74 ± 0.06
Xe-133	3.59 ± 0.04	3.16 ± 0.04	2.87 ± 0.04	2.39 ± 0.05
Xe-134	11.02 ± 0.02	10.8 ± 0.02	10.74 ± 0.02	10.2 ± 0.02
Xe-135	7.82 ± 0.03	8.67 ± 0.02	8.98 ± 0.02	8.96 ± 0.02
Xe-136	21.67 ± 0.02	23.4 ± 0.02	26.03 ± 0.01	27.4 ± 0.01
Xe-137	12.4 ± 0.02	13.6 ± 0.02	14.55 ± 0.02	15.6 ± 0.02
Xe-138	13.71 ± 0.02	14.7 ± 0.02	15.65 ± 0.02	18 ± 0.02
Xe-139	6.7 ± 0.03	7.52 ± 0.03	7.75 ± 0.03	8.72 ± 0.02
Xe-140	5.88 ± 0.03	5.88 ± 0.03	6.53 ± 0.03	7.54 ± 0.03
Xe-141	2.28 ± 0.05	2.14 ± 0.05	2.37 ± 0.05	2.75 ± 0.04
Xe-142	1.59 ± 0.06	1.53 ± 0.06	1.51 ± 0.06	1.7 ± 0.06
Xe-143	0.41 ± 0.11	0.43 ± 0.11	0.46 ± 0.11	0.44 ± 0.11
Xe-144	0.24 ± 0.15	0.21 ± 0.16	0.26 ± 0.14	0.26 ± 0.14
Xe-145	0.06 ± 0.29	0.04 ± 0.38	0.06 ± 0.3	0.04 ± 0.38
Xe-146	0.01 ± 1	0.04 ± 0.35	0.02 ± 0.5	0.02 ± 0.58
Cs-129	0.01 ± 1	-	-	-
Cs-130	-	0.02 ± 0.58	-	-
Cs-131	0.07 ± 0.27	0.03 ± 0.45	0.01 ± 0.71	-
Cs-132	0.17 ± 0.17	0.11 ± 0.22	0.05 ± 0.32	0.06 ± 0.29
Cs-133	0.95 ± 0.07	0.52 ± 0.1	0.42 ± 0.11	0.24 ± 0.15
Cs-134	1.14 ± 0.07	0.84 ± 0.08	0.73 ± 0.08	0.55 ± 0.1

Table C.1 Continued.

Isotope	50 MeV	40 MeV	35 MeV	30 MeV
Cs-135	4.42 ± 0.03	3.73 ± 0.04	3.31 ± 0.04	2.78 ± 0.04
Cs-136	5.9 ± 0.03	5.74 ± 0.03	5.96 ± 0.03	5.39 ± 0.03
Cs-137	15.08 ± 0.02	16.1 ± 0.02	16.37 ± 0.02	15.9 ± 0.02
Cs-138	8.84 ± 0.02	9.74 ± 0.02	10.02 ± 0.02	11 ± 0.02
Cs-139	14.8 ± 0.02	16.4 ± 0.02	18.2 ± 0.02	19 ± 0.02
Cs-140	11.01 ± 0.02	11.8 ± 0.02	13.21 ± 0.02	14 ± 0.02
Cs-141	10.55 ± 0.02	11.3 ± 0.02	11.68 ± 0.02	13.2 ± 0.02
Cs-142	5.98 ± 0.03	5.85 ± 0.03	6.57 ± 0.03	7 ± 0.03
Cs-143	4.03 ± 0.04	4.48 ± 0.03	4.65 ± 0.03	5.32 ± 0.03
Cs-144	1.62 ± 0.06	1.73 ± 0.06	1.72 ± 0.06	2.11 ± 0.05
Cs-145	0.95 ± 0.07	1.09 ± 0.07	1 ± 0.07	1.11 ± 0.07
Cs-146	0.38 ± 0.12	0.37 ± 0.12	0.35 ± 0.12	0.27 ± 0.14
Cs-147	0.16 ± 0.18	0.13 ± 0.2	0.15 ± 0.19	0.23 ± 0.15
Cs-148	0.03 ± 0.41	0.02 ± 0.58	0.03 ± 0.45	0.04 ± 0.35
Cs-149	0.02 ± 0.58	0.01 ± 0.71	-	-
Cs-150	0.01 ± 0.71	-	-	-
Ba-132	0.01 ± 1	-	-	-
Ba-133	-	-	-	-
Ba-134	0.07 ± 0.3	0.03 ± 0.45	0.02 ± 0.5	-
Ba-135	0.24 ± 0.14	0.15 ± 0.19	0.07 ± 0.27	0.04 ± 0.38
Ba-136	1.14 ± 0.07	0.72 ± 0.09	0.62 ± 0.09	0.38 ± 0.12
Ba-137	1.69 ± 0.06	1.34 ± 0.06	1.09 ± 0.07	0.97 ± 0.07
Ba-138	6.13 ± 0.03	5.95 ± 0.03	5.2 ± 0.03	5.1 ± 0.03
Ba-139	6.57 ± 0.03	6.34 ± 0.03	6.14 ± 0.03	6.01 ± 0.03
Ba-140	11.03 ± 0.02	11.5 ± 0.02	12.02 ± 0.02	12.2 ± 0.02
Ba-141	9.18 ± 0.02	10.7 ± 0.02	10.94 ± 0.02	11.5 ± 0.02
Ba-142	12.27 ± 0.02	13.2 ± 0.02	14.02 ± 0.02	15.2 ± 0.02
Ba-143	7.71 ± 0.03	8.43 ± 0.03	8.7 ± 0.02	10.2 ± 0.02
Ba-144	7.57 ± 0.03	7.8 ± 0.03	8.37 ± 0.03	1-.02
Ba-145	3.58 ± 0.04	3.96 ± 0.04	4.2 ± 0.04	4.97 ± 0.03
Ba-146	2.56 ± 0.05	2.56 ± 0.05	2.9 ± 0.04	3.01 ± 0.04
Ba-147	1.07 ± 0.07	1.04 ± 0.07	1.23 ± 0.07	1.39 ± 0.06
Ba-148	0.56 ± 0.1	0.57 ± 0.1	0.62 ± 0.09	0.52 ± 0.1
Ba-149	0.16 ± 0.18	0.18 ± 0.17	0.17 ± 0.17	0.2 ± 0.16
Ba-150	0.07 ± 0.26	0.12 ± 0.21	0.08 ± 0.25	0.07 ± 0.28
Ba-151	0.03 ± 0.53	0.02 ± 0.5	0.02 ± 0.5	0.02 ± 0.58
Ba-152	0.01 ± 1	-	-	-
La-136	0.03 ± 0.45	0.02 ± 0.58	0.01 ± 1	-
La-137	0.15 ± 0.19	0.06 ± 0.29	0.03 ± 0.41	0.02 ± 0.5
La-138	0.39 ± 0.12	0.26 ± 0.14	0.14 ± 0.19	0.1 ± 0.23

Table C.1 Continued.

Isotope	50 MeV	40 MeV	35 MeV	30 MeV
La-139	1.6 ± 0.06	1.12 ± 0.07	0.84 ± 0.08	0.74 ± 0.08
La-140	2.15 ± 0.05	1.79 ± 0.05	1.66 ± 0.06	1.32 ± 0.06
La-141	4.5 ± 0.03	4.13 ± 0.04	4.26 ± 0.04	3.57 ± 0.04
La-142	4.87 ± 0.03	5.41 ± 0.03	5.41 ± 0.03	5.01 ± 0.03
La-143	7.75 ± 0.03	8.21 ± 0.03	8.86 ± 0.02	9.27 ± 0.02
La-144	6.8 ± 0.03	7.4 ± 0.03	7.79 ± 0.03	8.85 ± 0.02
La-145	8.01 ± 0.03	8.62 ± 0.02	8.89 ± 0.02	1-.02
La-146	4.78 ± 0.03	5.04 ± 0.03	5.59 ± 0.03	6.01 ± 0.03
La-147	4.6 ± 0.03	4.98 ± 0.03	5.17 ± 0.03	5.69 ± 0.03
La-148	2.07 ± 0.05	2.11 ± 0.05	2.16 ± 0.05	2.44 ± 0.05
La-149	1.67 ± 0.06	1.68 ± 0.06	1.81 ± 0.05	2.07 ± 0.05
La-150	0.62 ± 0.09	0.49 ± 0.1	0.58 ± 0.1	0.65 ± 0.09
La-151	0.32 ± 0.13	0.21 ± 0.16	0.2 ± 0.16	0.23 ± 0.15
La-152	0.04 ± 0.33	0.09 ± 0.24	0.05 ± 0.32	0.08 ± 0.26
La-153	0.03 ± 0.45	0.02 ± 0.58	0.02 ± 0.58	0.02 ± 0.5
La-154	-	0.01 ± 1	-	0.01 ± 1
La-155	0.01 ± 0.71	-	-	-
Ce-138	0.02 ± 0.58	-	-	-
Ce-139	0.01 ± 1	0.01 ± 1	0.01 ± 1	-
Ce-140	0.26 ± 0.14	0.13 ± 0.2	0.09 ± 0.24	0.03 ± 0.45
Ce-141	0.43 ± 0.11	0.26 ± 0.14	0.18 ± 0.17	0.17 ± 0.17
Ce-142	1.08 ± 0.07	0.89 ± 0.08	0.67 ± 0.09	0.52 ± 0.1
Ce-143	1.56 ± 0.06	1.36 ± 0.06	1.3 ± 0.06	1.07 ± 0.07
Ce-144	3.22 ± 0.04	3.21 ± 0.04	3.14 ± 0.04	3 ± 0.04
Ce-145	3.3 ± 0.04	3.37 ± 0.04	3.45 ± 0.04	3.68 ± 0.04
Ce-146	5.43 ± 0.03	5.81 ± 0.03	5.74 ± 0.03	6.18 ± 0.03
Ce-147	3.73 ± 0.04	3.99 ± 0.04	4.19 ± 0.04	4.75 ± 0.03
Ce-148	4.29 ± 0.03	4.69 ± 0.03	5.13 ± 0.03	5.49 ± 0.03
Ce-149	2.74 ± 0.04	2.88 ± 0.04	2.9 ± 0.04	3.27 ± 0.04
Ce-150	2.43 ± 0.05	2.66 ± 0.04	2.72 ± 0.04	2.98 ± 0.04
Ce-151	1.09 ± 0.07	1.06 ± 0.07	1.3 ± 0.06	1.34 ± 0.06
Ce-152	0.58 ± 0.1	0.69 ± 0.09	0.83 ± 0.08	0.91 ± 0.08
Ce-153	0.17 ± 0.17	0.24 ± 0.15	0.24 ± 0.15	0.25 ± 0.15
Ce-154	0.13 ± 0.19	0.12 ± 0.21	0.13 ± 0.2	0.17 ± 0.18
Ce-155	0.04 ± 0.35	0.04 ± 0.38	0.01 ± 1	0.03 ± 0.41
Pr-141	0.02 ± 0.58	-	-	-
Pr-142	0.01 ± 0.71	-	-	-
Pr-143	0.21 ± 0.16	0.1 ± 0.23	0.04 ± 0.35	0.04 ± 0.35
Pr-144	0.06 ± 0.28	0.02 ± 0.58	0.03 ± 0.45	0.03 ± 0.41
Pr-145	0.68 ± 0.09	0.56 ± 0.1	0.6 ± 0.09	0.39 ± 0.12

Table C.1 Continued.

Isotope	50 MeV	40 MeV	35 MeV	30 MeV
Pr-146	1.13 ± 0.07	0.83 ± 0.08	0.89 ± 0.08	0.79 ± 0.08
Pr-147	1.97 ± 0.05	1.8 ± 0.05	1.79 ± 0.05	1.72 ± 0.06
Pr-148	1.94 ± 0.05	2.01 ± 0.05	1.89 ± 0.05	2.06 ± 0.05
Pr-149	2.61 ± 0.04	2.73 ± 0.04	3.04 ± 0.04	3.11 ± 0.04
Pr-150	2.36 ± 0.05	2.19 ± 0.05	2.41 ± 0.05	2.72 ± 0.04
Pr-151	2.38 ± 0.05	2.61 ± 0.04	2.75 ± 0.04	2.94 ± 0.04
Pr-152	1.22 ± 0.07	1.29 ± 0.06	1.36 ± 0.06	1.52 ± 0.06
Pr-153	0.91 ± 0.08	0.98 ± 0.07	1.13 ± 0.07	1.09 ± 0.07
Pr-154	0.36 ± 0.12	0.45 ± 0.11	0.39 ± 0.12	0.53 ± 0.1
Pr-155	0.24 ± 0.15	0.32 ± 0.13	0.29 ± 0.13	0.23 ± 0.15
Pr-156	0.05 ± 0.33	0.08 ± 0.25	0.07 ± 0.27	0.07 ± 0.28
Pr-157	0.01 ± 0.71	0.01 ± 0.71	0.03 ± 0.41	0.03 ± 0.45
Pr-158	-	-	-	-
Pr-159	0.01 ± 1	-	-	-
Nd-143	0.01 ± 1	-	-	-
Nd-144	0.02 ± 0.5	0.02 ± 0.58	0.01 ± 1	0.01 ± 1
Nd-145	0.03 ± 0.45	0.01 ± 0.71	0.02 ± 0.58	-
Nd-146	0.12 ± 0.21	0.05 ± 0.32	0.05 ± 0.33	0.02 ± 0.5
Nd-147	0.22 ± 0.15	0.2 ± 0.16	0.12 ± 0.21	0.08 ± 0.25
Nd-148	0.43 ± 0.11	0.45 ± 0.11	0.38 ± 0.12	0.27 ± 0.14
Nd-149	0.5 ± 0.11	0.49 ± 0.1	0.46 ± 0.11	0.34 ± 0.13
Nd-150	1.01 ± 0.07	1.02 ± 0.07	1.06 ± 0.07	0.96 ± 0.07
Nd-151	0.97 ± 0.07	1 ± 0.07	1.03 ± 0.07	1.07 ± 0.07
Nd-152	1.3 ± 0.06	1.34 ± 0.06	1.47 ± 0.06	1.63 ± 0.06
Nd-153	0.92 ± 0.08	0.94 ± 0.08	1.08 ± 0.07	1.09 ± 0.07
Nd-154	0.84 ± 0.08	0.93 ± 0.08	1.07 ± 0.07	1.13 ± 0.07
Nd-155	0.44 ± 0.11	0.47 ± 0.11	0.59 ± 0.09	0.56 ± 0.1
Nd-156	0.36 ± 0.12	0.26 ± 0.14	0.35 ± 0.12	0.33 ± 0.13
Nd-157	0.12 ± 0.21	0.15 ± 0.19	0.11 ± 0.22	0.12 ± 0.21
Nd-158	0.08 ± 0.25	0.03 ± 0.41	0.05 ± 0.33	0.07 ± 0.27
Nd-159	0.02 ± 0.58	-	-	-
Pm-147	0.01 ± 0.71	-	-	-
Pm-148	0.01 ± 1	-	-	-
Pm-149	0.05 ± 0.33	0.05 ± 0.33	0.01 ± 1	0.02 ± 0.58
Pm-150	0.12 ± 0.21	0.08 ± 0.25	0.07 ± 0.28	0.05 ± 0.33
Pm-151	0.28 ± 0.14	0.23 ± 0.15	0.18 ± 0.17	0.16 ± 0.18
Pm-152	0.33 ± 0.13	0.28 ± 0.14	0.26 ± 0.14	0.24 ± 0.15
Pm-153	0.5 ± 0.1	0.53 ± 0.1	0.56 ± 0.1	0.46 ± 0.11
Pm-154	0.43 ± 0.11	0.53 ± 0.1	0.32 ± 0.13	0.41 ± 0.11
Pm-155	0.46 ± 0.11	0.57 ± 0.1	0.56 ± 0.1	0.59 ± 0.09

Table C.1 Continued.

Isotope	50 MeV	40 MeV	35 MeV	30 MeV
Pm-156	0.35 ± 0.12	0.26 ± 0.14	0.35 ± 0.12	0.43 ± 0.11
Pm-157	0.31 ± 0.13	0.28 ± 0.14	0.37 ± 0.12	0.35 ± 0.12
Pm-158	0.13 ± 0.21	0.1 ± 0.23	0.18 ± 0.17	0.17 ± 0.17
Pm-159	0.07 ± 0.27	0.12 ± 0.21	0.07 ± 0.27	0.09 ± 0.24
Pm-160	0.02 ± 0.58	0.01 ± 1	0.02 ± 0.58	0.02 ± 0.58
Pm-161	0.01 ± 0.71	0.01 ± 0.71	0.03 ± 0.45	0.01 ± 1
Sm-151	0.02 ± 0.5	-	-	-
Sm-152	0.02 ± 0.5	0.03 ± 0.45	0.01 ± 1	0.02 ± 0.5
Sm-153	0.04 ± 0.43	0.03 ± 0.45	0.04 ± 0.35	0.03 ± 0.41
Sm-154	0.08 ± 0.25	0.1 ± 0.23	0.1 ± 0.23	0.04 ± 0.35
Sm-155	0.14 ± 0.2	0.11 ± 0.22	0.11 ± 0.22	0.08 ± 0.25
Sm-156	0.18 ± 0.17	0.16 ± 0.18	0.15 ± 0.19	0.13 ± 0.2
Sm-157	0.19 ± 0.16	0.16 ± 0.18	0.23 ± 0.15	0.13 ± 0.2
Sm-158	0.2 ± 0.17	0.15 ± 0.19	0.22 ± 0.16	0.16 ± 0.18
Sm-159	0.05 ± 0.3	0.14 ± 0.2	0.07 ± 0.28	0.12 ± 0.21
Sm-160	0.07 ± 0.28	0.06 ± 0.29	0.09 ± 0.24	0.06 ± 0.29
Sm-161	0.02 ± 0.58	0.03 ± 0.45	0.02 ± 0.58	0.03 ± 0.45
Sm-162	0.02 ± 0.58	0.01 ± 1	0.04 ± 0.38	0.03 ± 0.45
Sm-163	0.01 ± 1	-	-	-
Eu-154	0.02 ± 0.58	-	-	-
Eu-155	0.01 ± 0.71	-	-	-
Eu-156	0.01 ± 0.71	0.02 ± 0.58	0.01 ± 0.71	0.01 ± 0.71
Eu-157	0.04 ± 0.4	0.03 ± 0.41	0.03 ± 0.45	0.03 ± 0.41
Eu-158	0.04 ± 0.35	0.02 ± 0.5	0.04 ± 0.38	0.04 ± 0.35
Eu-159	0.06 ± 0.29	0.05 ± 0.33	0.07 ± 0.27	0.06 ± 0.3
Eu-160	0.05 ± 0.33	0.04 ± 0.38	0.04 ± 0.35	0.02 ± 0.58
Eu-161	0.04 ± 0.33	0.05 ± 0.32	0.05 ± 0.32	0.05 ± 0.33
Eu-162	0.05 ± 0.33	0.02 ± 0.58	0.03 ± 0.45	0.02 ± 0.5
Eu-163	0.01 ± 1	0.01 ± 0.71	0.01 ± 0.71	0.01 ± 0.71
Gd-159	0.02 ± 0.58	-	-	-
Gd-160	0.02 ± 0.5	0.04 ± 0.38	0.03 ± 0.45	0.01 ± 0.71
Gd-161	0.02 ± 0.58	0.02 ± 0.58	0.01 ± 0.71	0.01 ± 0.71
Gd-162	0.03 ± 0.45	0.01 ± 1	0.03 ± 0.45	0.03 ± 0.45
Gd-163	0.01 ± 1	0.03 ± 0.45	0.01 ± 0.71	-
Gd-164	0.01 ± 1	-	-	0.01 ± 1
Gd-165	0.01 ± 0.5	-	0.01 ± 0.71	0.02 ± 0.58
Gd-166	0.01 ± 1	0.02 ± 0.5	0.01 ± 1	0.01 ± 0.71
Pm-156	0.35 ± 0.12	0.26 ± 0.14	0.35 ± 0.12	0.43 ± 0.11
Pm-157	0.31 ± 0.13	0.28 ± 0.14	0.37 ± 0.12	0.35 ± 0.12
Pm-158	0.13 ± 0.21	0.1 ± 0.23	0.18 ± 0.17	0.17 ± 0.17

Table C.1 Continued.

Isotope	50 MeV	40 MeV	35 MeV	30 MeV
Pm-159	0.07 ± 0.27	0.12 ± 0.21	0.07 ± 0.27	0.09 ± 0.24
Pm-160	0.02 ± 0.58	0.01 ± 1	0.02 ± 0.58	0.02 ± 0.58
Pm-161	0.01 ± 0.71	0.01 ± 0.71	0.03 ± 0.45	0.01 ± 1
Sm-151	0.02 ± 0.5	-	-	-
Sm-152	0.02 ± 0.5	0.03 ± 0.45	0.01 ± 1	0.02 ± 0.5
Sm-153	0.04 ± 0.43	0.03 ± 0.45	0.04 ± 0.35	0.03 ± 0.41
Sm-154	0.08 ± 0.25	0.1 ± 0.23	0.1 ± 0.23	0.04 ± 0.35
Sm-155	0.14 ± 0.2	0.11 ± 0.22	0.11 ± 0.22	0.08 ± 0.25
Sm-156	0.18 ± 0.17	0.16 ± 0.18	0.15 ± 0.19	0.13 ± 0.2
Sm-157	0.19 ± 0.16	0.16 ± 0.18	0.23 ± 0.15	0.13 ± 0.2
Sm-158	0.2 ± 0.17	0.15 ± 0.19	0.22 ± 0.16	0.16 ± 0.18
Sm-159	0.05 ± 0.3	0.14 ± 0.2	0.07 ± 0.28	0.12 ± 0.21
Sm-160	0.07 ± 0.28	0.06 ± 0.29	0.09 ± 0.24	0.06 ± 0.29
Sm-161	0.02 ± 0.58	0.03 ± 0.45	0.02 ± 0.58	0.03 ± 0.45
Sm-162	0.02 ± 0.58	0.01 ± 1	0.04 ± 0.38	0.03 ± 0.45
Sm-163	0.01 ± 1	-	-	-
Eu-154	0.02 ± 0.58	-	-	-
Eu-155	0.01 ± 0.71	-	-	-
Eu-156	0.01 ± 0.71	0.02 ± 0.58	0.01 ± 0.71	0.01 ± 0.71
Eu-157	0.04 ± 0.4	0.03 ± 0.41	0.03 ± 0.45	0.03 ± 0.41
Eu-158	0.04 ± 0.35	0.02 ± 0.5	0.04 ± 0.38	0.04 ± 0.35
Eu-159	0.06 ± 0.29	0.05 ± 0.33	0.07 ± 0.27	0.06 ± 0.3
Eu-160	0.05 ± 0.33	0.04 ± 0.38	0.04 ± 0.35	0.02 ± 0.58
Eu-161	0.04 ± 0.33	0.05 ± 0.32	0.05 ± 0.32	0.05 ± 0.33
Eu-162	0.05 ± 0.33	0.02 ± 0.58	0.03 ± 0.45	0.02 ± 0.5
Eu-163	0.01 ± 1	0.01 ± 0.71	0.01 ± 0.71	0.01 ± 0.71
Gd-159	0.02 ± 0.58	-	-	-
Gd-160	0.02 ± 0.5	0.04 ± 0.38	0.03 ± 0.45	0.01 ± 0.71
Gd-161	0.02 ± 0.58	0.02 ± 0.58	0.01 ± 0.71	0.01 ± 0.71
Gd-162	0.03 ± 0.45	0.01 ± 1	0.03 ± 0.45	0.03 ± 0.45
Gd-163	0.01 ± 1	0.03 ± 0.45	0.01 ± 0.71	-
Gd-164	0.01 ± 1	-	-	0.01 ± 1
Gd-165	0.01 ± 0.5	-	0.01 ± 0.71	0.02 ± 0.58
Gd-166	0.01 ± 1	0.02 ± 0.5	0.01 ± 1	0.01 ± 0.71
Tb-159	0.01 ± 1	-	0.01 ± 1	-
Tb-163	0.02 ± 0.58	-	-	0.01 ± 1
Tb-164	0.01 ± 1	0.01 ± 0.71	0.01 ± 0.71	-
Tb-165	0.02 ± 0.58	-	-	0.01 ± 0.71
Tb-166	0.01 ± 1	0.01 ± 1	-	-
Tb-167	0.01 ± 1	-	-	-

Table C.1 Continued.

Isotope	50 MeV	40 MeV	35 MeV	30 MeV
Tb-168	0.01 ± 1	-	-	-
Dy-168	0.01 ± 1	0.01 ± 1	-	-
Er-169	0.01 ± 1	-	-	-
Fr-224	0.01 ± 1	-	-	-
Ra-225	0.01 ± 1	-	-	-
Ra-226	0.02 ± 0.75	-	-	-
Ra-227	0.11 ± 0.22	-	0.01 ± 1	-
Ra-228	0.18 ± 0.17	0.04 ± 0.38	-	-
Ra-229	0.02 ± 0.5	0.02 ± 0.5	-	0.01 ± 1
Ra-230	0.01 ± 1	-	-	-
Ac-224	0.22 ± 0.15	-	-	-
Ac-225	3.2 ± 0.04	0.02 ± 0.5	-	-
Ac-226	5.1 ± 0.03	0.86 ± 0.08	0.03 ± 0.41	-
Ac-227	3.53 ± 0.04	2.72 ± 0.04	0.99 ± 0.07	0.12 ± 0.21
Ac-228	1.35 ± 0.06	1.28 ± 0.06	1.31 ± 0.06	0.49 ± 0.1
Ac-229	1.91 ± 0.05	0.46 ± 0.11	0.41 ± 0.11	0.5 ± 0.1
Ac-230	8.05 ± 0.03	0.65 ± 0.09	0.23 ± 0.15	0.03 ± 0.41
Ac-231	42.87 ± 0.01	9.68 ± 0.02	2.9 ± 0.04	0.92 ± 0.08
Ac-232	25.17 ± 0.01	14.1 ± 0.02	6.15 ± 0.03	2.51 ± 0.05
Th-226	0.5 ± 0.1	-	-	-
Th-227	4.19 ± 0.04	0.09 ± 0.24	-	-
Th-228	51.89 ± 0.01	5.25 ± 0.03	1.06 ± 0.07	0.02 ± 0.58
Th-229	144.4 ± 0.01	44.75 ± 0.01	10.19 ± 0.02	2.69 ± 0.04
Th-230	359.8 ± 0	328 ± 0	219.6 ± 0	75.8 ± 0.01
Th-231	357.9 ± 0	382 ± 0	384.2 ± 0	339 ± 0
Th-232	362.1 ± 0	417 ± 0	443.3 ± 0	46-
Th-233	44.42 ± 0.01	59 ± 0.01	67.72 ± 0.01	80.6 ± 0.01
Pa-226	0.03 ± 0.45	-	-	-
Pa-227	6.58 ± 0.03	0.05 ± 0.32	-	-
Pa-228	15.39 ± 0.02	18.9 ± 0.02	2.3 ± 0.05	-
Pa-229	37.57 ± 0.01	57.58 ± 0.01	86.86 ± 0.01	59.87 ± 0.01
Pa-230	67.37 ± 0.01	81.8 ± 0.01	93.94 ± 0.01	142 ± 0.01
Pa-231	112.1 ± 0.01	149 ± 0.01	173.9 ± 0.01	202 ± 0.01
Pa-232	65.37 ± 0.01	88.1 ± 0.01	101.9 ± 0.01	121 ± 0.01
Pa-233	17.98 ± 0.02	22 ± 0.02	25.22 ± 0.01	27.6 ± 0.01

Vita

Naser Burahmah was born in Kuwait City, Kuwait. He graduated from Saleh Shehab Highschool in Kuwait in 2010. He moved to Knoxville, Tennessee to complete his Bachelor of Science in Nuclear Engineering in 2015. He continued his education at the University of Tennessee where he received his Master of Science in Nuclear Engineering in May 2017.